University of Alberta

Investigation into the Use of Braiding in Golf Shaft Design

by

Douglas Steven S. Swanek

A thesis submitted to the Faculty of Graduate Studies and Research
in partial fulfillment of the requirements for the degree of

Master of Science

Department of Mechanical Engineering

Edmonton, Alberta
Spring 2007

Your file Votre référence
ISBN: 978-0-494-30031-2
Our file Notre référence
ISBN: 978-0-494-30031-2

ABSTRACT

Presently, braiding is not a popular method used in the production of golf shafts. The objective of this thesis is to design a golf shaft using braided lamina that is comparable in terms of mass, deflection-force and angle of twist to commercially available composite and steel shafts.

To achieve this, a model for a 2D conical braided composite was developed. The goals for the model were to: (1) calculate/maintain a minimum 95% cover factor and (2) predict the corresponding elastic constants. The model was validated by comparison with previous work.

Castigliano's Theorem was used to calculate the deflection-force and angle of twist of the design shaft assuming small deflections. Geometric calculations show this condition was verified. The mass of the design shaft was calculated based on the geometry and density of the shaft and its constituent materials.

Design golf shafts were comprised of both braided and unidirectional layers and compared to commercially available composite and steel shafts. Two shafts with a deflection-force of 11.47 N and 13.09 N, an angle of twist of 2.81° and 2.39° and mass of 67.8 g and 87.7 g, respectively, were designed using lamina with a 70% fibre volume fraction. These results are comparable to both commercial composite and steel shafts.

Lastly, a preliminary investigation was conducted to evaluate the use of foam materials as an internal solid core to provide additional rigidity without adding significant mass. From the materials evaluated, the *maximum* improvement of 14.9% and 8.19% in deflection-force and twist, respectively, is offset by a *minimum* mass increase of 17.8%.

ACKNOWLEDGEMENTS

I would like to thank Dr. Jason Carey for all of his support, guidance and patience during my time in the graduate program. His assistance and encouragement were vital in completing both the research and thesis. I consider him both a mentor and a friend.

I'd also like to thank all of the other individuals in the lab for their help and friendship: Cagri, Alessandro, Jamaal, Mark, Lynne, Jenna, Patrick, John and Richard. Additionally, thanks to Roger Marchand and Bernie Faulkner, in the machine shop, whose assistance was always appreciated.

I would like to thank all of my friends and family for their years of unwavering support. To my parents, I will never be able to tell how much I appreciate everything that you have done for me in my life. Everything that I have accomplished is a tribute to your kindness, patience, understanding and patience (can't mention that enough). To my sister, you are an inspiration to me and motivate me to accomplish more than I thought myself capable. Thanks all my friends for all of their support and good times we've had over the years (too many to count).

Lastly, thanks also go out to Drs. Mertiny, Gervais, Liggins and Budney for graciously donating their time in participating on the examination committee.

At the time I finished the undergraduate program, I didn't think I would ever return for a graduate degree. However, I did and I have thoroughly enjoyed the experience. It's funny how life works out.

"Do or do not, there is no try" – Yoda

TABLE OF CONTENTS

GLOSSARY

- **Braiding:** an automated and versatile process used to produce composites with interlaced strands. No two interlaced strands twist around each other.
- **Braid angle:** Acute angle measured between the strand and mandrel axis.
- **Brazier effect:** Plastic deformation of a circular tube in pure bending that results in the ovalization of the cross-section.
- **Carrier:** Part of a braiding machine used to carry strands during the braiding process and usually rotates in a plane normal to the mandrel.
- **CLPT:** Classical laminate plate theory.
- **Convergence zone:** Region where the strand meets the mandrel.
- **Cover factor (CF)**: Ratio of the mandrel area covered by the strands to the total surface area of the mandrel.
- **Cut-off area:** Elimination of overhanging strand area at the corners of a unit cell.
- **Damper:** A device that eliminates or progressively diminishes vibrations or oscillations.
- **Deflection-force:** Force required deflecting the tip of a cantilevered golf shaft a pre-determined distance.
- **Diamond braid:** Braided composite where strands travel in an alternating one over, one under pattern.
- **Fancy braid:** A term that is applied to a braid that is not classified as either a flat or tubular braid.
- **FE:** Finite element.
- **FGM:** Fabric geometry model.

- **Fibre volume fraction:** Measure of the average volume of fibres in a strand relative to the total strand volume.
- **Flat braid:** A braided composite that is ribbonlike in appearance.
- **Flex:** Rating of the stiffness of a golf club shaft. Flex can be categorized, from lowest to highest, as: L (ladies), A (amateur), R (regular), S (stiff) and X (extra stiff).
- **Hercules braid:** Braided composite where strands travel in an alternating three over, three under pattern.
- **Jam angle:** Braid angle where adjacent strands are tightly packed against each other, thereby preventing a further increase in braid angle.
- **Kickpoint:** The point along the length of a shaft that exhibits the greatest amount of bend. The grip end of the club is secured and the tip deflected by a point load (also called flex point or bend point).
- **Loading (golf shaft):** accumulation of spring energy in a golf shaft due to the downward acceleration during the downswing.
- **Lorythmic:** A scale system invented by Robert Adams to determine the swingweight about a fulcrum point 14" from the top of the grip. Swingweight is expressed with a letter-number designation ranging from A0 to G0.
- **Mandrel:** Central core used for the formation of braided composites with a varying or constant cross-section.
- **Overlap area:** Neglecting the overlapping area of strands in a unit cell to ensure the overlapping area is not considered twice.
- **PAN:** Polyacrylonitrile.

- **Pitch:** Axial distance travelled by a point in one revolution on a helical path.
- **Regular braid:** Braided composite where strands travel in an alternating two over, two under pattern.
- **Strand:** Bundle of fibres combined into a single element.
- **Strand undulation:** The alternating over/under path of a strand across adjacent strands in a braided or woven composite.
- **Torque (engineering):** The moment of a force that produces torsion and rotation about an axis.
- **Torque (golf):** Measurement (in degrees) of the magnitude a shaft will twist under a given load.
- **Twist:** Magnitude of angular deflection, measured in degrees, resulting from a torque applied to a golf shaft (also referred to as angle of twist).
- **UD:** Unidirectional. In this work, UD refers to a lamina with fibres oriented parallel (0°) to the mandrel axis.
- **Unit cell:** representation of a section along the length of a braided composite that is repeatable around the corresponding perimeter.
- **Unloading (golf shaft):** release of spring energy in a golf shaft during the latter stages of the downswing.
- **Woven textile:** Composite consisting of interlaced strands where adjacent strands are oriented at 90° to each other.

1 INTRODUCTION

Since the creation of the game of golf in 13th century Scotland, the golf club has been an essential part of the game. Until the 20th century, golf shafts were constructed of various types of wood [1]. In the early 1900's, solid, iron rod shafts were introduced [1]. The first hollow steel, stepped, tapered shaft was developed in 1927 and the design is still used today [1]. The first use of composite materials in shaft design was in the 1950's when a fibreglass layer was fit over a thin steel core [1]. The first hollow, graphite shafts were manufactured in the 1970's using filament winding [1]. These shafts had flexural stiffness comparable to steel but had the advantage of being lighter [1]. However they did not gain wide popularity until the 1980's due to a lack of torsional stiffness [1]. In the 1980's, shaft manufacturers began to use better quality materials and production techniques to improve the torsional stiffness of graphite shafts [1]. Shaft manufacturers realized that changing the orientation of fibres, with respect to the longitudinal axis of the shaft, increased torsional stiffness [1]. Currently, the majority of driver and wood shafts are of graphite composites. Additionally, many iron sets will offer a model with either steel or graphite shafts. The current popularity of composite golf shafts can be attributed to their lightweight and the variability of their mechanical properties.

Currently, composite golf shafts are manufactured using various methods. Hand lay-up and filament winding are two predominant methods used to produce a shaft with the desired mass, flexural and torsional stiffness.

Braiding is not currently a popular manufacturing technique used to produce golf club shafts. Braiding involves winding strands around a mandrel in an interweaving and interlocking pattern. Braiding may also be used in conjunction with other manufacturing

techniques such as hand lay-up. Braiding may be a superior manufacturing method due to the increased interlaminar strength provided by the interlocking strands. It has been shown that a braided composite has a higher shear modulus than a unidirectional (UD) composite made of the same material using an identical fibre volume fraction (V_f) [2]. However, braided composites exhibit a lower longitudinal modulus than UD composites due to strand undulations [2]. Effective braid longitudinal elastic modulus is lower than an UD lamina elastic modulus due to the off-axis loading of undulating strands [3]. Therefore, for a given cross-section the flexural rigidity of a braided laminate will be lower than an UD composite. Braiding may be more beneficial for torsional reinforcement than to increase flexural rigidity.

1.1 Thesis Objectives

The objective of this thesis project is to investigate the use of braiding to manufacture golf club shafts with comparable flexural and torsional rigidity of commercially available steel and composite shafts. Currently, braiding is not a prevalent method used to produce golf club shafts. The primary research objectives are:

1) Evaluate suitable fibre and matrix materials for proposed golf shafts.
2) Model a 2D conical braided composite.
3) Calculate the longitudinal modulus, E_x and in-plane shear modulus, G_{xy}, of a 2D conical braided composite using Classic Laminate Plate Theory.
4) Develop a laminate layer configuration using both braided and unidirectional lamina to produce a golf shaft with comparable flexural and torsional rigidity to commercial shafts.

5) Compare the mass and low-load, small deflection, static bending and torsional deflection of the braided golf shaft to commercial steel and composite shafts.
6) Investigate foam core materials to determine ability to increase shaft rigidity while controlling overall shaft mass.

1.2 Thesis Outline

The thesis is divided into chapters that investigate various aspects of modeling and designing a composite golf shaft. In Chapter 2 the review of published literature relating to golf club shafts, braided composites, foam core materials and relevant patents is detailed. Design parameters that are important in golf shaft design are discussed in Chapter 3. Selection of suitable materials is specified in Chapter 4. In Chapter 5 the proposed cover factor and elastic constants models are discussed and validated. In Chapter 6 the methodology involved in determining the static deflection and angle of twist for a golf shaft is covered. In Chapter 7, design of a golf shaft using both unidirectional and braided layers is investigated. Multiple materials and laminate stacking sequences are evaluated to determine if a design comparable to commercially available golf shafts is achievable. In Chapter 8, the preliminary investigation into using a foam core inside of a golf shaft is discussed. Finally, in Chapter 9 conclusions and recommendations for future work on the braided golf club shaft are specified.

2 LITERATURE REVIEW

Previous work available on golf club shafts and conical braided 2D composites is reviewed in this chapter. This includes details of an analysis of golf club shafts, various models developed to calculate the cover factor and elastic constants, the use of foam cores in composite structures and existing patents. Finally the thesis rationale concludes this chapter.

2.1 Golf Club Shafts

The golf swing, before impact with the golf ball, can be divided into two separate phases: (1) the backswing and (2) the downswing. Of less importance regarding shaft requirements is the backswing which initiates when the player begins to bring the club back (away from the ball) and terminates when the player reaches the top of the swing, just before the start of the downswing. For golf shaft design, the deformation of the shaft during the downswing is of interest since it influences the golf shot [4]. At the beginning of the downswing, the shaft is "loaded" by the initial downward acceleration [5]. Eventually during the downswing, the shaft effectively "unloads" and straightens out due the stored energy in the shaft [5]. Ideally, the shaft is fully "unloaded" at impact with the golf ball [5]. This takes place over a very small time interval, approximately 225 ms, and ends once the ball is contacted [6]. In that time, the clubhead can attain a velocity in excess of 45 m/s before impact with the golf ball [6]. Therefore, it can be expected that the shaft will deform during the swing. The deformation of the golf shaft during the swing assists in determining which parameters are important for shaft design. Numerous researchers, such as Milne and Davis [6], Horwood [4] and Butler and Winfield [7], have

conducted analysis into the role of the shaft during the downswing. Milne and Davis [6] modelled the dynamic behaviour of the shaft during the downswing. The resulting general behaviour is shown in Figure 2-1.

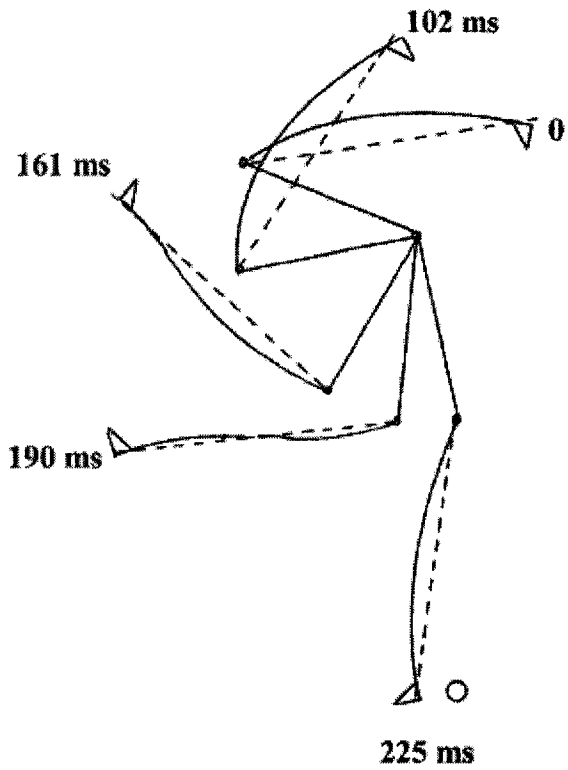

Figure 2-1: Shaft deflection during the downswing (deflection is magnified 5X) [8]

The time scale is referenced from the initiation of the downswing, measured in milliseconds (ms). At the initiation of the downswing, the shaft is bent down due the centrifugal force applied by the player and the inertia of the clubhead [8]. Through the progression of the downswing, the shaft straightens and bends forward just before impact [8]. Progression of the shaft from bent backward-to-bent forward can be seen as a wave-like oscillation at 190 ms, with a full oscillation occurring over the entire downswing. The bent-forward orientation of the shaft at impact is due to the centrifugal bending

moment applied by the clubhead to the shaft. The center of mass of the clubhead is offset behind the longitudinal axis of the shaft and due to the high clubhead speed (during the swing); the effective weight of the clubhead is magnified 150 times [6]. Milne and Davis [6] also used strain gauges, attached at three separate locations on the shaft, to analyze the bending moment on the shaft during the downswing. This was done with three different golfers, each of varying ability. Results were in good agreement with the findings of the simulation. Research done by Horwood [4] and Butler and Winfield [7] also supports the results of Milne and Davis. They also used strain gauges attached to the shaft to track the shaft deformation during the swing and found similar behaviour of the shaft during the downswing.

When the club is at rest, the angle between the vertical and the clubface is referred to as loft. Dynamic loft is an increase in the loft due to the deformation (bent-forward) of the shaft at impact [6]. An increase in the dynamic loft results in a higher ball trajectory, since the bent-forward action of the shaft at impact (Figure 2-2) causes the dynamic loft to increase.

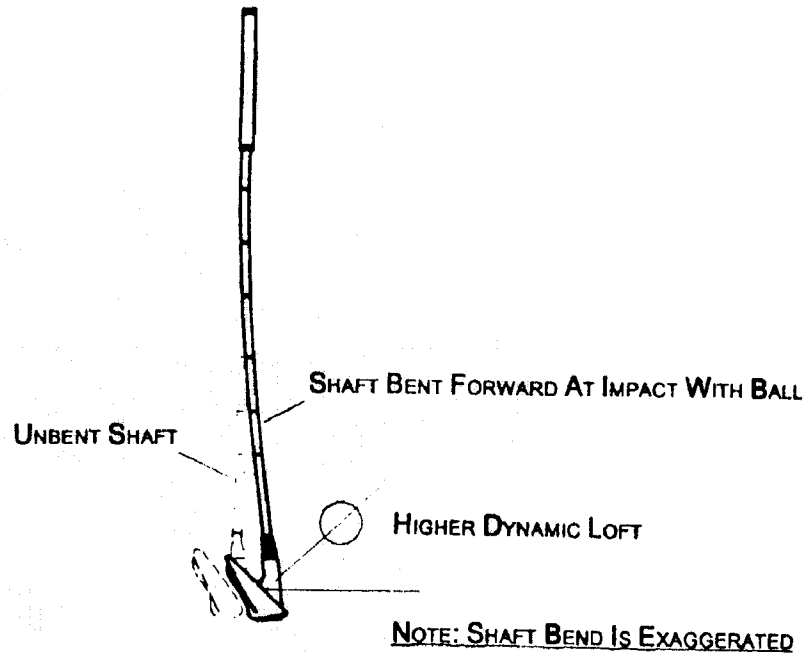

Figure 2-2: Bending of shaft at impact [4]

If the shaft is not sufficiently stiff for a player, the shaft will prematurely or excessively "unload" and further increase the dynamic loft of the clubhead. Likewise, if a shaft is too stiff, the shaft will minimally "load" and "unload", which will result in a low ball flight and decreased distance [9].

Additionally, the inertia force that causes the increase in dynamic loft also causes twisting of the shaft that affects clubhead alignment at impact [4]. Depending on the torsional stiffness of the shaft, this same inertia force may cause the clubhead into either a "closed", "square" or "open" position, which are illustrated in Figure 2-3 [9].

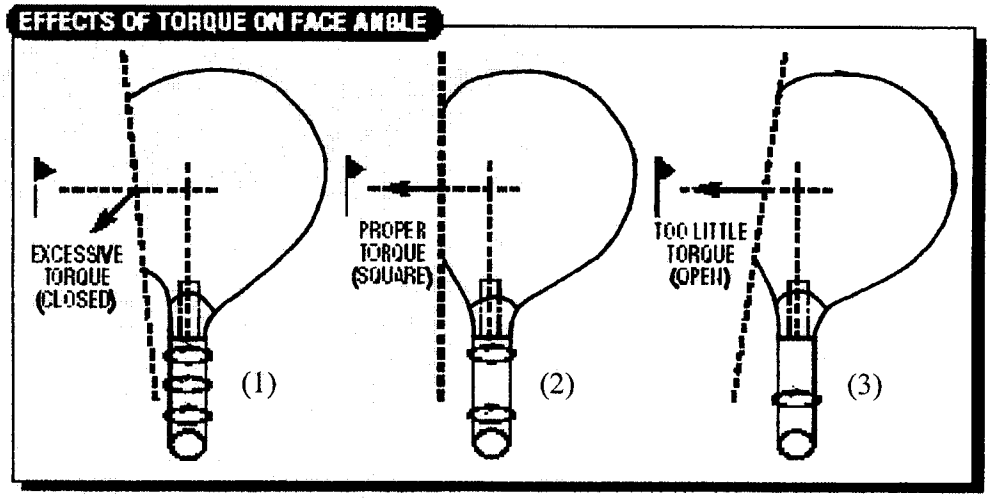

Figure 2-3: Torque (twist) of clubhead at impact; (1) indicates a "closed" position, (2) denotes a "square" position and (3) indicates an "open" position [9]

In addition, the offset of the clubhead from the shaft at impact will place an additional torque on the shaft, which may also affect clubhead alignment.

Figure 2-3 (1) shows a "closed" clubhead position. If a shaft does not have sufficient stiffness for a player, the inertial forces may cause the clubface to become excessively "closed" and the result could be a hook or pull (for a right-handed golfer) [5].

Figure 2-3 (2) shows a "square" clubface position, which is the desired orientation of the clubhead at impact [9]. A shaft with a torsional stiffness that matches the swing of the golfer will generate a "square" position at impact and a straight shot.

Figure 2-3 (3) details an "open" clubhead position. For a right-handed golfer, an "open" clubface points to the right of the intended target. An "open" clubface may occur due to an excessively stiff shaft or off-center hits on the clubface. A shaft that is too stiff for a player will not rotate during the swing and remain in an "open" position [9]. Off-center hits produce a greater torque on the shaft the further impact occurs from the shaft. If the shaft does not have sufficient torsional stiffness, the induced torque may cause the clubface to open upon contact with the ball.

Therefore, a proper shaft flex for a player will result in a "square" clubhead position and optimal "unloading" of the shaft at impact [9].

It has also been shown by Butler and Winfield [7] and Horwood [4] that the inertia of the clubhead will cause the toe of the clubhead to deflect down. This is due do the center of gravity of the clubhead being offset from the shaft by several centimetres [8]. This causes the shaft to "droop" during the swing (Figure 2-4). Results by Butler and Winfield found the magnitude of the "drooping" in the range of 0.52 cm to 5.44 cm [7].

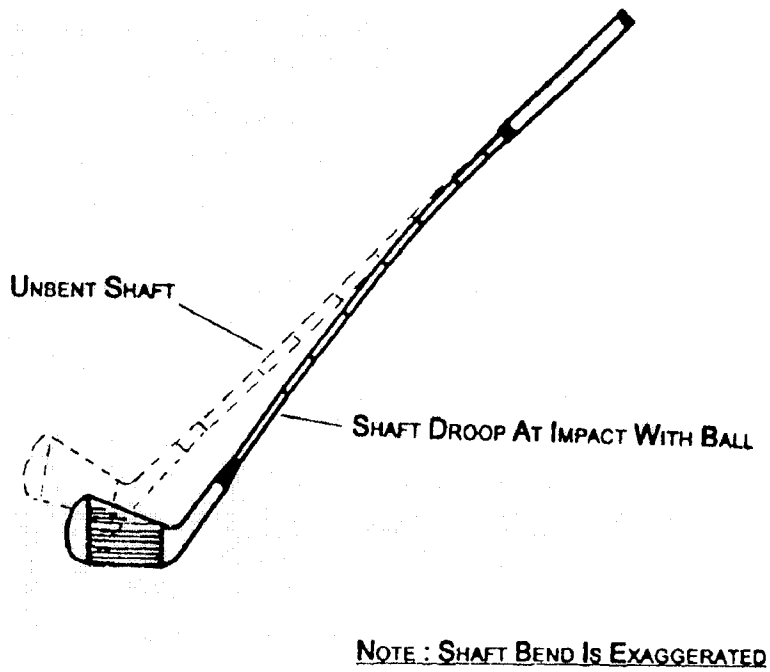

Figure 2-4: Bending of the shaft at impact, referred to as "drooping" [4]

Pelz [10] investigated the difference in drive distance and shot dispersion of steel and graphite (composite) golf shafts. Both the steel and graphite shafts were 1092 mm (43 inches) in length. It was found that the drive distance of the composite shafts was 3.0 yards longer than the steel shafts. This may appear minimal but with the competitive

nature of golf equipment design is a legitimate advantage over steel shafts. The greater drive distance of the graphite shafts may be due to their typically lower mass.

Steel shafts range in mass from 90 g to 130 g and graphite shafts from 50 g to 80 g [11]. The most popular mass range for graphite wood shafts is 60 – 70 g [11]. A lower shaft mass can allow the player to generate greater clubhead speed [8], which can result in greater drive distance [11]. Steel shafts are known to provide a tighter shot dispersion than graphite shafts. Pelz [10] found that the steel shafts had an average shot dispersion 8 yards lower than the composite shafts. This indicates that the shots from the steel shafts were more consistent, in terms of lateral deviation, than those from the composite shafts. Typically, steel shafts have greater torsional stiffness than composite shafts [12]. A greater twist during the swing and at impact (i.e. a lower torsional stiffness) results in higher dispersion of shots [13]. Despite the lower torsional stiffness of composite golf shafts, they are still very popular with golfers for their flexural stiffness and low mass.

Composite golf club shafts have been a major area of development in golf equipment. The ability to tailor flexural and torsional stiffness of composite golf shafts makes them attractive to players of all abilities [13]. Although braiding is not a popular manufacturing technique for golf shafts, Fujikura has recently begun using triaxial braiding in the tip section of their Rombax model shafts [14].

The flexural (bending) stiffness of a golf shaft is expressed in the shaft industry as flex [13] and is measured by either the static deflection or frequency of the shaft. To measure static deflection, the shaft is clamped at the butt end, a small load is placed on the tip and the resulting deflection is measured in inches or millimetres [15]. A greater the deflection corresponds to a lower flex. To determine the frequency, the butt end of the

shaft is clamped and a mass is placed on the shaft tip [15]. The tip is then plucked and the frequency is then measured. Frequency is commonly measured in cycles per minute (cpm). A stiffer shaft is characterized by a higher frequency [5]. The golf shaft industry has divided flex into 5 categories: L (ladies), A (amateur, senior), R (regular), S (stiff) and X (extra stiff) [15]. However, there is no industry standard to determine the different magnitudes of flex [5]. Therefore, for one company the R flex may be an S flex for another. Additionally, the tip stiffness of a golf shaft may be determined. The tip end is clamped and the deflection of the butt (free end) is determined when subjected to a load [16]. The tip stiffness is used to predict the launch characteristics of the shaft [16]. Generally, greater tip stiffness results in a lower launch trajectory, while low tip stiffness may produce a higher launch angle [16]. The torsional stiffness is expressed as the angle of twist when the butt end of the shaft is clamped and a torque is applied to the tip [17]. The Rules of Golf [18] stipulate the shaft must "bend in such a way that the deflection is the same regardless of how the shaft is rotated about its longitudinal axis" at any point along its length [18]. Additionally, the shaft must "twist the same in both directions" when a torque is applied to any point along the length [18]. This adds design constraints to golf shaft design.

There is abundant information on the dynamic characteristics of the golf shaft during the swing. However, there is minimal research on the composite layering and the use of braiding in manufacturing golf shafts, which is of interest in this research. Matsumoto [13] and Cheong [15] investigated the mechanical properties of golf shafts based on the composite layering and lamina fibre orientation using hand lay-up; while Howell [17] detailed the same but in reference to filament winding.

Cheong [15] and Howell [17] each discussed static torsion and static deflection tests, as ways to characterize shaft bending and torsional stiffness. Cheong [15] modelled the composite structure of a golf shaft and evaluated the corresponding deflection, angle of twist, kick point and natural frequency. The modelled shaft consisted of variable or bias layers that were sandwiched between layers whose orientations were held constant. This was done to examine the influence of fibre angle on the mechanical properties. The results indicate that the fibre angle has a significant influence on the mechanical properties of the golf shaft.

Matsumodo [13] investigated the torsional stiffness and vibration damping of golf shafts made from high modulus carbon fibres. The initial ball speed and flight path following impact was evaluated for a higher torque-degree (6.7°) and a lower torque-degree (2.8°) shaft. The vibration damping of pitch-based and PAN-based shafts was investigated using low torque-degree shafts (1.7° to 2.8°). The bias layers consisted of commercially available PAN-based and pitch-based carbon fibre prepregs. Parameters such as length, tip and butt diameter, flex and straight layer materials were held constant for each of the tested shafts. From the results, the shafts manufactured from the pitch-based prepregs exhibited greater torsional vibration damping, initial ball speed and more stable launch direction that PAN-based fibre golf shafts.

Howell [17] discussed the methodology for golf shaft design using filament winding. Design parameters such as fibre and resin selection, fibre orientation with respect to the longitudinal shaft axis and layer stacking sequence were detailed. Fibres typically used in filament wound golf shaft are standard, intermediate and high modulus carbon fibres. The fibre orientation, with respect to the shaft longitudinal axis, influences

the bending and/or torsional stiffness; a 0° fibre angle increases the flexural modulus while a 45° fibre angle is optimal for torsion. Additionally, the layering sequence will influence the stiffness of the shaft. A 0°-ply will provide greater bending stiffness if placed on the outer diameter of the shaft than the inner diameter due to an increase of the moment of inertia. Likewise for a 45°-ply the torsional stiffness improves the further the layer is placed from the inner diameter.

Takemura [19] modelled the cylindrical tip section of a golf shaft using finite element (FE) analysis and compared to experimental results. The shaft consisted of an outer layer of low-modulus fibres with an inner layer of high-modulus fibres. The cylinder was supported at the ends and an impact hammer hit the cylinder at the mid-span. The FE analysis was able to replicate experimental results, which indicated that the low-modulus outer layer increased the compressive strength of the cylinder. This was due to the higher compressive failure strain of the low-modulus fibres.

2.2 Braided 2D Composites

The braiding process has been used commercially for over 100 years. Initially, this technology was used to manufacture various textiles, such as rope, cylindrical tubing and rugs [20]. In the manufacture of composite materials, braiding is primarily used to produce flat or tubular forms [20]. Braiding is a relatively easy, low-cost and automated manufacturing process and therefore may be used for high volume production [21]. Since the current application is golf shaft design, the circular braiding process will be exclusively discussed.

In the process, strands are deposited to a transverse moving mandrel via strand carriers (carriers) that rotate around the centrally placed mandrel. The mandrel may be of

a constant or varying cross-section but is assumed axisymmetric, such as golf shafts [22]. Half of the strands rotate in a clockwise direction and form a positive braid angle, $+\theta$, while the other half rotate in a counter clockwise direction and form an equal but negative braid angle, $-\theta$ [22]. The result is an interweaving pattern [23]. The velocities of the mandrel and carriers can be manipulated to change the braid angle [24].

2.2.1 Cover Factor

Research on determining the cover factor of a 2D conical braided composite has been done by Brunnschweiler [23,25], Michaeli and Rosenbaum [24], Soebroto [26], Pastore and Ko [27], Du and Popper [22,28], Zhang [20], Mazzawi [29] and Rawal [30].

Brunnschweiler [23,25] discussed the history, manufacturing, structural and tensile properties of braided fabrics and composites. There are three main braiding configurations: diamond, regular and Hercules. Diamond, regular and Hercules braid patterns are shown in Figure 2-5.

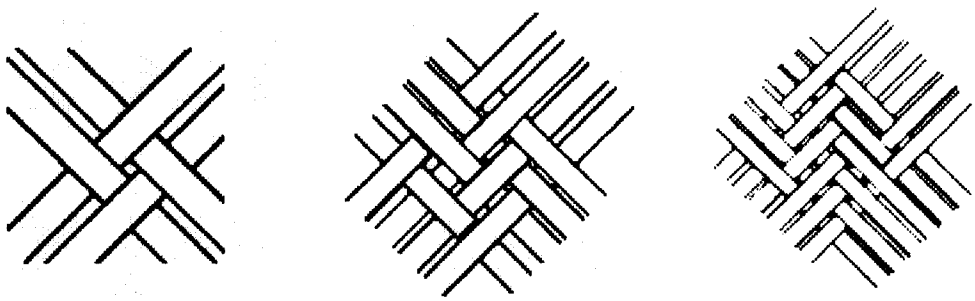

Figure 2-5: Diamond, regular and Hercules braiding patterns [adapted from 31]

A diamond braid or 1x1 pattern is a single strand overlap pattern, meaning that a strand continually passes over an adjacent strand and under the next. A regular braid, also known as a 2x2 pattern has a double strand overlap, indicating that a strand passes over two adjacent strands and then under the next two. Finally, a Hercules braid or 3x3 is a

triple strand overlapping pattern where a single strand passes over three neighbouring strands and under the next three adjacent ones [23].

Braids can be flat, tubular and fancy [23]. Flat braids follow a zig-zag path and are ribbon-like in appearance. Tubular braids have a circular cross-section and may be used for tubing or placed over a core. Finally, fancy braids are any braid that is not considered flat or tubular.

Brunnschweiler [25] also detailed the maximum and minimum jam angles for a given number of strands and strand width. The jam angle is where the strands are pressed against each other and inhibit movement in a particular direction, which indicates a 100% cover factor.

Michaeli and Rosenbaum [24] detailed a control system for a braiding machine to manage the braid angle. The system controlled the braid angle based on the velocities of the carrier and mandrel and the diameter of the mandrel. However, it did not consider braiding parameters such as the cover factor.

Soebroto et al [26], and Pastore and Ko [27], related the braiding process parameters to the resulting geometry of a tubular braided composite. The composite surface is divided into a repeatable rectangular unit cell representative of the entire composite in terms of structure and mechanical properties. The process factors that determined the fibre geometry were the carrier angular velocity and mandrel velocity. The cover factor was determined based on the ratio of the area covered by the strands to the unit cell area.

Du and Popper [22, 28] developed a mathematical process model to determine the cover factor of an axisymmetric mandrel. The model related the dependence of the braid

angle and cover factor on parameters such as carrier angular velocity, mandrel velocity, strand width, number of carriers, mandrel radius and the taper angle (half-cone angle) of the mandrel. Additionally, the jamming angles due to geometrical considerations were discussed.

Zhang [20] investigated the validity of the assumption that the strands (yarns) may be considered straight in the convergence zone, which is the area where the strands are deposited onto the mandrel. Previous models, such as those by Du and Popper [22], used the straight yarn assumption. The model proposed by Zhang [20] considered the frictional forces between strands due to relative sliding during the interweaving. The results indicated that for smaller braiders (< 64 carriers) the friction forces were small and therefore, the straight yarn assumption was valid.

Mazzawi [29] uses a geometric model based on the braid angle formed through one revolution of a conical mandrel. The resulting braid angle is dependent on the velocities of both the carriers and mandrel. Due to the taper of a conical mandrel, a trapezoidal unit cell was used rather than a rectangular or square unit cell as used by Pastore [27]. The conical strand path varies in pitch and curvature along the mandrel length due to the change in cross-section, which results in a changing braid angle if the carrier and mandrel velocities are held constant. The results of the conical model were compared to a previously developed model by Du and Popper [22]. A negligible difference in cover factor was found between the two models.

Rawal and Potluri [30] used a 3D geometrical model to determine the mathematical relationship between the braid angle and helical path of strands on mandrels of various shapes. Circular, conical and square prism mandrel shapes were used

in the model development. This was used to relate the process parameters of braiding to the resulting braid angle and cover factor.

Cover factor of a braided composite, is one of the many variables required to predict the elastic constants.

2.2.2 Elastic Constants Predictive Models

Models to predict the elastic constants of 2D diamond-braid composites have been conducted by numerous researchers. Models can be divided into three basic categories: finite element (FE), fabric geometry models (FGM) and those based on the Classic Laminate Plate Theory (CLPT).

Falzon [32] evaluated multiple models, including FE, FGM and CLPT models, used to estimate the elastic constants of interest; namely the longitudinal modulus, E_x, in-plane shear modulus, G_{xy} and other elastic constants of woven textiles. Woven textiles only differ from braided textiles in that woven fabrics are constrained to having the strands intersect at 90°. It was found that FE models were complex, required substantial computing time and did not provide greater accuracy in predicting elastic constants. FE models are more applicable to strength analysis where a greater level of complexity is required [32].

FGM models were found to be sufficient in predicting elastic constants; however strand undulations are either neglected or assumed as straight lines.

CLPT models were found to be accurate and simple [32]. Ishikawa and Chou [33] developed early CLPT models for 2D composites: (1) mosaic model (2) fibre undulation model and (3) bridging model. The mosaic model used an assemblage of asymmetrical cross-ply laminates to predict the elastic behaviour [33]. The fibre undulation model is

similar to the mosaic model except the fibre undulation model uses a sinusoidal function to model the fibre undulations between the overlapping strands. The bridging model was originally used for satin weaves and combines elements of both the mosaic and fibre undulation models. In the bridging model, only the undulation path of the fill yarn uses a sinusoidal function.

Huang [34] used the bridging model, originally developed by Ishikawa and Chou [33] for satin fabrics, to determine the mechanical properties of woven and braided fabrics. The unit cell is divided into four symmetric/identical subcells with a sinusoidal function used to approximate the undulation path. A favourable comparison with experimental results was found.

Naik and Ganesh [35] used a unit cell approach to calculate the thermoelastic properties of woven fabrics. The unit cell would be representative of the composite structure and considered the strand undulations, fibre volume fraction, strand cross-section and weave geometry. Various assumptions on modelling the strand undulations were investigated including: circular, sinusoidal and element array model with parallel-series combination. From comparison with experimental results, the sinusoidal approximation modelled the undulation path the best.

Raju and Wang [36] use a unit cell approach and a sinusoidal function, as in Ishikawa and Chou [33], to model the undulation path. The unit cell is divided into multiple regions that consist of unidirectional fibres and matrix material.

Carey [37] generalized the model developed by Raju and Wang [36] to determine the elastic constants of open and closed mesh braided composites. The unit cell is divided into multiple regions that consist of one of the following: unidirectional fibre and matrix

material, matrix material only or fibre undulations and matrix material [37]. The model also uses a sinusoidal function to approximate the undulation path. The results of the model were in excellent agreement with experimental results for the Kevlar 49/epoxy braided tubes in predicting the longitudinal modulus, E_x. Additionally, the predicted values of the in-plane shear modulus, G_{xy}, were comparable to those found in previous models [31].

In conclusion, CLPT models will be used as they account for the strand undulations, are relatively simple and have been found to suitably predict elastic constants for braided and woven composites.

2.3 Core Materials as Composite Reinforcement

A preliminary evaluation into the use of foam core materials in the design of golf shafts is conducted in this work. The literature review is limited to previous foam core research with tubular structures since the application deals with golf shafts. There are three main types of core materials: foam, honeycomb and cellulose [38]. Foams include both thermoset and thermoplastic polymers, honeycombs may be metallic or non-metallic materials and cellulose core materials that include cork and wood [38]. Foams are classified into 5 categories, based on density: very light (3 – 50 kg/m^3), light (50 – 200 kg/m^3), medium (200 – 500 kg/m^3), heavy (500 – 700 kg.m^3) and superheavy (> 700 kg/m^3) [39].

Kanny et al [40] conducted an experimental analysis on PVC foam materials. The densities ranged from 75-300 kg/m^3 and were statically tested, using a 3-point bend test, to determine the bending modulus. It was found that the bending modulus increased as the material density increased.

Cecchini [41] used foam cores to increase the resistance of cylindrical tubes to the Brazier effect. A mathematical optimization of isotropic and orthotropic cylinder materials was detailed. The isotropic cylinder was aluminium with aluminium foam core and the orthotropic cylinder was a carbon fibre reinforced plastic (CFRP) with a polymeric foam core. It was found that the aluminium cylinder and core could theoretically be as much as 50% lighter than a hollow aluminium cylinder for a given Brazier failure bending moment. A theoretical reduction in mass of 30% was found for the CFRP cylinder with polymeric foam compared to a hollow CFRP cylinder.

Harte [42] tested foam-filled braided tubes, in tension and compression, to analyze deformation energy absorption to failure. Additionally, analytical models were developed to determine dependence of energy absorption on tube wall strength, the ratio of tube wall thickness to tube diameter and the foam density. It was found that the amount of energy absorbed increased as the ratios of tube radius to wall thickness and tube wall yield strength to foam core wall strength also increased. The maximum energy absorption per unit mass and unit volume occurred when the ratio of the relative density of the foam to cell wall material was 0.2 and 0.3, respectively.

Mantena [43] investigated the impact response of foam-filled steel tubes. Three foams of varying density were modelled under compressive quasi-static conditions using finite element (FE) analysis. The area under the load-deflection curve, for both elastic and plastic deformation, was used to calculate the absorbed energy. It was found that the energy absorption decreased with decreasing density. The difference in stiffness between the steel tube and foam density was a reason for the energy absorption capabilities of the foam materials.

Brachos [44] investigated the energy absorption capabilities of rectangular and cylindrical braided tubes both hollow and filled with foam materials. The hollow cylinders exhibited greater energy absorption than the rectangular hollow tubes. Additionally, both the cylindrical and rectangular tubes have greater energy absorption with an increase in wall thickness. Adding a foam core increased the energy absorption capabilities of both tube cross-sections.

Ekstrom [45] studied the affect of core materials on the reduction in vibration transmitted through a steel and composite golf shaft. Dampers from two separate vendors were tested. Little information was provided regarding the damper materials. It was found that the damper from Vendor2 was as effective as "putting paper towel into the shaft". However, the dampers from Vendor1 were much more effective in reducing vibration. Dampers from Vendor1 reduced vibrations 97.6% in the graphite shaft and 46% in the steel shaft. It was concluded that to effectively reduce vibration, the damper should be set to match the frequency of the golf shaft.

True Temper Sports Inc. [46] utilizes a technology called Sensicore, which is a polymer core inside the shaft, to reduce vibration in select models of steel iron shafts. It is claimed that the core will provide up to 70% reduction in vibration at impact. A patent search for additional information on this technology was unsuccessful.

Foam core materials provide several advantages when used in tubular structures, which include increased energy absorption, vibration dampening and stiffening.

2.4 Applicable Patents

A search of applicable patents relating to: (1) use of braiding in golf manufacturing and (2) using cores in composite structures was conducted. The results are summarized below. Table 2-1 details patents that involve braiding and golf shafts. The multiple patents held by Ashida [47, 49,50,52, 52] are the closest to the work being undertaken in this thesis. None of the listed patents use a combination of biaxial braided and unidirectional layers. Additionally, none of the patents entail using an outer braided layer with a minimum cover factor of 95%.

Table 2-2 summarizes the results of a search for patents related to braided composites using foam cores. Harte [42], Mantena [43] and Brachos [44] detailed the energy absorption capabilities of foam core materials in tubular structures. Energy absorption is greater for tubular structures with foams cores than hollow structures. Additionally, an increase in foam core density increases the resulting energy absorption. Ekstrom [45] and True Temper [46] have shown that foam core materials increase the vibration dampening in both composite and steel golf club shafts. Grove [61] utilizes a center beam to be inserted into a golf shaft but does not state constructing a golf shaft around a core. Sutherland [57] applies a braided sleeve over a core for use in the design of baseball bats, whereas this research applies to the design of golf shafts. Cundiff [58] uses braided and unidirectional layers over a foam core to wind tunnel blades. Crow [59] uses a plug (formed of a sound absorbing material) that is set inside the tapered section of a composite or steel shaft. None of the listed patents utilize a foam core along the entire length of a composite golf shaft, specifically a braided shaft, which is proposed in this work.

Table 2-1: Patents relating to braided shafts

Patent Number	Patent Author	Year	Patent Name	Invention Premise
US7037212 [47]	Ashida, H. et al	2006	Fiber Reinforced Plastic Golf Shaft	Using a braided layer and having a linear change in braid angle along the shaft
US6652389 [48]	Hismatsu, et al.	2003	Golf Club Shaft	Golf shaft is produced using triaxial braided layers.
US6572490 [49] CA2363756 [50]	Ashida, H.	2003 2001	FRP Golf Club Shaft	Varying the braid angle of an inner biaxial braided layer between ±45° and the angle of an outer triaxial braided layer between ±10°.
US6666778 [51] CA2363812 [52]	Ashida, H.	2001 2001	FRP Golf Club Shaft	Braided golf shaft with strands at multiple angles. A portion of the braided layer is set such that it minimizes the space between the strands. This is applied to both biaxial and triaxial braided layers.
US5419231 [53] CA2104669 [54]	Earle III, et al.	1995 1992	Asymmetric braiding of improved fibre reinforced products	Use asymmetric braiding to construct tubular products. Utilizes both asymmetric biaxial and triaxial layers.
US5653646 [55]	Negishi, et al.	1995	Golf Club Shaft and Method of Producing the Same	A shaft is composed of a filament wound layer and a reinforcing layer formed by partially inserting a braid layer onto a desired position on the filament wound layer.
US5083780 [56]	Walton; T.C, Fenton; F.	1992	Golf Club Shaft Having Selective Reinforcement	Steel shaft with a braid shell on the outer surface. Braided shell does not cover the entire outer steel shaft surface.

Table 2-2: Patents relating to composites and internal cores

Patent Number	Patent Author	Year	Patent Name	Invention Premise
US7008339 [57]	Sutherland	2006	Composite Over-wrapped Lightweight Core	Producing a baseball bat with a polymer composite braided outer skin wrapped around a rigid inner core. Core may be wood, metal or foam.
US6872340 [58]	Cundiff, et al.	2005	Resin Transfer Molding Process	Producing a wind tunnel blade where foam core sections are covered by a braided sleeve and intermediate unidirectional tows
US6117021 [59]	Crow, et al.	2000	Golf Club Shaft	Steel or composite shaft with in internal plug inside the tapered section. The plug is formed from a sound absorbing material.
US5855790 [60]	Bocoviz., et al.	1999	Method of Making a Flow-Straightener Vane	Producing a composite vane using unidirectional or braided layers. Vane may be hollow or have an internal core of cellular or lightweight foam.
CA2154370 [61]	Grove, D.W.	1997	Center Beam Golf Club Shaft	Inserting a center beam into the hollow golf shaft. Center beam may be composite, graphite or metal.
US5580627 [62]	Goodwin, et al.	1996	Molded Products Made from Preforms of Tubular Braids	Applying a tubular braided layer over a bladder or foam core. Composite is then molded and core is removed.

2.5 Conclusion

A literature review was conducted to introduce previous research conducted on various aspects of this work. Aspects of golf shaft deformation and design were first outlined. It was shown that the shaft plays a significant role in the golf swing. The flexural and torsional stiffness of the shaft will affect the orientation of the clubhead at impact. The stiffness of golf shafts can be obtained using static testing by determining the deflection and angle of twist. The stiffness and use of composite shafts has been investigated. Various types of materials and fibre angles have been used to evaluate their use in shaft design. It has been found that the flexural and torsional stiffness is dependent on the material and fibre angles.

Models to determine the cover factor and elastic constants of diamond unit cell braided composites were introduced. Cover factor models either use process parameters or unit cell approaches. CLPT is selected for this work based on its simplicity and accuracy in predicting elastic constants.

A preliminary investigation into using a foam core, for flexural or torsional reinforcement, of a golf shaft was introduced. The literature reviewed was confined to tubular structures for obvious reasons. Foam cores have been used with golf shafts to reduce vibration in the shaft following impact. They have been found to significantly reduce vibrations in both composite and steel shafts. Additionally, research with foam cores has mainly been applied to investigating the impact and crush behaviour of metallic or non-metallic tubular structures. However, no literature was found applying to evaluation of foam cores for an increase in stiffness of tubular structures.

Patents revealed the use of braiding in the design of golf shafts. Additionally, core materials have also been used in golf shafts. None of the listed patents use a composite shaft formed over a foam core.

In conclusion, using braided composites in the design of golf shafts is an area that requires further investigation. Development of a model that can determine both the cover factor and elastic constants of a braided lamina would provide a relatively new method of composite analysis. Investigating the influence of foam core materials on the mechanical properties of braided composites has not been thoroughly researched.

3 CHARACTERISTICS OF GOLF SHAFT DESIGN

Golf shafts are designed based on 3 major parameters: (1) mass, (2) flexural stiffness and (3) torsional stiffness.

Mass is determined by weighing a raw or un-cut shaft. An un-cut shaft is a shaft that has not yet been trimmed to manufacturer's specifications. Un-cut wood and driver shafts are typically 1168 mm (46 in). This allows for a direct comparison between different shaft models based on mass.

Flexural stiffness is expressed as flex by the golf industry. Flex may be established based on the deflection of a shaft with the butt end cantilevered and a load applied to the tip [15]. A stiffer shaft is characterized as having a smaller deflection. The problem is that there is no industry standard for the stiffness range corresponding to a particular flex [5]. Therefore, an R-flex shaft from one company may be an S-flex for another. Figure 3-1, illustrates an example of a flex (deflection) test apparatus.

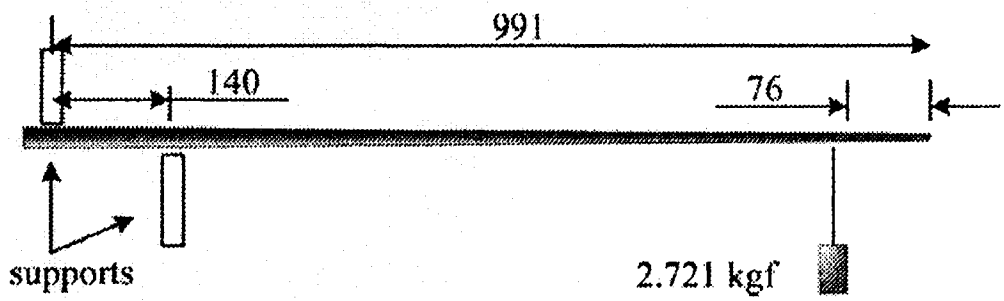

Figure 3-1: Deflection test apparatus [15]

In this example, the cut shaft length is 991 mm. The butt clamp length is 140 mm and a load of 2.721 kgf* is applied 76 mm from the tip. The problem is that

* Kilograms-force (kgf) is the mass that produces the corresponding force. To determine the force (in newtons, N), multiply kilograms-force by the gravitational constant.

manufacturers set up the deflection test apparatus using different butt clamp lengths, loads and distance from the tip. It is important to properly fit golfers with the right shaft flex for their swing speeds. If a shaft is too rigid, there will be negligible unloading of the shaft during the downswing and impact [5]. This may effectively decrease the dynamic loft of the club and result in a lower launch trajectory. Conversely if the shaft too flexible, the shaft will unload excessively and result in a higher launch path. This indicates that the clubhead will lead the shaft at impact.

The angle of twist (a measure of torsional stiffness) is measured by clamping the butt end of the shaft and applying a torque to the tip [15]. The resulting angle of twist (twist), measured in degrees, is associated with the torsional rigidity of the shaft. If shaft has a lower angle of twist, it is said to have a greater torsional rigidity. An example of a typical torsion-testing machine is illustrated in Figure 3-2. A torque of 1.35 N·m (0.138 kgf·m) is applied 51 mm from the tip, with a span length of 1041 mm.

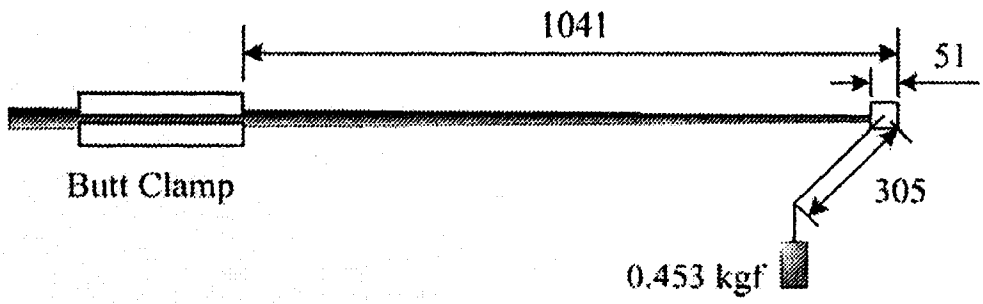

Figure 3-2: Typical torsion test apparatus [15]

As with deflection, if the shaft is not sufficiently rigid the clubface will face left of the target, for a right-handed golfer. This is referred to as a "closed" clubface position. This may result in a pull or hook to the left of the target. If a shaft is too torsionally rigid for a golfer, the clubface will be less "closed". If the player cannot rotate his/her wrists to

orient the clubface as it was at address, the result could be a clubface in the "open" position at impact. For a right-handed golfer, an "open" clubface will face to the right of the intended target resulting in a slice or push.

As with deflection testing, there is no standard methodology to measure torsion. The testing machine may be similar but the length of the butt clamp and the magnitude of the applied torque may differ between manufacturers.

The challenge is to adequately compare various golf shafts when there are no industry standards. Dynacraft [12] has compiled data on the mass, deflection-force and twist for numerous composite and steel golf shafts. The deflection testing methodology used by Dynacraft differs from what is typically employed. Instead of measuring the deflection of the shaft from a given load, the load required to deflect (deflection-force) the tip of the shaft 101.6 mm (4 in.) was determined. Each shaft was fit to a pre-determined swingweight.

Swingweighting (SW) is used to assist in properly fitting a club to a player. Swingweighting may be defined as the moment needed to balance a golf club on a fulcrum 14" (0.356 m) - or 12" (0.305 m) in some cases - from the butt end [5]. For example, if a golf club is placed on a table, with all but 14" of the club hanging over the edge, the resulting moment required to prevent the club from tipping is the swingweight. The swingweight may also be calculated by using the balance point (BP) of the club [5]. The balance point is the location on the golf club where the resulting moments are equal on either side of the fulcrum.

$$SW = M_s(BP - 0.356) \tag{3-1}$$

Where M_s is the mass of the club (in grams) and BP is the location of the balance point (measured in metres from the butt end). This will result in the moment (in m-grams) about an axis 0.356 m from the butt end [5]. The resulting moment is then related to the Lorythmic Scale, which was created by Robert Adams in the 1920's [63]. The Lorythmic Scale consists of an arbitrarily set letter-number system, which remains the most popular system used today [63]. Table 3-1 relates the resulting SW moment to the arbitrary letter-number swingweight scale for the C-0 to D-9 range. The Lorythmic Scale ranges from A-0 (very light) to G-9 (very heavy) [5]. Typically, men's clubs are measured in the low D's and women's in the low-mid C's [5].

Table 3-1: Example of club moment and corresponding swingweight point [5]

Swingweight	Moment (m-grams)	Swingweight	Moment (m-grams)
C-0	140.97	D-0	153.67
C-1	142.24	D-1	154.94
C-2	143.51	D-2	156.21
C-3	144.78	D-3	157.48
C-4	146.05	D-4	158.75
C-5	147.32	D-5	160.02
C-6	148.59	D-6	161.29
C-7	149.86	D-7	162.56
C-8	151.13	D-8	163.83
C-9	152.4	D-9	165.1

Another method used to fit clubs to a player is called frequency matching. Since frequency is a measure of flex, frequency matching essentially matches the flex feel for a club set [5]. There are two types of frequency matching: (1) constant frequency and (2) sloped frequency [5]. Constant frequency matching involves fitting clubs to a player based on a single frequency [5]. Sloped frequency matching uses a plotted curve that

designates a greater frequency to clubs as the length decreases [5]. Therefore, if a set is matched using sloped frequency, a 9-iron will be specified with a greater frequency than the 5-iron.

The results of the proposed golf shaft design will be compared to the Dynacraft results for multiple composite and steel shafts. Composite and steel shafts with S (stiff) and X (extra stiff) flexes were used in the comparison. It is desirable that the proposed braided shafts have comparable mass, deflection-force and twist to S and X flex shafts, because the mechanical properties of composite structures are variable and the laminate properties could be altered to produce a shaft with a lower flex. A significant factor in golf shaft design is material selection, which is discussed in the next chapter.

4 SELECTION OF SUITABLE MATERIALS

To produce a composite golf club shaft, proper fibre and matrix materials must be selected. There is typically a compromise between stiffness and weight. For a given shaft model, typically, an increase in stiffness will result in an increase in shaft mass.

Table 4-1: Typical relationship between mass and flex for composite golf shafts [12]

Manufacturer	Model	Shaft Material	Flex	Mass (g)
Aldila	NV 65	Composite	R	66
			S	67.8
			X	69.3
True Temper	Dynalite Gold	Steel	R	121.7
			S	123.8

This is evident by viewing specifications of a golf shaft manufacturer in Table 4-1. The mass increases with stiffness for both the composite Aldila and steel True Temper shaft models. For an individual golfer, an optimal design would comprise of a shaft with a combination of suitable flex and low mass. The lower mass would allow for a greater generation of club head speed [17], while the proper flex would allow for proper orientation of the clubhead at impact [9]. Ideal materials would both have low densities and high longitudinal and shear moduli. This would allow for a shaft to attain the required flex with a lower volume of material. Lower density materials would assist in minimizing mass with a lower material volume. Detailed below is the selection of fibre and matrix materials for golf shaft design and the corresponding equations used to calculate unidirectional lamina properties for the proposed braid model. When discussing design parameters of golf shafts, stiffness is used to describe resistance to bending or twisting. Stiffness is a structural property taken along the entire shaft length. When

predicting elastic constants local properties are calculated. Rigidity is a local property that is based on the geometry of the structure. Flexural rigidity is the product of the moment of inertia, I, and elastic modulus, E_x. Axial rigidity is determined from the elastic modulus, E and cross-sectional area, A, while torsional rigidity is the product of the in-plane shear modulus, G_{xy}, and polar moment of inertia, J. The elastic constants, E_x and G_{xy}, of a braided composite are dependant on the properties of both the fibres and matrix materials.

4.1 Fibre Material Selection

Typically, carbon-based fibres are used in producing golf shafts due to the relatively high longitudinal modulus compared to other fibres types such as Kevlar and E-glass [64]. Characteristic values of Kevlar, E-glass and carbon fibre are in Table 4-2.

Table 4-2: Elastic constants of various fibre materials [64]

Material	Longitudinal Modulus E_f (GPa)	Shear Modulus G_f (GPa)	Density ρ_f (kg/m^3)	Specific Modulus $E_{o,f}$ ($GPa/(kg/m^3)$)
Carbon Fibre	230	22	1800	0.128
Kevlar	124	3	1400	0.089
E-Glass	85	35.4	2500	0.034

Carbon fibres have a greater specific modulus than the Kevlar and E-glass by factors of 1.4 and 3.8, respectively. Carbon fibre also has the second highest shear modulus and density. It is necessary to consider both mass and stiffness/rigidity in the golf shaft design. Therefore for a given cross-section, the carbon fibres will produce the greatest rigidity to mass ratio. This combination makes carbon fibres the best choice for fibre materials and will be used exclusively in the following sections.

Golf shafts are made using a combination of various carbon fibre types. Carbon fibres may be classified according to a dominant mechanical property. Some fibres considered emphasize high modulus (HM) or high strength (HS). High strength fibres are characterized by a greater tensile strength. High modulus fibres exhibit a higher tensile modulus but lower tensile strength. Additionally, the high modulus fibre may be classified, in relative terms, as: standard (SM), intermediate (IM) or high modulus (HM). The SM fibre has average modulus values, while the HM has a higher longitudinal modulus but an equal shear modulus and similar density to SM. The HS has a greater tensile strength and longitudinal modulus but similar shear modulus and density to SM and HM.

In the research done by Matsumodo [13] and Takemura [19], HS and HM carbon fibres were used in golf shaft construction. They did not point out a specific lamina stacking sequence to indicate where HS and HM fibres would provide the greatest reinforcement. Table 4-3 summarizes the mechanical properties of high modulus and high strength fibres, which may be considered in the shaft design. From Table 4-3, the density of the fibres is fairly constant and only varies by 2.25 % over the range. The M40J, a high modulus fibre, has the highest longitudinal modulus but the lowest tensile strength, while the T800H, a high strength fibre, has the 2nd highest longitudinal modulus and the highest tensile strength. To complete the material selection, a suitable resin must be chosen.

Table 4-3: Properties of high strength and high modulus carbon fibres [19, 31]

Material	Longitudinal Modulus, E_f (GPa)	Tensile Strength, S_f (GPa)	Density, ρ_f (kg/m^3)
AS4 (SM)	228	3.53	1800
T700S (SM)	230	4.90	1800
T800H (HS)	294	5.49	1810
M40J (HM)	377	4.41	1770

4.2 Matrix Material Selection

The desired matrix material should exhibit high longitudinal modulus and low density, which would contribute to a rigid and light shaft. Some typical values of matrix materials are summarized in Table 4-4.

Metal and ceramic matrix materials exhibit a greater specific modulus than the thermosets or thermoplastics. However, the density of the aluminium and alumina is too high for this application because minimizing mass is a design consideration. Ceramic matrix materials are susceptible to flaws, which result in a severe decrease in strength [65]. The two main groups of polymer matrix materials are thermosets and thermoplastics. Thermosets are cured and cannot be re-melted or reformed [65]. This is due to the formation of 3D molecular chains called cross-linking [66]. As the number of cross-links increases, the more rigid the thermoset becomes [66]. Since liquid resin is used at room temperature, thermosets are easier to use in manufacturing and provide better fibre impregnation than thermoplastics [66]. Thermoplastics have been shown to be more difficult to use in manufacturing of golf shafts due to the high viscosity the thermoplastic attains when heated, which makes it difficult to use in resin transfer moulding (RTM) and other resin infusion processes [67]. Additionally, thermoplastics create a weak bond with the fibres and can exhibit high strain at low stresses [68]. For

this reason, epoxy, the most common thermoset, was used in the design of the golf shaft. From Table 4-4, epoxy resin exhibits the highest tensile modulus and specific modulus of the polymer matrix materials. Additionally, the density of epoxy was among the lowest of the polymers. Epoxy has the second lowest shrinkage of the resin materials listed in Table 4-4 (once resin shrinkage values are averaged over their given range), which reduces the probability of large shear stresses forming at the resin and fibre interface [64]. The low viscosity and flow rate of epoxy allows for good fibre impregnation and prevention of strand misalignment during processing [64]. Proper strand alignment is vital to the performance of the golf shaft since the elastic properties can be critically diminished if strands are not properly aligned. Given all of the factors, epoxy should be the matrix material used in the golf shaft design.

Table 4-4: Properties of various matrix materials [65, unless otherwise specified]

Resin Material	Material Class	Density, ρ_m (g/cm^3)	Tensile Modulus, E_m (GPa)	Tensile Strength, S_m (MPa)	Specific Modulus, E_{0m} ($GPa \cdot cm^3/g$)	Shrinkage [69] (mm/mm)
Epoxy	Thermoset	1.2 - 1.4	2.5 - 5.0	50 - 110	1.78 - 3.57	0.5
Phenolic	Thermoset	1.2 - 1.4	2.7 - 4.1	35 - 60	2.25 - 2.93	0.4 – 1.1
Polyester	Thermoset	1.1 - 1.4	1.6 - 4.1	35 - 95	1.45 - 2.93	0.25
Nylon	Thermoplastic	1.1	1.3 - 1.35	55 - 90	1.18 - 1.23	0.3 – 1.9
PEEK	Thermoplastic	1.3 - 1.35	3.5 - 4.4	100	2.69 - 3.26	0.3 – 1.4
Polyethylene	Thermoplastic	0.9 - 1.0	0.7 - 1.4	20 - 35	0.78 - 1.40	0.6
Aluminum	Metal	2.7	69	300	25.5	NA
Alumina	Ceramic	3.9	380	NA	97.44	NA

4.3 Core Material Selection

The core material to be used as a stiffener of the golf shaft needs to enhance the bending and torsional rigidity while adding little mass. The evaluation of various core materials is based on a combination of density and elastic constants.

Ashby charts, seen in Figure 4-1, are useful tools to assess the type of core material that would be suitable for this application [70].

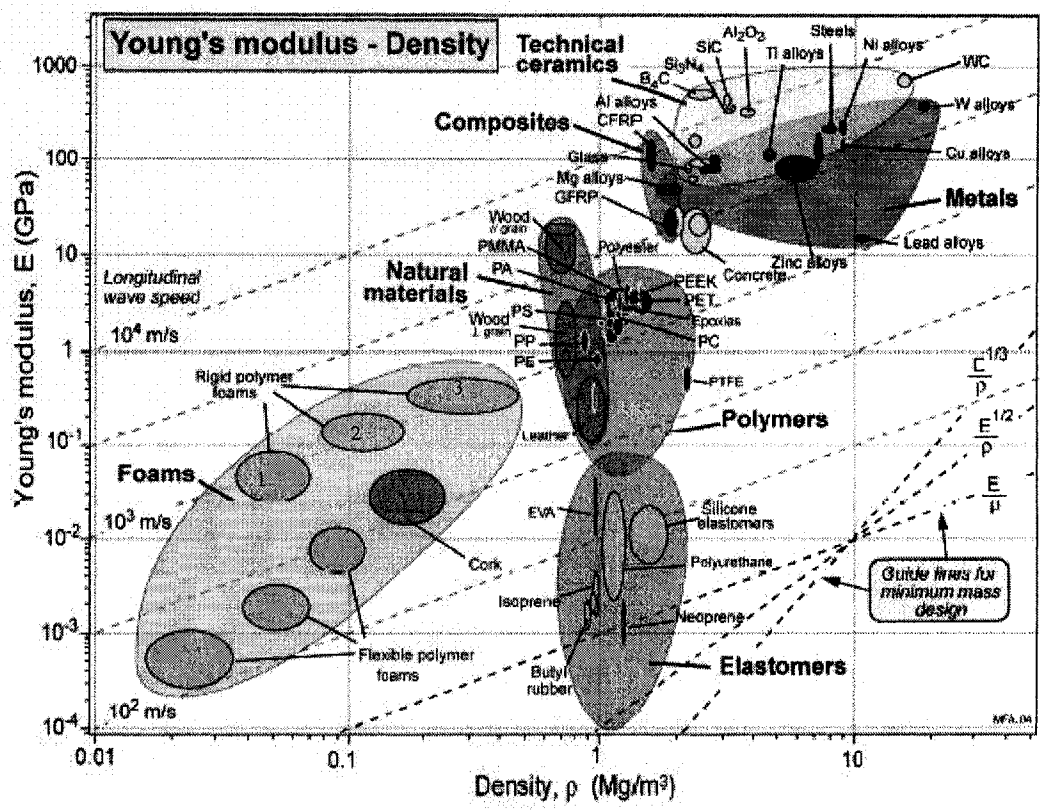

Figure 4-1: Ashby chart illustrating Young's modulus versus density for a variety of materials [adapted from 70]

Composite golf shafts may be categorized as carbon fibre reinforced plastics (CFRP). A model core material should have a lower density than the constituent materials of the golf shaft, specifically the fibre and resin. As seen in Figure 4-1, this eliminates the

metals, composites and technical ceramics and leaves natural materials, polymers, elastomers and foams. However, the core material should also have a high Young's modulus. Therefore, the ratio of Young's modulus to density, also known as specific modulus, would be ideal criteria to consider in choosing a suitable core material. However, a high specific modulus can be misleading since the material could still have a high density (relative to composites) and an exceptionally high modulus. Since the core material should not add significant mass, the material density is also an important parameter. The selection of an ideal type of core material was based on a combination of specific modulus and density. The specific modulus of polymers ranges from 0.45-6.4 MPa/(kg/m^3), while elastomers and foams range from 0.005-0.072 MPa/(kg/m^3) and 0.00045-2.85 MPa/(kg/m^3), respectively. Even though the polymers have greater specific modulus than foams, the foams have a lower density. The ideal foam core materials would be in the rigid polymer foam groups denoted in Figure 4-1 as 1, 2 or 3. These types of foam have a greater specific modulus, than the flexible polymer foams, while the density is relatively low compared to CFRP. Foam materials are characterized as having either a closed-cell structure or an open-cell structure [71]. Closed-cell structures consist of cells that do not interconnect, while almost all of the cells interconnect in open-cell foams [71]. Table 4-5 details rigid and semi-rigid, closed-cell foam materials that may be suitable for the application of this work.

Table 4-5: Rigid and semi-rigid, closed-cell foam core materials [69]

Material	Density ρ_{fc} (kg/m^3)	Longitudinal Modulus E (GPa)	Shear Modulus G (GPa)	Specific Modulus E/ρ_{fc} ($MPa/(kg/m^3)$)
Sawbones Rigid Polyurethane	800	2.000	0.262	2.500
Cymat Aluminum Foam	300	1.000	1.000	3.333
Degussa Rohacell 110 IG PMI	110	0.160	0.050	1.455
DIAB Klegecell R 260 PVC	205	0.290	0.115	1.415
DIAB Divinylcell HT 110 IPN	111	0.175	0.040	1.577
DIAB Divinylcell H 250 Semi-rigid PVC	256	0.300	0.108	1.172

Even though polymers can have a specific modulus of 6.4 $MPa/(kg/m^3)$, it is at the upper density range of 1250 kg/m^3. This density is close to the typical CFRP density of 1500 kg/m^3. Therefore, using this material would add significant mass to the shaft. The two materials that may provide the greatest reinforcement, without greatly increasing mass, are the Sawbones and Cymat. The Sawbones has one of the highest specific modulus but also has a higher density, of 800 kg/m^3, which is 2.67 times greater than the Cymat (second highest). The Cymat has the highest specific modulus, second highest longitudinal modulus and highest shear modulus. The remaining materials are close in terms of specific modulus, which is due to the low density and relatively low longitudinal modulus.

Each of these materials was evaluated, with the design shaft, for improving flexural and torsional rigidity but minimizing an increase in shaft mass.

4.4 Unidirectional Lamina Elastic Constants

The elastic constants of a unidirectional lamina can either be considered in- or out-of-plane. The out-of-plane, or through-thickness, direction can be considered to be along the 3-axis, while the in-plane directions are in the 1- and 2-directions, as shown in Figure 4-2. Equations used to determine the in-plane elastic constants of a unidirectional lamina are provided below in Equations 4-1 to 4-11 and are available in [72].

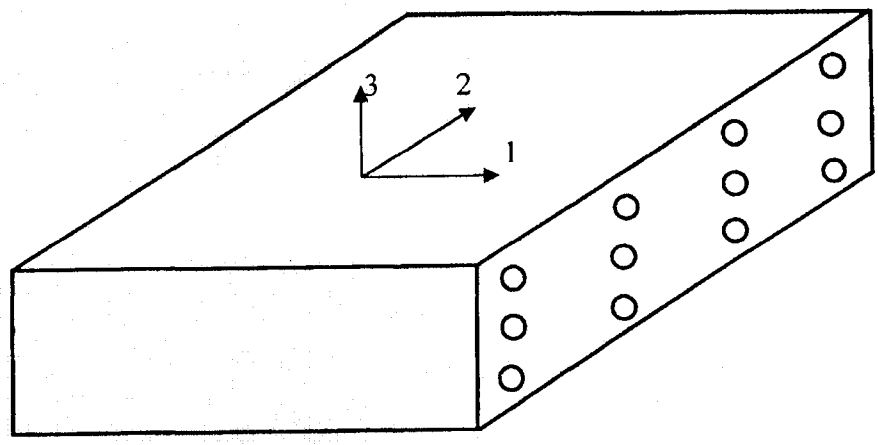

Figure 4-2: General axis orientation with unidirectional (UD) fibres [64]

The longitudinal modulus, E_{11}, and major Poisson's ratio, υ_{12}, are derived using the rule of mixtures predictions (ROM) concept, thus are dependent on the volume fractions of both the fibre and matrix materials [72] such that:

$$E_{11} = V_f E_f + V_m E_m \tag{4-1}$$

where V_f is the fibre volume fraction, E_f is the fibre longitudinal modulus, E_m is the matrix modulus and V_m is the matrix volume fraction, and:

$$v_{12} = v_f V_f + v_m V_m \tag{4-2}$$

where v_f is the fibre Poisson's ratio, v_m is the matrix Poisson's ratio.

The transverse modulus, E_{22}, and in-plane shear modulus, G_{12}, are determined using equations developed by Halpin-Tsai [72].

$$\frac{E_{22}}{E_m} = \frac{1+\xi\eta_{22}V_f}{1-\eta_{22}V_f} \tag{4-3}$$

where

$$\eta_{22} = \frac{(E_f/E_m)-1}{(E_f/E_m)+\xi} \tag{4-4}$$

and where ξ is the reinforcing factor and is dependent on the fibre and packing geometry and loading conditions. Fibres are assumed to be circular fibres and in a square packing geometry. For this assumption, ξ =2 for the transverse and in-plane shear moduli. The latter is solved as:

$$\frac{G_{12}}{G_m} = \frac{1+\xi\eta_{12}V_f}{1-\eta_{12}V_f} \tag{4-5}$$

where

$$\eta_{12} = \frac{(G_f/G_m)-1}{(G_f/G_m)+\xi} \tag{4-6}$$

and where G_f is the fibre shear modulus and G_m is the matrix shear modulus.

The minor Poisson's ratio, v_{21}, is found as:

$$v_{21} = \frac{v_{12}E_{22}}{E_{11}} \tag{4-7}$$

In addition to the in-plane elastic constants, out-of-plane elastic constants are also required to determine braided composite elastic constants. The equation for the out-of-

plane shear modulus, G_{23}, was found by Barbero using the stress-partitioning parameter technique [73] as:

$$\frac{G_{23}}{G_m} = \frac{V_f + \eta_{23}(1 - V_f)}{\eta_{23}(1 - V_f) + V_f G_m / G_f} \tag{4-8}$$

where

$$\eta_{23} = \frac{3 - 4\nu_m + G_m / G_f}{4(1 - V_f)} \tag{4-9}$$

Ko [3] defined the out-of-plane Poisson's ratio, $v_{f,23}$, as:

$$\nu_{23} = V_f \nu_{f,23} + V_m (2\nu_m - \nu_{21}) \tag{4-10}$$

Assume transverse isotropy, the elastic constants, E_{33}, G_{13} and v_{13} in the orthogonal direction are defined:

$$\begin{aligned} E_{33} &= E_{22} \\ G_{13} &= G_{12} \\ \nu_{13} &= \nu_{12} \end{aligned} \tag{4-11}$$

These equations were used in the braid model introduced in the next chapter to determine the elastic constants of a braided lamina.

5 PROPOSED BRAID MODEL

5.1 Introduction

A model to predict both the cover factor and elastic constants of a braided lamina was developed based on previous work [29,37]. Separate models for the cover factor and elastic constants were utilized. A condition of the design is to maintain a cover factor greater than 95%, the reason for which is discussed in the following chapter. The elastic constants are predicted using CLPT. Each model is evaluated separately and then combined into a complete braid model. This complete model is also evaluated.

5.2 Assumptions for Proposed Braid Model

The assumptions used in the proposed braid model are listed below:

- The wall thickness is assumed to be thin, i.e. the ratio of the inner diameter to the wall thickness is greater than 10.
- Strands do not twist during the braiding process.
- Each strand is assumed to have a constant dry rectangular cross-section, consisting of the strand width, w_y, and strand thickness, h_c [37].
- Strands are assumed to be parallel inside of the rectangular unit cell [37].
- The strand undulation angle, β, is measured with respect to the horizontal and undulates as a sinusoidal function. The strand cross-section remains perpendicular to the fibres [37].
- Basic assumptions of CLPT, which are contained in various composite textbooks, such as Kaw's "Mechanics of Composite Materials" [64].

5.3 Cover Factor Predictive Model

5.3.1 Model Development

The model developed by Mazzawi [29] was used as a basis to determine the cover factor on a conical mandrel. The model is based on the geometry of the strand on the conical mandrel, which is generated from such process conditions such as the carrier and mandrel velocities. The goals of using the model are to attain a minimum cover factor of 95%, since there is a rapid decrease in mechanical properties with a decrease in cover factor beyond this point [74] and to provide a model useful for future manufacturing purposes. A cover factor in between 95% - 100% is a reason range and would result in a relatively small loss in mechanical properties. An example of a braided composite with such a high cover factor is a closed mesh braid.

The Mazzawi model is based on a trapezoidal unit cell [29]. The model uses a number of assumptions from a braiding model developed by Du and Popper [22] namely, (1) the mandrel is a surface of revolution and is symmetric, therefore, only one braiding strand is needed to represent all others; (2) the strand is straight in the convergence zone and interlacing effects between strands are neglected; (3) the strand does not slip relative to the mandrel; and (4) the cover factor or elastic properties will not vary for a unit cell at a given position along the mandrel. Assumptions (2) and (3) are support by previous research [20]. It was found that for a braided composite manufactured using less than 64 carriers that the strand remains straight in the convergence zone. Additionally, the friction forces are small and therefore, the strands should not slip relative to the mandrel [20]. Hence, a single unit cell can accurately represent the cover factor and elastic properties

anywhere on the perimeter of the composite at that position along the mandrel. This holds true along the entire mandrel length.

The trapezoidal unit cell utilizes the area covered by the strands in the unit cell to determine the cover factor. The unit cell is determined through the geometry of the conical mandrel surface and is based on the braid formation through one revolution of the mandrel [29]. As the braid progresses along the mandrel length, in the direction of increasing diameter, it forms a helical path due to the rotation of the mandrel. The helical path of a strand on a conical mandrel results in a curved fibre path that varies in curvature and slope from point to point on the mandrel [22]. The resulting helical path establishes the pitch of the strand through one revolution. The relationship between the angular and axial velocities is determined using the pitch. Pitch is the axial distance a strand travels after it has rotated through one full revolution.

The cover factor depends on determining: fibre length (L), braid angle (θ), cut-off and overlap area (A_{oc}) and the unit cell area (A_{uc}). The trapezoidal unit cell configuration and dimensions are shown in Figure 5-1.

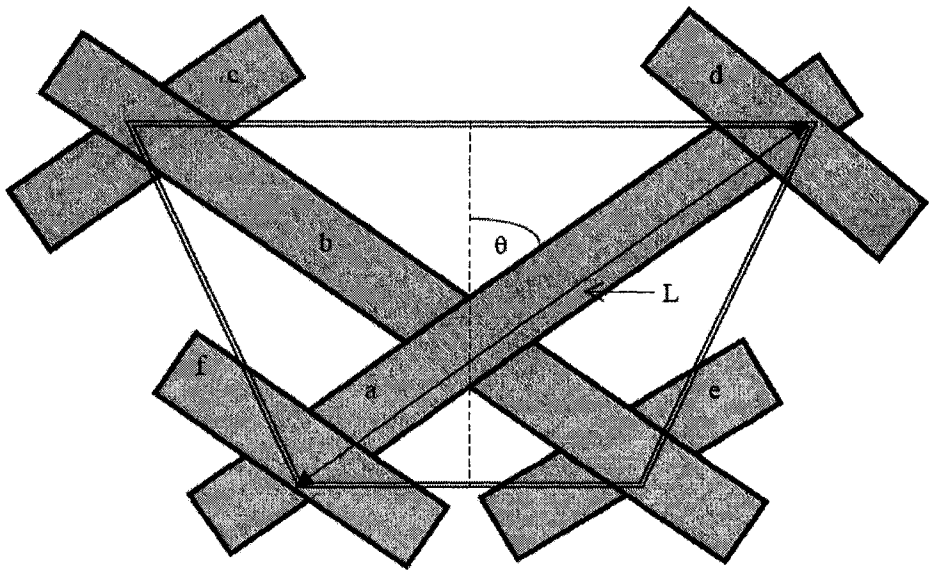

Figure 5-1: Trapezoidal unit cell with strand designations [modified from 29]; double solid line denotes the trapezoidal unit cell boundary

The fibre orientation and jam angle must be calculated to determine if the fibre angle is greater than the jam angle. If the fibre angle is greater than the jam angle then the braided formation will be jammed. The jam angle is based on a cover factor equal to 100%. The fibre length (L) is based on the main fibre(s) that run diagonally across the unit cell and is determined as:

$$L = \sqrt{\left[\frac{2\pi}{N_c}(r_2 + r_1)^2\right]^2 + (r_2 - r_1)^2 + (z_2 - z_1)^2} \qquad \textbf{(5-1)}$$

where z_1 and z_2 represent lower and upper boundaries of the unit cell, r_1 and r_2 the radius of mandrel at the lower and upper unit cell boundaries and N_c is the number of braider carriers. The lower and upper boundaries (z_1, z_2) are measured as the distance travelled along the mandrel length.

The braid angle of the strand on the mandrel depends on the pitch created by both the axial velocity of the mandrel and the angular velocity of the carriers. If the rotational and axial velocities are held constant, the pitch also remains constant and the braid angle decreases due to an increase in mandrel radius. The braid angle depends on the pitch resulting from the ratio of axial to angular velocity and the radius at the unit cell boundaries (r_2, r_1). The equation for the braid angle, θ, is given as:

$$\tan(\theta) = \frac{2\pi(r_2 + r_1)}{N_c\sqrt{(z_2 - z_1)^2 + (r_2 - r_1)^2}} \tag{5-2}$$

The area covered by fibres in the unit cell depends on six different strands, designated as a, b, c, d, e and f, as illustrated in Figure 5-1. However, ll strands, a, b, c, d, e, and f contribute to the cover factor, with the majority accounted for by strands a and b [29]. Equation 5-3 calculates the cut-off and overlap area, A_{oc}, of the fibres in the unit cell. Overlap is simply the overlapping of strands a and b and the cut-off area eliminates the area of strands a and b outside of the unit cell.

$$A_{oc} = w_y^2\left[\frac{\tan(\theta)(\tan^2(\theta)+1)}{\tan^2(\theta)-\tan^2(\zeta)}\right] \tag{5-3}$$

where w_y is the stand width and the curvature angle, ζ, is given as:

$$\sin(\zeta) = \frac{w_y \sin(\gamma)}{4r\cos(\theta)} \tag{5-4}$$

where γ is the half-cone angle, which is the angle of the mandrel with respect to its longitudinal axis and r is the radius at the midpoint along the unit cell. The cell area, A_{uc}, is based on the geometry of the conical segment and is:

$$A_{uc} = \frac{2\pi}{N_c}(r_2 + r_1)\sqrt{(z_2 - z_1)^2 + (r_2 - r_1)^2} \quad \textbf{(5-5)}$$

Lastly, the cover factor (CF) is determined using these parameters and is found as:

$$CF = \frac{2Lw_y - A_{oc}}{A_{uc}} \quad \textbf{(5-6)}$$

For a cylindrical mandrel, where the half-cone angle is zero, the (r_2-r_1) terms cancel because the radius remains constant.

A model was developed to determine the cover factor of a 2D braid on a conical mandrel. This model was used since a golf shaft contains a tapered section along its length. A trapezoidal unit cell provides a better match to the geometrical shape of a conical composite compared to a rectangular unit cell [29].

5.3.2 Cover Factor Model Validation

The cover factor model was validated by comparing results with those of Du and Popper [22]. A conical composite with a cone angle (2γ) of 16.5 °, an initial radius of 15.85 mm, travelling 76.32 mm axially per revolution using 36 carriers was used as the comparative example. The resulting difference in cover factor between the current model and Du and Popper was found to be a maximum of 0.111%. A summary of the results for the difference in cover factor between the two models along the axial travel is detailed in Table 5-1.

Table 5-1: Comparison of the current model to previous model for cover factor

Carrier Position (degrees)	Distance Traveled (mm)	Radius (mm)	Cover Factor		Difference (%)
			Current Model	Du & Popper	
20	4.24	15.85	0.9938	0.9948	0.101
40	8.48	16.47	0.9917	0.9928	0.108
60	12.72	17.08	0.9896	0.9907	0.107
80	16.96	17.70	0.9874	0.9885	0.111
100	21.20	18.31	0.9853	0.9863	0.105
120	25.44	18.93	0.9832	0.9842	0.102
140	29.68	19.54	0.9811	0.9821	0.103
160	33.92	20.16	0.9792	0.9801	0.089
180	38.16	20.77	0.9772	0.9781	0.093
200	42.40	21.39	0.9754	0.9762	0.083
220	46.64	22.00	0.9736	0.9744	0.081
240	50.88	22.62	0.9719	0.9726	0.077
260	55.12	23.23	0.9703	0.971	0.070
280	59.36	23.85	0.9687	0.9694	0.071
300	63.60	24.46	0.9672	0.9679	0.069
320	67.84	25.08	0.9659	0.9664	0.053
340	72.08	25.69	0.9645	0.965	0.055
360	76.32	26.31	0.9632	0.9637	0.053

A general decrease in the cover factor occurs as the mandrel progresses along its axial travel. This indicates that the mandrel is either travelling too fast or the carriers are not rotating quickly enough to account for the increase in radius. Either the mandrel or carrier velocity would have to change to maintain a constant cover factor.

5.4 Braid Elastic Constants Model

5.4.1 Model Development

The model used to determine the elastic constants for a braided conical composite, with a minimum cover factor of 95%, is based on previous work [37]. The model is based on the Classic Laminate Plate Theory, utilizes a unit cell approach and models the

undulation region using a sinusoidal function. Unlike determining cover factor, the calculation of elastic constants is dependent on each of the six strands (each diagonal and one in each corner) shown in Figure 5-1. However, the unit cell has now been divided into 13 separate regions (R_1-R_{13}) and the unit cell is assumed to be rectangular.

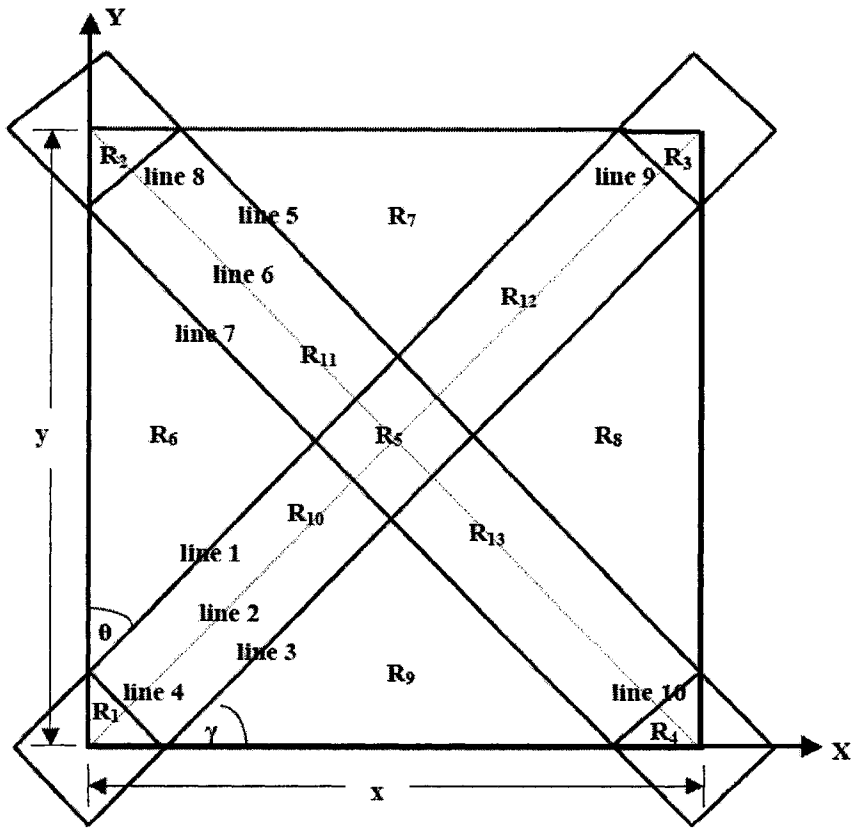

Figure 5-2: Rectangular unit cell with the 13 regions [adapted from 37]

A trapezoidal unit cell was used to determine the cover factor; however, this unit cell is complex for determining the elastic constants due to the variation in unit cell width. Therefore, to justify the use of a rectangular instead of a trapezoidal unit cell, the difference in unit cell area will be determined since it is assumed that unit cell thickness is constant. It is assumed that a difference in area less than 5% is acceptable. The half-cone angle, γ, for a golf club shaft is very small at approximately 0.30°; therefore, the

difference between the trapezoidal and rectangular unit cells is assumed to be negligible in this case. A rectangular unit cell would allow for assumptions, used by [37], to be applied. Figure 5-3 illustrates the trapezoid-to-rectangular assumption, where a small half-cone angle will minimize the distance K and the area difference between both geometries.

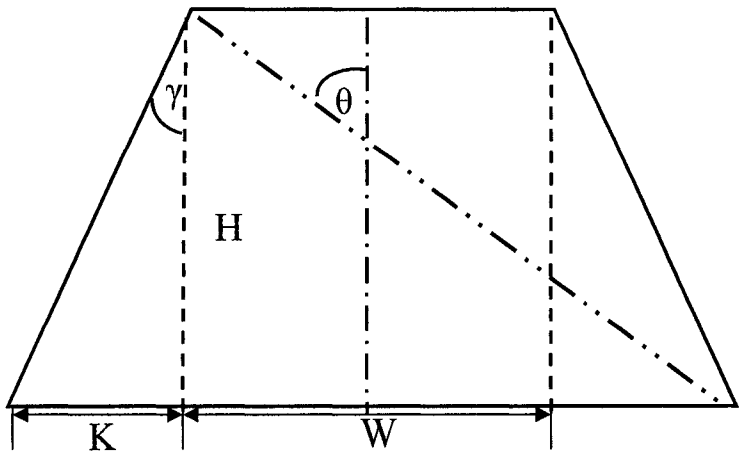

Figure 5-3: Trapezoidal unit cell with rectangular unit cell fit; dashed line indicates rectangular unit cell, solid line indicates trapezoidal unit cell, long-short dash is the longitudinal axis, short-short-long dash is the fibre strand

From Figure 5-3, the parameters that would influence a variation in area between the trapezoidal and rectangular unit cells are the half-cone angle, γ, the height of the unit cell, H, and the resulting value of K. The relationship between half-cone angle and the corresponding variance in unit cell area are listed in Table 5-2. The half-cone angle corresponds to the upper bound of the ratio of H:W that would yield a 5% area difference between the rectangular and trapezoidal unit cells. The rectangular width, W, is held constant while the unit cell height, H, is varied. For example, for a H:W ratio of 0.05:1, a half-cone angle of 46.47° would result in an area difference of 5%. The method in [37] can be applied to this work if this condition is satisfied. This will be verified as part of the validation for the overall predictive model.

Table 5-2: Influence of half-cone angle on the variance between trapezoidal and rectangular unit cell area

W	H	Half-Cone Angle (deg.)	Rectangular Area	Trapezoidal Area	Difference (%)
1.00	0.05	46.47	0.0500	0.0526	5.0
1.00	0.10	27.76	0.1000	0.1053	5.0
1.00	0.25	11.89	0.2500	0.2632	5.0
1.00	0.50	6.01	0.5000	0.5263	5.0
1.00	1.00	3.01	1.0000	1.0526	5.0
1.00	5.00	0.60	5.0000	5.2632	5.0
1.00	10.00	0.30	10.0000	10.5263	5.0
1.00	15.00	0.20	15.0000	15.7895	5.0
1.00	20.00	0.15	20.0000	21.0526	5.0

Figure 5-2 illustrates the unit cell that contains 13 regions as follows: regions R_1-R_5 contain overlapping fibre strands and matrix, regions R_6-R_9 are pure matrix and regions R_{10}-R_{13} contain undulating fibre strands and matrix. In Figure 5-2, X and Y denote the unit cell coordinate system, θ is the braid angle and γ is the complimentary braid angle. It is assumed that lines 4, 5, 6, 7 and 9 are parallel, as are lines 1, 2, 3, 8 and 10. Additionally, the boundaries of R_5 are all of the same length, L_e, and can be solved as [37]:

$$L_e = \frac{w_y}{\cos(2\theta - \pi/2)} \tag{5-7}$$

The line boundaries of the thirteen regions, as seen in Figure 5-2, which will be of use for equations used for integration of the volumetric averaged stiffness matrices, are defined by [37] as:

$$
\begin{aligned}
line_1 &: y = x\tan(\gamma) + L_e\cos(\theta) \\
line_2 &: y = x\tan(\gamma) \\
line_3 &: y = x\tan(\gamma) - L_e\cos(\theta) \\
line_4 &: y = -x\tan(\gamma) + L_e\cos(\theta) \\
line_5 &: y = -x\tan(\gamma) + Y + L_e\cos(\theta) \\
line_6 &: y = -x\tan(\gamma) + Y \\
line_7 &: y = -x\tan(\gamma) + Y - L_e\cos(\theta) \\
line_8 &: y = x\tan(\gamma) + Y - L_e\cos(\theta) \\
line_9 &: y = -x\tan(\gamma) + 2Y - L_e\cos(\theta) \\
line_{10} &: y = x\tan(\gamma) - Y + L_e\cos(\theta)
\end{aligned}
\tag{5-8}
$$

The modified CLPT model considers fibre undulation in regions R_{10}-R_{13}. The undulation path, h(d), of the fibres is modeled as a cosine function. This undulation path is uniformly followed throughout the entire strand thickness, h_c, and over the entire undulation length, a_u. At any distance, d, along the undulation length the undulation angle, β, changes. This is illustrated in Figure 5-4.

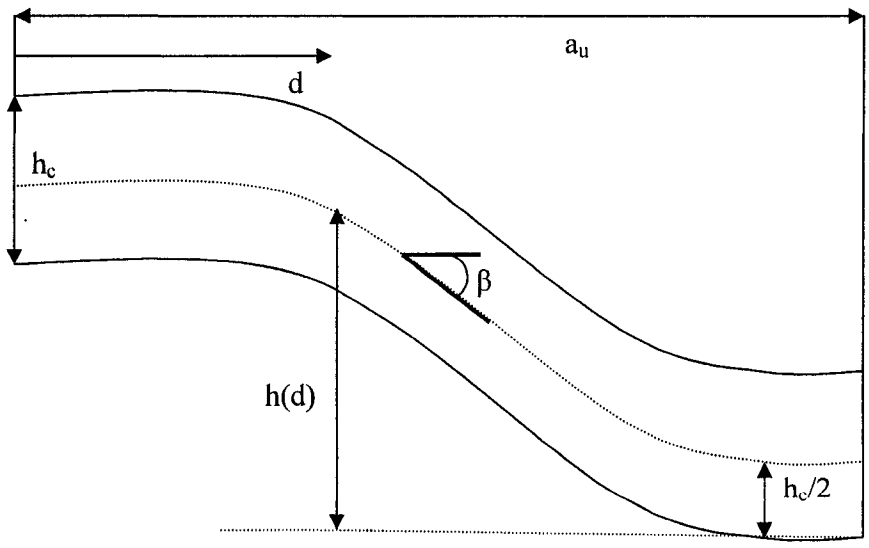

Figure 5-4: Undulation parameters of the rectangular unit cell [modified from 37]

The governing equations of the modified CLPT model are partially repeated here, for completeness the reader is directed to the literature. The undulating strand path, of Figure 5-4, is assumed to follow a cosine function such as:

$$h(d) = (1 + \cos\{\pi(d / a_u))h_c / 2 \quad \textbf{(5-9)}$$

while the undulation strand angle, β, taken with respect to the horizontal is measured as:

$$\tan(\beta) = \frac{dh(d_{(x,y)})}{dd_{(x,y)}} \quad \textbf{(5-10)}.$$

Regional differences in stiffness must be addressed individually. Regional stiffness matrices must be transformed to the global coordinate system. For regions R_1-R_5 (overlapping regions) stiffness matrices were transformed to account for the braid angle, θ. The laminate properties are expressed as the transformed stiffness matrix, $[\overline{Q}]$:

$$[\overline{Q}] = [T_\theta][Q][T_\theta]^{-T} \quad \textbf{(5-11)}$$

Since the pure matrix regions (R_6-R_9) are homogeneous and isotropic, transformation of the matrix stiffness matrix is not required. For the undulating regions (R_{10}-R_{13}) the stiffness matrix must be transformed through braid and undulation angles to global coordinates and was developed by Naik and Ganesh [35] as:

$$[\overline{Q}_u] = [T_\vartheta]^{-1}[Q_{(\beta)}][T_\vartheta]^{-T} \quad \textbf{(5-12)}$$

where:

$$[Q_{(\beta)}] = \begin{bmatrix} \frac{E_x(\beta)}{D_\upsilon} & \frac{\upsilon_{21}(\beta)E_y(\beta)}{D_\upsilon} & 0 \\ \frac{\upsilon_{21}(\beta)E_y(\beta)}{D_\upsilon} & \frac{E_y(\beta)}{D_\upsilon} & 0 \\ 0 & 0 & G_{12}(\beta) \end{bmatrix} \quad \textbf{(5-13)}$$

and

$$E_x(\beta) = \frac{1}{(\cos^4\beta)/E_{11} + (1/G_{13} - 2\upsilon_{31}/E_{11})\cos^2\beta\sin^2\beta + (\sin^4\beta)/E_{33}}, \quad \textbf{(5-14)}$$

$$\upsilon_{21}(\beta) = E_x(\beta)\left[\upsilon_{31}\frac{\cos^2\beta}{E_{11}} + \upsilon_{23}\frac{\sin^{2\beta}}{E_{33}}\right], \quad \textbf{(5-15)}$$

$$G_{12}(\beta) = \left[\frac{\cos^2\beta}{G_{12}} + \frac{\sin^2\beta}{G_{23}}\right]^{-1}, \quad \textbf{(5-16)}$$

$$E_y(\beta) = E_{22} = E_{33} \quad \textbf{(5-17)}$$

and,

$$D_\upsilon = 1 - (\upsilon_{21}(\beta))^2\frac{E_{22}}{E_x(\beta)} \quad \textbf{(5-18).}$$

Finally, the stiffness relationship from the CLPT for a braided unit cell can be expressed as [75]:

$$\begin{Bmatrix} N \\ M \end{Bmatrix} = \begin{bmatrix} [A^*] & [B^*] \\ [B^*] & [D^*] \end{bmatrix} \begin{Bmatrix} \varepsilon^0 \\ \kappa^0 \end{Bmatrix} \quad \textbf{(5-19)}$$

where ε^0, κ^0 represent the mid-plane strain and curvature and N and M are the stress and moment resultants.

Volume-weighted stiffness matrices [A*], [B*] and [D*] were determined and are representative for the entire unit cell. They are determined through the summation of regional stiffness matrices [A], [B] and [D] calculated for each of the 13 regions. Stiffness matrices [A], [B] and [D] are found through integration over the region volume and divided by the projected area of the region on the mid-plane [37].

$$[A]=\int_x\left(\int_y\left(\int_z[\bar{Q}]dz\right)dy\right)dx$$
$$[B]=\int_x\left(\int_y\left(\int_z[\bar{Q}]zdz\right)dy\right)dx \quad \textbf{(5-20)}$$
$$[D]=\int_x\left(\int_y\left(\int_z[\bar{Q}]z^2dz\right)dy\right)dx$$

In the above equations, $[\bar{Q}]$ is the stiffness matrix for the layer of fibre strand or matrix in the composite. The final forms of the regional stiffness matrices for regions R_1-R_9 are similar in form as those for the overlapping regions, which are:

$$[A]=a_{xy}[([Q_c(-\theta)]+[Q_c(\theta)])h_c+[Q_m]t_m] \quad \textbf{(5-21)}$$

$$[B]=\frac{1}{2}a_{xy}\begin{Bmatrix}[Q_c(-\theta)]\left(\left(\frac{t_m}{2}\right)^2-\left(-h_c-\frac{t_m}{2}\right)^2\right)+\ldots\\ [Q_c(\theta)]\left(-\left(\frac{t_m}{2}\right)^2+\left(h_c+\frac{t_m}{2}\right)^2\right)+\ldots\\ [Q_m]\left(\left(h_c+\frac{t_m}{2}\right)^2-\left(-h_c-\frac{t_m}{2}\right)^2\right)\end{Bmatrix} \quad \textbf{(5-22)}$$

$$[D]=\frac{1}{3}a_{xy}\begin{Bmatrix}[Q_c(-\theta)]\left(\left(\frac{t_m}{2}\right)^3-\left(-h_c-\frac{t_m}{2}\right)^3\right)+\ldots\\ [Q_c(\theta)]\left(-\left(\frac{t_m}{2}\right)^3+\left(h_c+\frac{t_m}{2}\right)^3\right)+\ldots\\ [Q_m]\left(\left(h_c+\frac{t_m}{2}\right)^3-\left(-h_c-\frac{t_m}{2}\right)^3\right)\end{Bmatrix} \quad \textbf{(5-23)}$$

where $[Q_c(\theta)]$ is the stiffness matrix rotated in the positive braid angle, $[Q_c(-\theta)]$ is the stiffness matrix rotated in the negative braid angle and a_{xy} is a constant relating to the regional area in the unit cell.

$$a_{xy} = \int_{x_1}^{x_2}\int_{y_1}^{y_2} dydx \tag{5-24}$$

These equations are solved using numerical methods in the case of regional stiffness matrices for the undulation regions (R_{10}-R_{13}) using a 10^{th} order Gauss-Legendre quadrature integration method, such that:

$$I = \frac{a-b}{2}\sum_{i=1}^{10} w_i f(d_i) \tag{5-25}$$

where

$$d_i = \frac{a+b}{2} + \frac{a-b}{2}\xi_i \tag{5-26}$$

where parameter d_i is a function of a_u and the quadrature zeros (ξ) [76,77]. The integration was calculated at 10 unequally spaced points (n=10) along the undulation length, a_u. Each point was multiplied by the weighting factor, w_i, with the sum of all of the integration points multiplied by the difference of the integration bounds, a and b, and L_e.

Table 5-3: Zeros and weights for Gauss-Legendre Quadrature for n=10

i	Zeros ($\pm\xi_i$)	Weights (w_i)
1, 10	0.1488743390	0.2955242247
2, 9	0.4333953941	0.2692667193
3, 8	0.6794095683	0.2190863625
4, 7	0.8650633667	0.1494513492
5, 6	0.9739065285	0.0666713443

The 3 x 3 volume-weighted stiffness matrices [A*], [B*] and [D*] are calculated over the 13 regions depicted in Figure 5-2. The simplified equations are below.

$$\begin{aligned}[A^*] &= \frac{1}{P_A}[A]^* \\ [B^*] &= \frac{1}{P_A}[B]^* \\ [D^*] &= \frac{1}{P_A}[D]^*\end{aligned} \tag{5-27}$$

where P_A is the projected unit cell area on the midplane, and

$$\begin{aligned}[A]^* &= \sum_{n=1}^{13}[A]_n \\ [B]^* &= \sum_{n=1}^{13}[B]_n \\ [D]^* &= \sum_{n=1}^{13}[D]_n\end{aligned} \tag{5-28}$$

where [A], [B] and [D] were defined earlier for each of the 13 regions.

By the method described by Tsai-Hahn, the elastic moduli can be determined along the X and Y axis (global unit cell axes as shown in Figure 5-2):

$$\begin{aligned}E_x &= \frac{1}{a_{1,1}t} \\ E_y &= \frac{1}{a_{2,2}t} \\ \mu_{x,y} &= \frac{-a_{1,2}}{a_{1,1}} \\ G_{xy} &= \frac{1}{a_{3,3}t}\end{aligned} \tag{5-29}$$

where, t is the total thickness of unit cell and $a_{i,j}$ component of compliance matrix [C], given as,

$$[a]=\begin{bmatrix} a_{1,1} & a_{1,2} & a_{1,3} \\ a_{2,1} & a_{2,2} & a_{2,3} \\ a_{3,1} & a_{3,2} & a_{3,3} \end{bmatrix} \tag{5-30}$$

From the inverse of the stiffness matrix [S], such that:

$$\begin{aligned} [S] &= \begin{bmatrix} [A^*] & [B^*] \\ [B^*] & [D^*] \end{bmatrix} \\ [S]^{-1} &= [C] \\ [C] &= \begin{bmatrix} [a] & [b] \\ [b] & [d] \end{bmatrix} \end{aligned} \tag{5-31}$$

where:

$$[a]=[A^*]^{-1}+[A^*]^{-1}[B^*]^{-1}\left([D^*]-[B^*][A^*]^{-1}\right)^{-1}[B][A^{*-1}] \tag{5-32}$$

5.4.2 Model Validation

To validate the elastic constant portion of the overall braid model, results were compared to previous results for an e-glass/polyester and carbon/epoxy composite using material properties and the unit cell geometry provided in the literature [37]. Figure 5-5, contains the comparison of the results for the longitudinal modulus, E_x, from [37] and the predictive model. It should be noted the values from the literature were taken from a graph and therefore are only approximations of the actual values and could account for some variability.

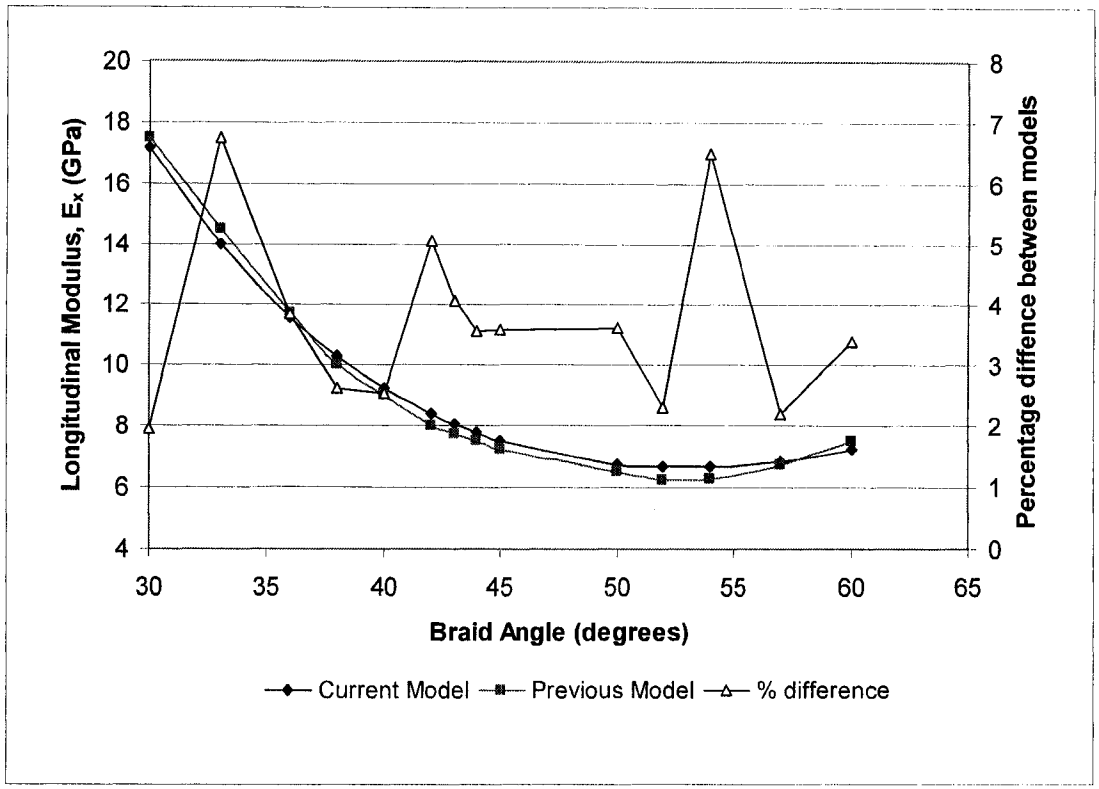

Figure 5-5: Comparison of results for the longitudinal modulus, E_x between the current and previous model [37] for an e-glass/polyester composite

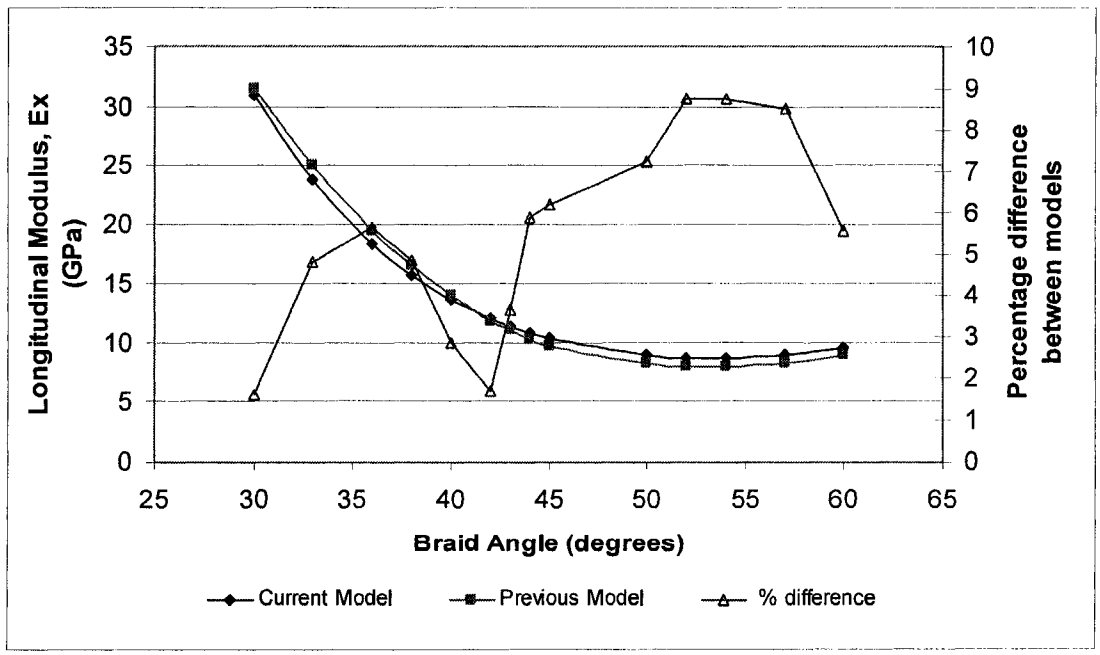

Figure 5-6: Comparison of results for the longitudinal modulus, E_x, between the current and previous model [37] for a carbon/epoxy composite

The comparative results for the longitudinal modulus, E_x, between the current and previous model yield results with a small variance for the e-glass/polyester composite between 1.9 - 6.7%, with an average difference of 3.7%. The difference in model results for the carbon/epoxy composite ranged from 1.6% to 8.5%, with an average difference of 5.4%. Based on the approximate values taken from a graphic [37], it is believed that the predictive model is capable of calculating composite elastic constants within acceptable error.

5.5 Overall Predictive Model

The cover factor and elastic constants models were combined to form an overall braid model to predict the elastic constants of a 2D conical braided composite with a minimum cover factor of 95%. Analyzing the results for a conical composite with a half-cone angle taken from a commercially available composite golf shaft will now validate this model. The results for the elastic constants and cover factor were evaluated. The cover factor was held to a minimum of 95%. Additionally, the difference in trapezoidal and rectangular unit cell area was determined to ensure the 5% difference criterion (as previously detailed in Section 5.3.2) is upheld.

5.5.1 Braid Model Validation and Results

The evaluation of the braid model was for the tapered mid-section of a golf shaft, which is 727 mm in length and varies in diameter from 15.2 mm (at the butt end) to 8.51 mm (at the tip section). These dimensions result in a half-cone angle of 0.27°. It is assumed that the carrier and mandrel velocities are held constant over the mandrel length.

Additionally, eight (8) strand carriers were used in the model validation. A carbon/epoxy composite was used with a fibre volume fraction of 60%.

The results of the analysis for the cover factor and the elastic constants are below in Figure 5-7 to Figure 5-13 for the carbon/epoxy composite, where length zero refers to the tip end of the shaft conical section.

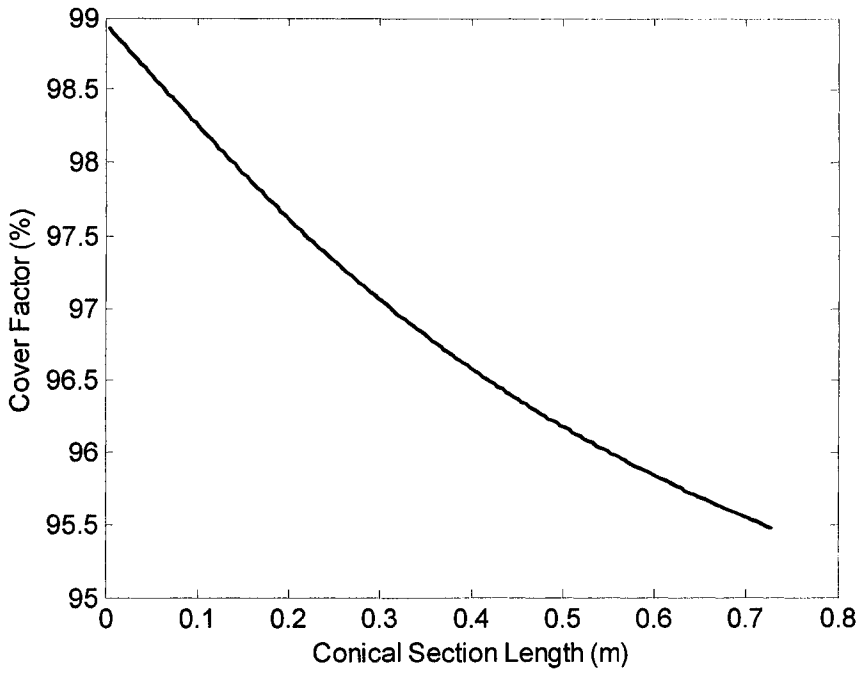

Figure 5-7: Cover factor along the mandrel tapered length for a carbon/epoxy composite

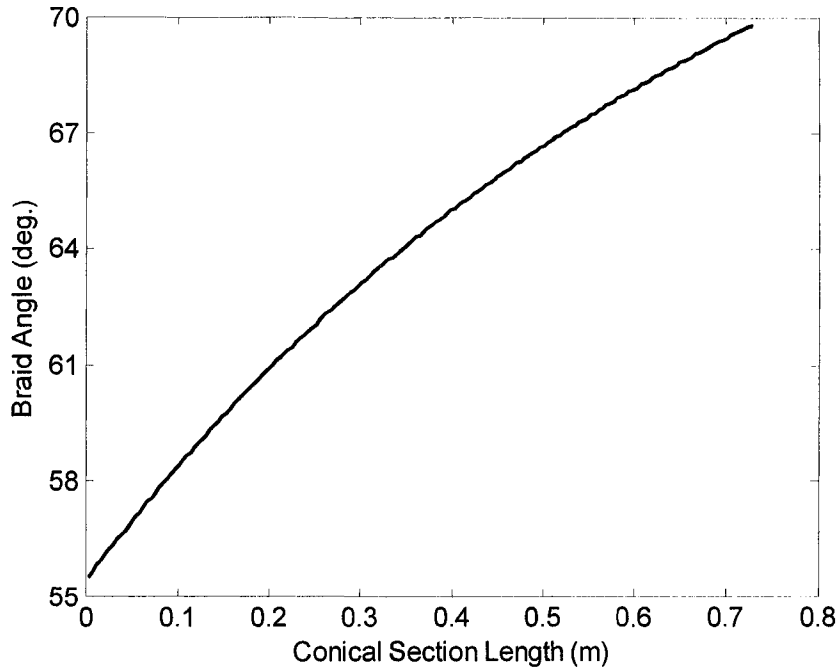

Figure 5-8: Braid angle along the mandrel tapered length for a carbon/epoxy composite

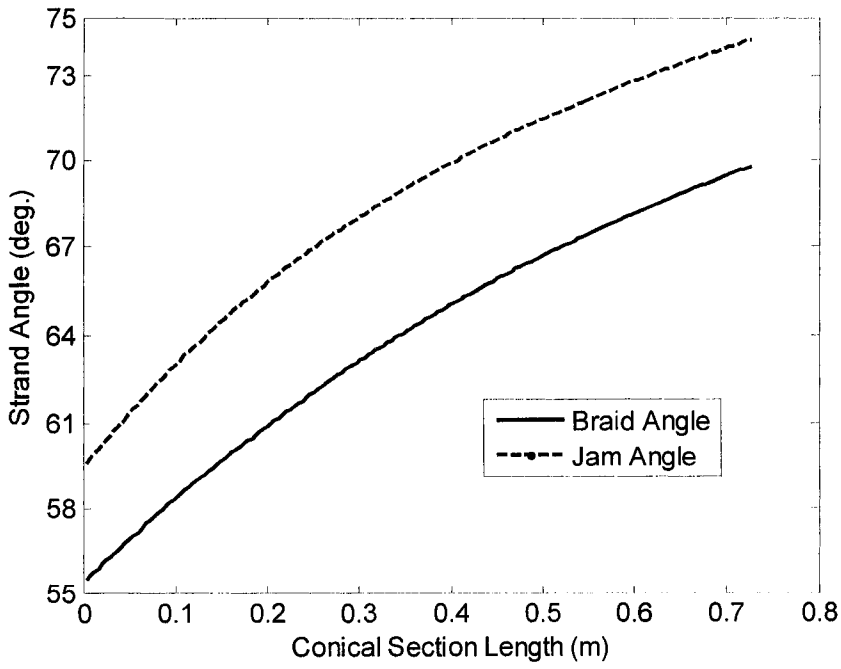

Figure 5-9: Braid and jam angle along the mandrel tapered length for a carbon/epoxy composite

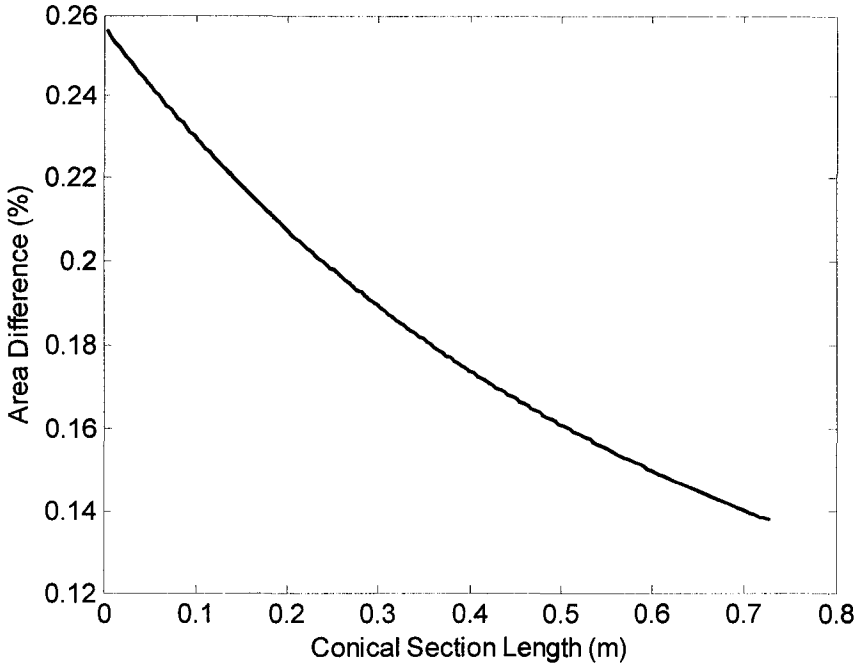

Figure 5-10: Area difference between trapezoidal and rectangular unit cells along the mandrel tapered length for a carbon/epoxy composite

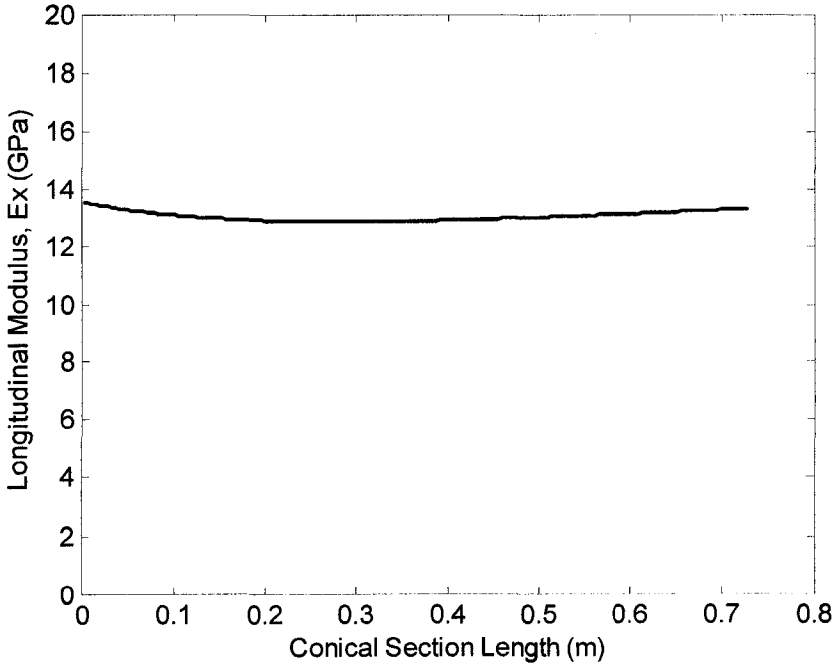

Figure 5-11: Longitudinal modulus, E_x, along the mandrel tapered length for a carbon/epoxy composite

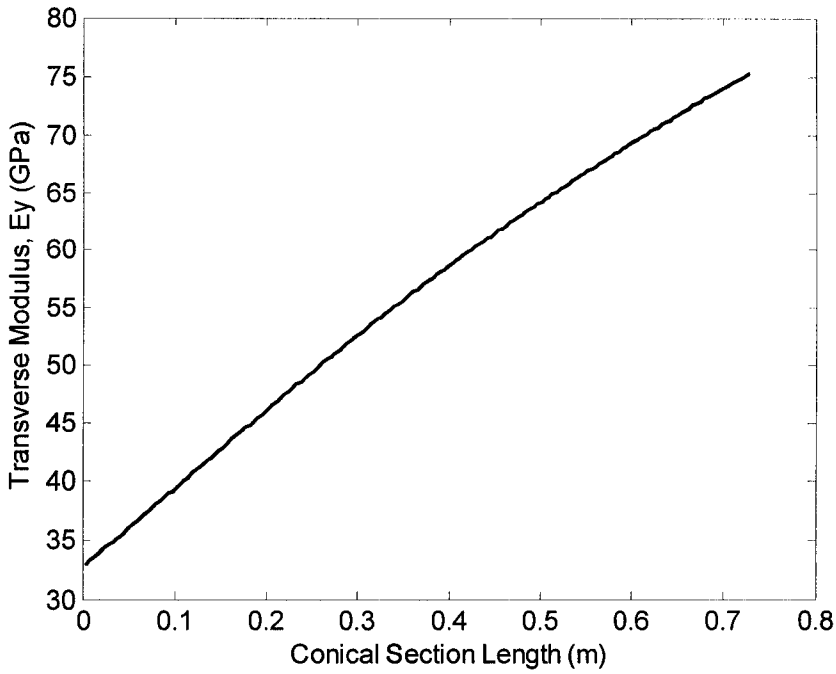

Figure 5-12: Transverse modulus, E_y, along the mandrel tapered length for a carbon/epoxy composite

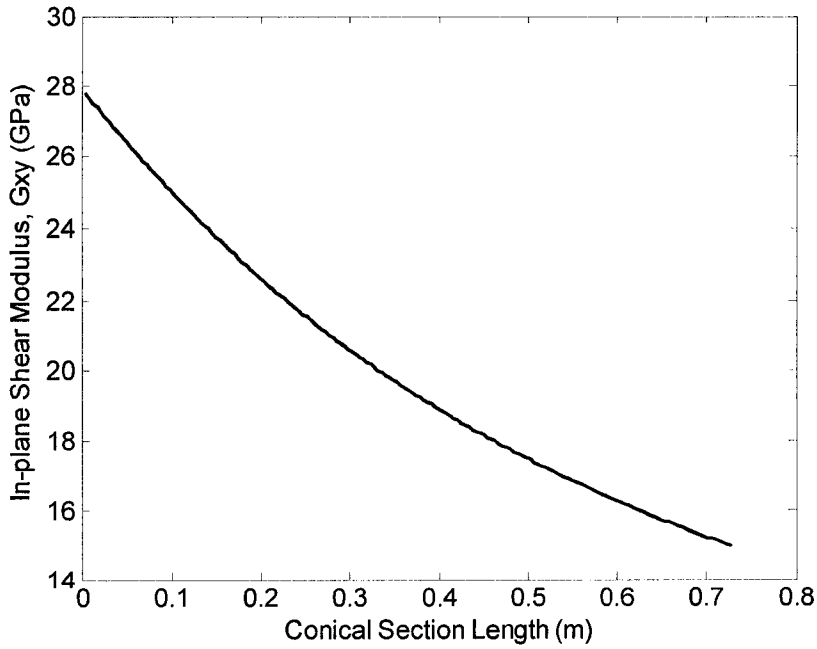

Figure 5-13: In-plane shear modulus, G_{xy}, along the mandrel tapered length for a carbon/epoxy composite

The cover factor decreased from an initial value of 99% to 95.5%, which satisfies the minimum 95% cover factor condition. The cover factor decreased more rapidly over the first 0.3 m of the mandrel than the remaining mandrel length.

The braid angle increased non-linearly from approximately 56° – 69° over the mandrel length. The slope is steeper, indicating a greater rate of increase, from 56° to 62.5°, over the first 0.3 m of the mandrel, followed by a lower rate over the remaining mandrel length. The braid angle along the mandrel is below the jam angle; therefore, this braiding process condition is satisfied.

The difference in the area between the trapezoid and rectangular unit cells varied between 0.14% and 0.255%, which is negligible and largely satisfies the maximum allowable area difference of 5%. Therefore, the rectangular-trapezoidal unit cell assumption, detailed in Section 5.4.1, is valid in this case. The predicted elastic constant values should be accurate.

From the results, the longitudinal modulus yielded a magnitude of approximately 13.5 GPa, over the mandrel length. The longitudinal modulus profile follows the general curvature of E_x for the elastic constant portion of the model (Figure 5-5 and Figure 5-6). In those figures, the longitudinal modulus decreased to a minimum at around 55° and then increased again.

The transverse modulus follows a near linear increase, from approximately 33 GPa – 75 GPa, over the mandrel length. The near linear increase is expected due to the braid angles formed over the mandrel. From studies by Carey [78] and Huang [79], the changes of the elastic constants of braided composites with braid angle are given. From each study, E_y begins to increase non-linearly with braid angles greater than

approximately 52°. The magnitudes of E_y differ for each study, and these results, due to the differences in materials used in the analysis. However, the similarity in trends indicates that the relationship is not material based but is dependent on braid angle.

From Figure 5-13, the in-plane shear modulus, G_{xy}, decreases non-linearly, from 28 GPa – 15 GPa, over the mandrel length. These results correspond to those reported in the literature [78] except that they only present results to 62°. Additionally, these results correspond to Howell [17], where it is stated that a 45° fibre angle is optimal for shear stiffness of filament wound golf shafts.

5.5.2 Model Validation for a Golf Shaft

The conical, or tapered, section of a golf shaft has been modelled. However, a golf shaft also consists of a two cylindrical sections, the tip and butt ends. Therefore, these sections must be included in the model. The model of the golf shaft starts at the tip end and progresses to the butt end. The outer diameter of the tip section was 8.51 mm and 15.2 mm at the butt end. As with the tapered section, a carbon/epoxy composite was used with a fibre volume fraction of 60%. The carrier angular and mandrel velocities are held constant. Eight strand carriers were used in the model validation. The results of the analysis for the cover factor and elastic constants are below in Figure 5-14 to Figure 5-20.

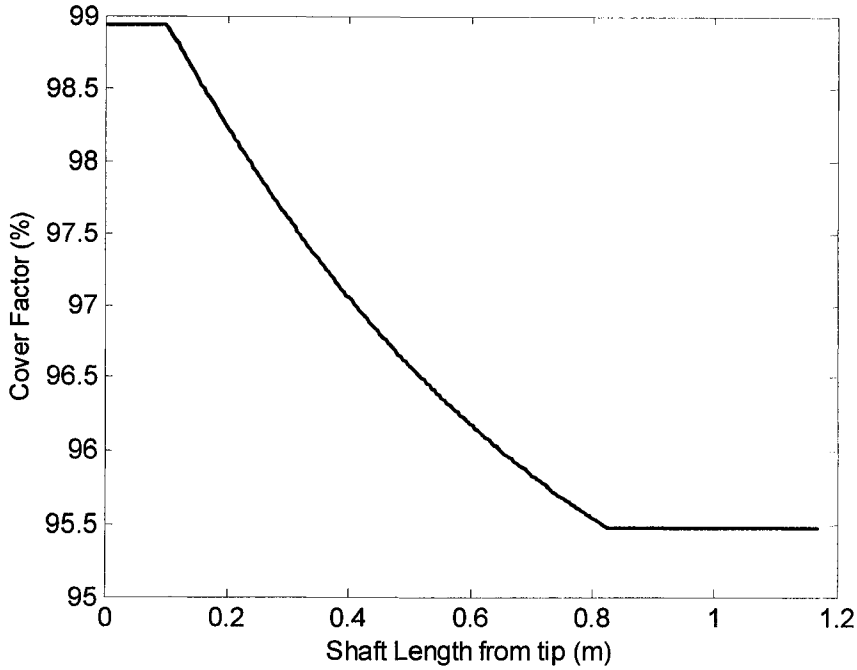

Figure 5-14: Cover factor along the golf shaft

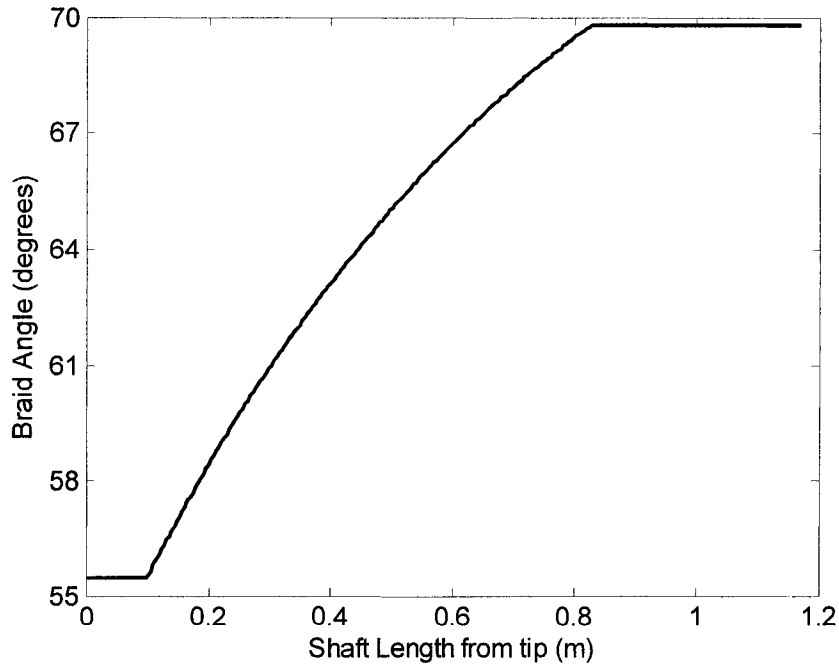

Figure 5-15: Braid angle along the golf shaft

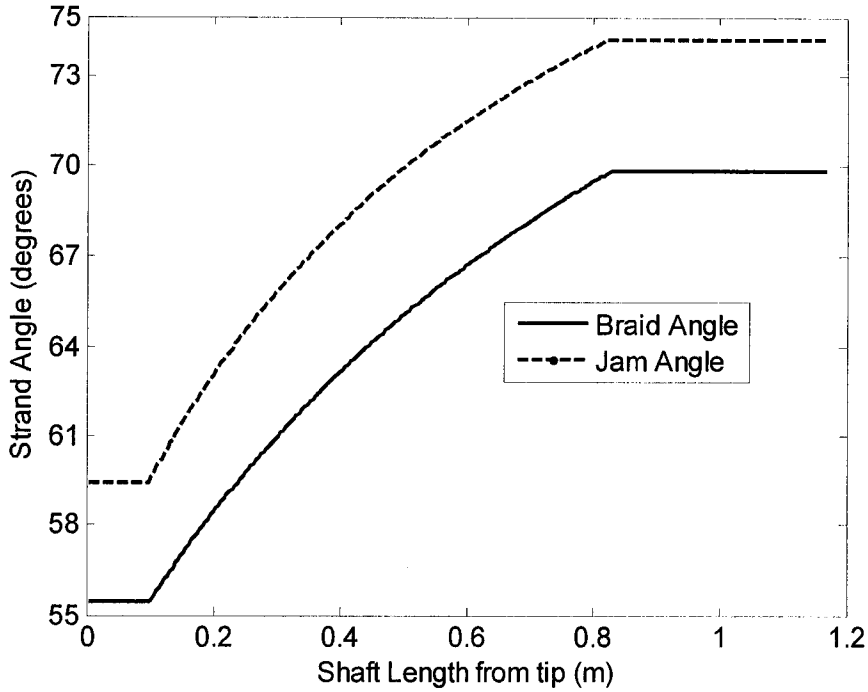

Figure 5-16: Braid and jam angle along the golf shaft

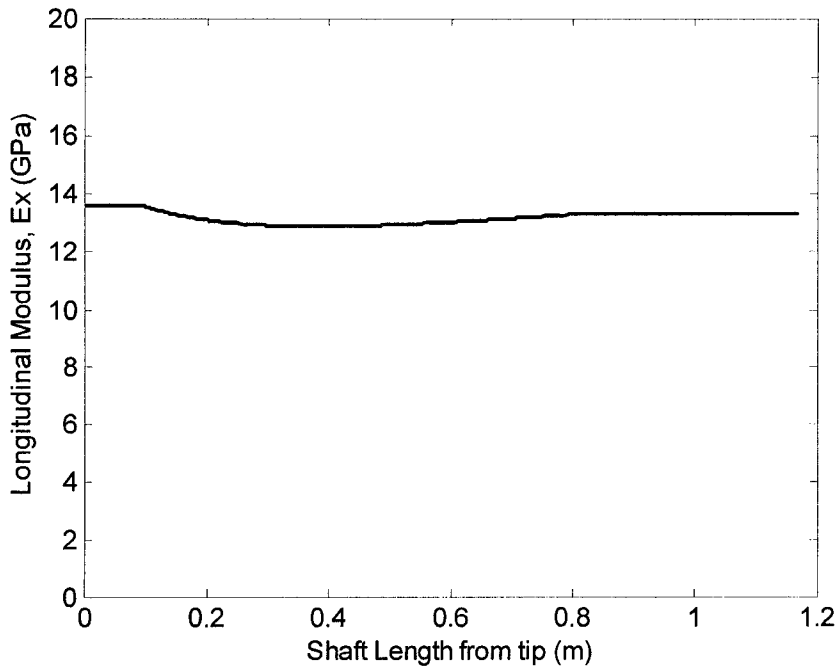

Figure 5-17: Longitudinal modulus along the golf shaft

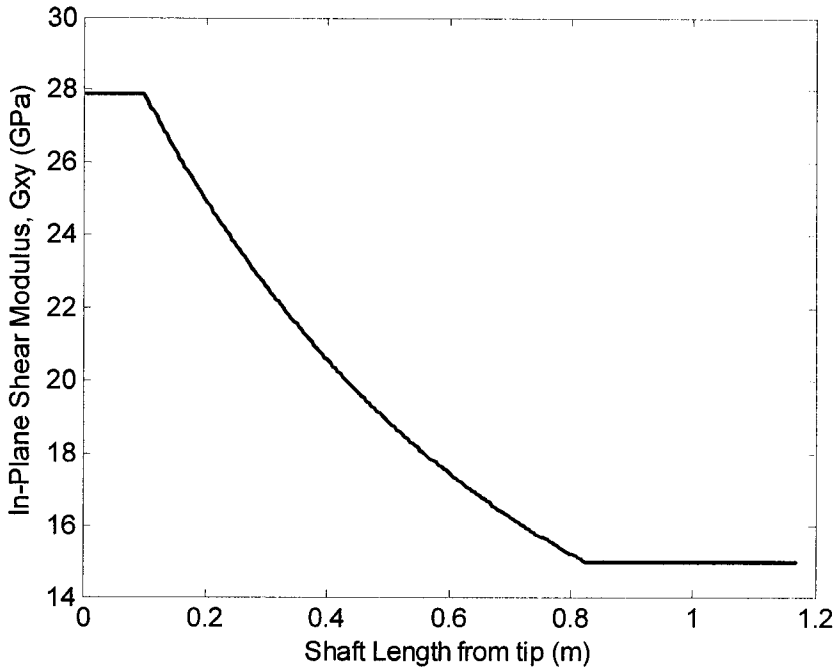

Figure 5-18: In-plane shear modulus along the golf shaft

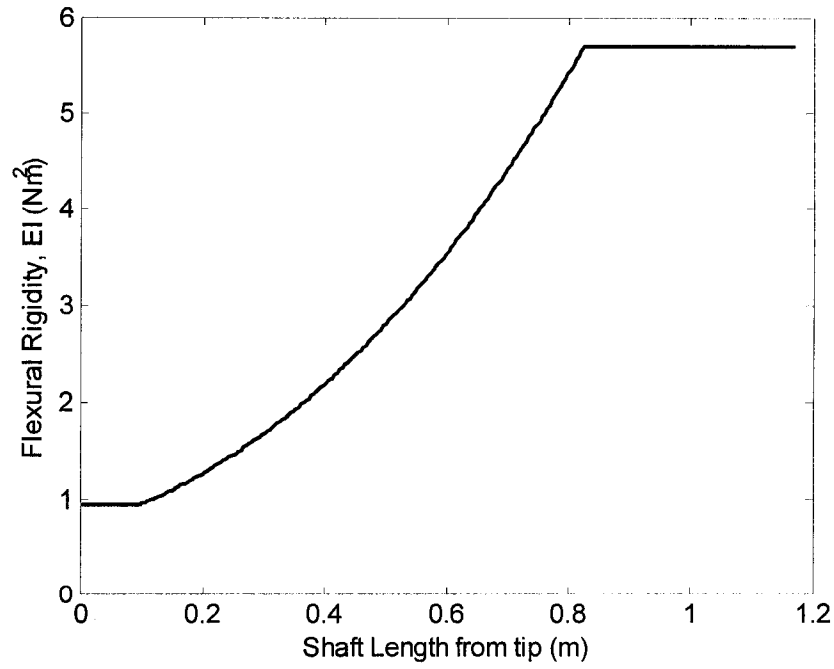

Figure 5-19: Flexural rigidity along the golf shaft

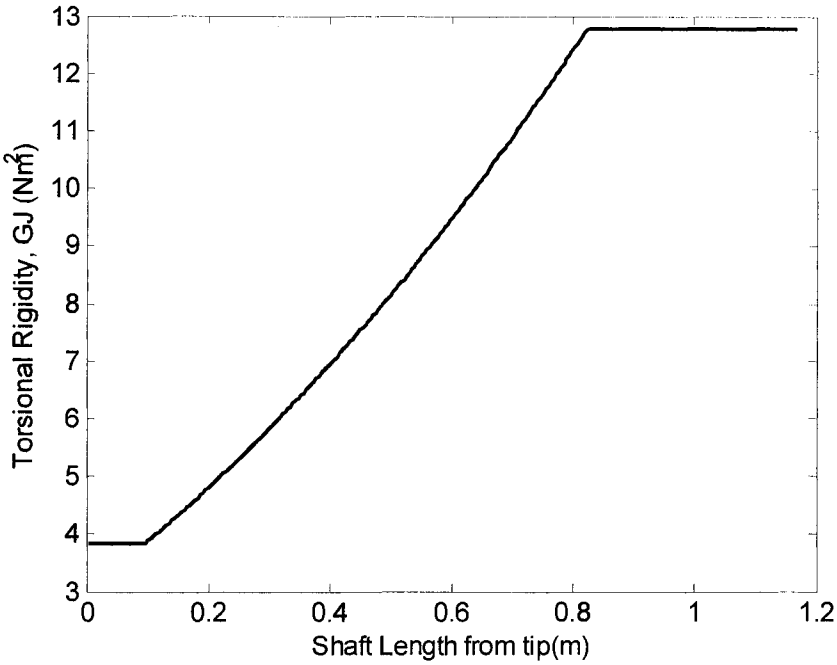

Figure 5-20: Torsional rigidity along the golf shaft

The results for the golf shaft model match those of the previous section for the conical section. This is expected since the material and mandrel dimensions remained constant. Obviously, the only differences are for the cylindrical tip and butt end sections. The magnitude for each parameter analyzed remaining constant is expected for the cylindrical sections. The cover factor, braid angle and jam angle are constant since the radius of the section does not change. The braid angle satisfies the jam angle. The only difference between a cylindrical and conical mandrel is the half-cone angle. For a cylindrical mandrel the half-cone angle is zero. If the braid angle does not change, the elastic constants will remain constant. If the elastic constants and cross-sectional area of the composite do not change, then the flexural and torsional rigidity will remain constant.

In this chapter, a predictive model was developed using MATLAB to determine the cover factor and corresponding elastic constants for a conical 2D braided composite.

The individual components of the predictive model, i.e. the cover factor and elastic constants, were validated using previous results. For the overall predictive model, the cover factor was required to remain above 95% and a maximum difference, between trapezoidal and rectangular unit cell areas, of 5% was permitted. Both of these conditions were satisfied. The results of the predictive golf shaft model will be used to determine golf shaft design parameters such as deflection-force and angle of twist.

6 DEFLECTION AND TWIST CALCULATIONS FOR GOLF SHAFTS

The deflection-force and twist of the braided golf shaft were compared to commercially available steel and composite shafts. To analyze deflection-force and twist of the braided shaft, Castigliano's Theorem was used. The methods presented in this chapter are used for the multiple stacking sequences modelled in the following chapters. Experimental and manufacturer specifications were used to determine the deflection-force and twist of the commercial shafts.

6.1 Castigliano's Theorem for Deflection

Castigliano's Theorem was used to determine the tip deflection of the braided golf shaft in the direction of applied load. Castigliano's Theorem is applicable for small displacements and linear deflections. It was assumed that the golf shaft was cantilevered with a small force, applied to the tip, sufficient to cause a downward deflection-force of 101.6 mm (4 inches). Cantilevered shaft lengths of 1059 mm and 1122 mm correspond to cut lengths of shafts used in previous shaft testing [12]. The small deflection assumption is valid since shaft lengths of 1059 mm and 1122 mm and tips deflections of 101.4 mm both results in 5 mm of axial deflection, which corresponds in a 0.4% difference for both lengths. Therefore, internal moment differences are negligible. In addition, elastic deformation is assumed. A 101.4 mm deflection was used to produce results comparable to previously compiled shaft data [12]. It is the force required (deflection-force) to cause 101.4 mm of deflection that will be calculated and not the deflection generated from an applied force. The shaft mass was also included in the analysis to provide a more accurate comparison to the commercial shafts. Various laminate stacking sequences were used in

the deflection-force analysis. Additionally, the deflection-force was calculated for a shaft with and without foam core to determine the influence of the core on the flexural rigidity. A cantilevered shaft with a deflection-force load, F, and torque, T, applied to the tip end is presented in Figure 6-1.

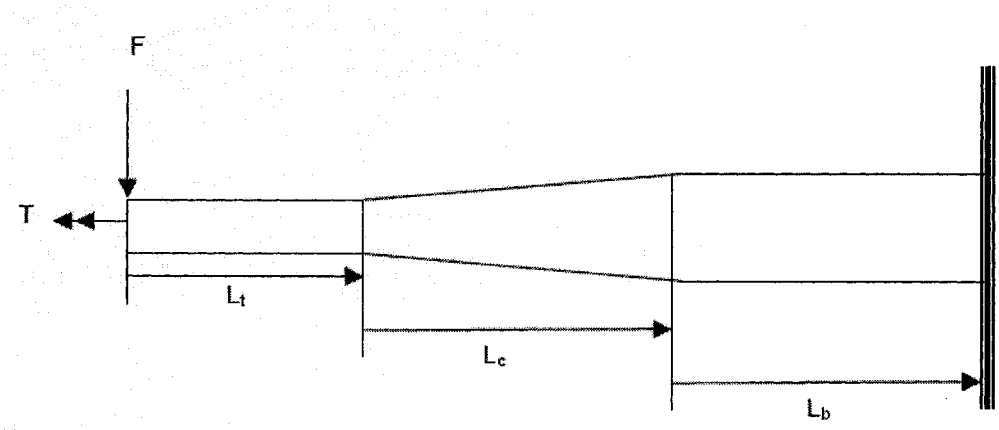

Figure 6-1: Diagram of shaft for deflection analysis

As seen in Figure 6-1, L_t, L_c and L_b are the total lengths of each of the three sections of the shaft. The first length, L_t, is the length of the tip section. The second length, L_c, is comprised of the conical (tapered) section. Finally, the third section, L_b, includes the butt section. Castigliano's Theorem is based on the complimentary strain energy, U^*, for a system with a linear material response. The strain energy is a function of the forces, F, applied to the system. The deflection, q, of a point in the system is solved by taking the partial derivative of the strain energy with respect to the force, F_i, applied at point i.

$$q_i = \frac{\partial U^*}{\partial F_i}, \quad for\ i = 1...n \tag{6-1}$$

In this analysis there were multiple forces, i.e. the force applied at the tip and the mass of the shaft. The deflection, at a point, is given as:

$$q_i = \sum_{j=1}^{n} \int \frac{M_j}{E_j I_j} \frac{\partial M_j}{\partial F_i} dz + \sum_{j=1}^{n} \int \frac{V_j}{A_j E_j} \frac{\partial V_j}{\partial F_i} dz \qquad \textbf{(6-2)}$$

where M_j, E_j, I_j, V_j and A_j are the moment, Young's modulus, moment of inertia, shear force and cross-sectional area of the each section of a system. Strain energy due to transverse shear (2nd summation term) is assumed to be negligible in comparison to the strain energy due to the moment (1st summation term) and therefore may be neglected.

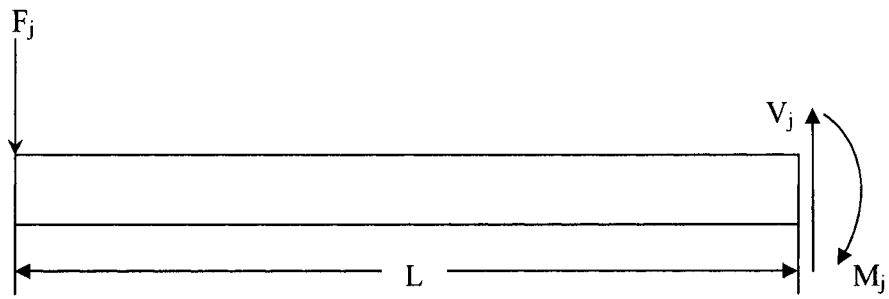

Figure 6-2: Example free body diagram of a cantilevered, hollow shaft

Using the terms in Equation 6-2, the resulting moment, M_j, and shear force, V_j for a shaft of length, L, are given below.

$$\begin{aligned} M_j &= F_i L \\ V_j &= F_i \\ \frac{\partial M_j}{\partial F_i} &= L \\ \frac{\partial V_j}{\partial F_i} &= 1 \end{aligned} \qquad \textbf{(6-3)}$$

Longer shafts have greater moment strain energy. Additionally, if the outer diameter of the beam were lower than unity, then the moment of inertia, I_j, would be greater than the cross-sectional area, A_j. Therefore, for a long, slender beam, the quantities that comprise the moment strain energy (1st summation term) will be larger than those that make up

transverse shear strain energy (2nd summation term). This assumption is then valid for a long, slender beam.

Since the cross-sectional area of the shaft changes between the tip, tapered and butt section the analysis was divided into three sections: the tip, tapered (conical) and butt sections. The total deflection of the shaft is:

$$q=\int_0^{L_t}\frac{M_t}{E_tI_t}\frac{\partial M_t}{\partial F}dz_t+\int_0^{L_c}\frac{M_c}{E(z)_cI(z)_c}\frac{\partial M_c}{\partial F}dz_c+\int_0^{L_b}\frac{M_b}{E_bI_b}\frac{\partial M_b}{\partial F}dz_b \qquad \textbf{(6-4)}$$

where t, c and b represent the tip, tapered (conical) and butt sections, respectively.

The deflection of the tip section was determined using the free body diagram (FBD) of Figure 6-3.

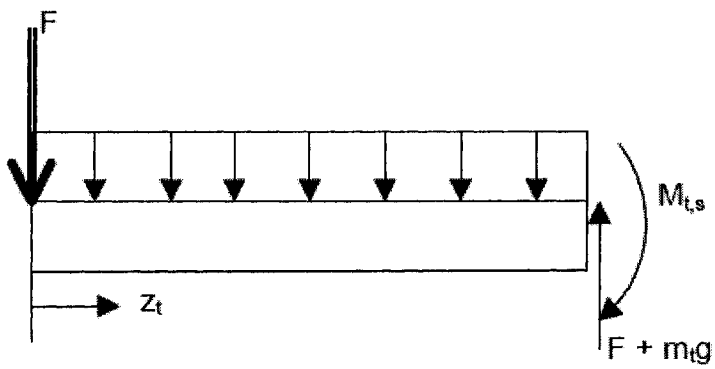

Figure 6-3: Free body diagram of the tip shaft section

where:

$$M_{t,s}=Fz_t+1/2\,k_tz_t^2$$
$$\partial M_{t,s}/\partial F=z_t \qquad \textbf{(6-5)}$$

and m_t is the mass of the tip section.

In the tip section, $E_{t,s}$ and $I_{t,s}$ are constant since the tip section is cylindrical. The force due to the mass, located at the centre of gravity can be analyzed as a uniformly distributed load, $k_{t,s}$.

$$k_{t,s} = \rho_s g \pi \left(r_{o,t}^2 - r_{i,t}^2 \right) \tag{6-6}$$

Where ρ_s is the shaft material density and $r_{o,t}$ and $r_{i,t}$ are the outer and inner radii. The subscripts, i and o, signify the inner and outer dimensions of the shaft, respectively.

The tapered (conical) section, denoted with subscript c, was more complex to analyze due to the changing cross-section, Young's modulus, $E_{c,s}$ and moment of inertia, $I_{c,s}$ over the length. The change in $E_{c,s}$ is due to the change in braid angle of the CF layer as the diameter of the conical section. The moment of inertia, $I_{c,s}$, changes as result of the increasing shaft cross-section.

The flexural rigidity, EI, is a product of the longitudinal modulus and moment of inertia, which both change over the conical section. In order to calculate the deflection of the conical section, the change in the flexural rigidity was approximated using a cubic function. The cubic function was fit to values of EI over the length of the conical section.

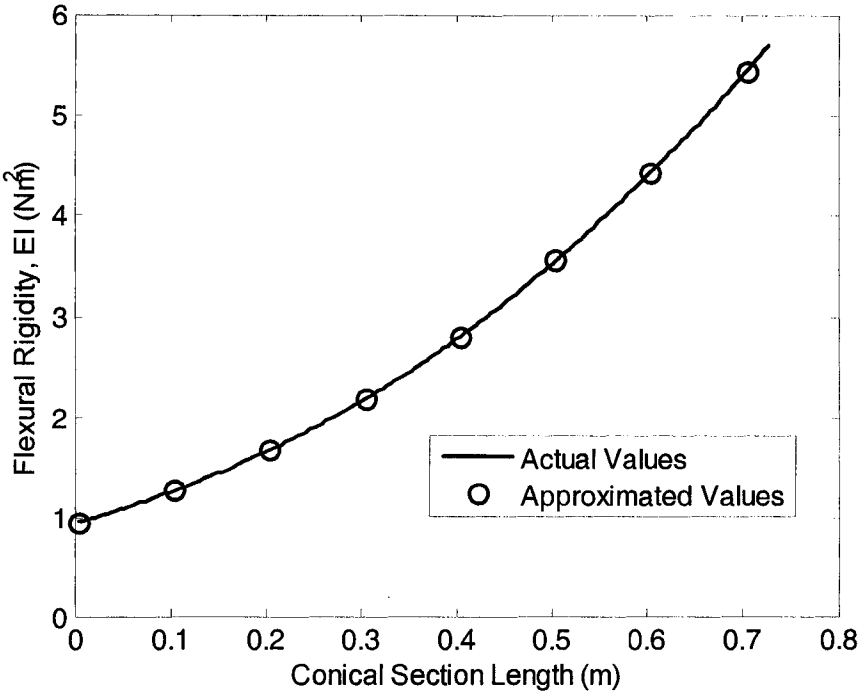

Figure 6-4: Best-fit approximation of the flexural rigidity of the conical shaft section

The approximated values for the flexural rigidity are denoted as EI_A and are solved as:

$$EI_A = 1.8341x^3 + 4.0404x^2 + 2.7706x + 1.099 \quad \textbf{(6-7)}$$

The cubic approximation closely matches the actual values for EI. The difference between the approximated values and the actual values is detailed in Table 6-1.

Table 6-1: Approximated, actual and errors for the flexural rigidity of the conical section

Distance (m)	EI (GPa)	EI_A (GPa)	EI error (%)
0.00425	1.023	1.022	0.122
0.10200	1.336	1.336	0.036
0.20400	1.759	1.759	0.010
0.30175	2.265	2.264	0.035
0.40375	2.908	2.908	0.004
0.50150	3.647	3.647	0.004
0.60350	4.556	4.557	0.014
0.70125	5.573	5.572	0.016

The values in Figure 6-4 are for shaft with only the minimum 95% cover factor layer made from AS4 carbon fibres. The error in the approximated values is a maximum of 0.122%, which indicates the approximation is very close to the actual values.

Additionally, the force due to the mass is not a uniformly distributed load but also follows a cubic function. This is due to the cubic increase in volume of the conical section. The force due to the mass will increase in the same manner as the volume because the shaft material density is constant. The volume curve is shown in Figure 6-5.

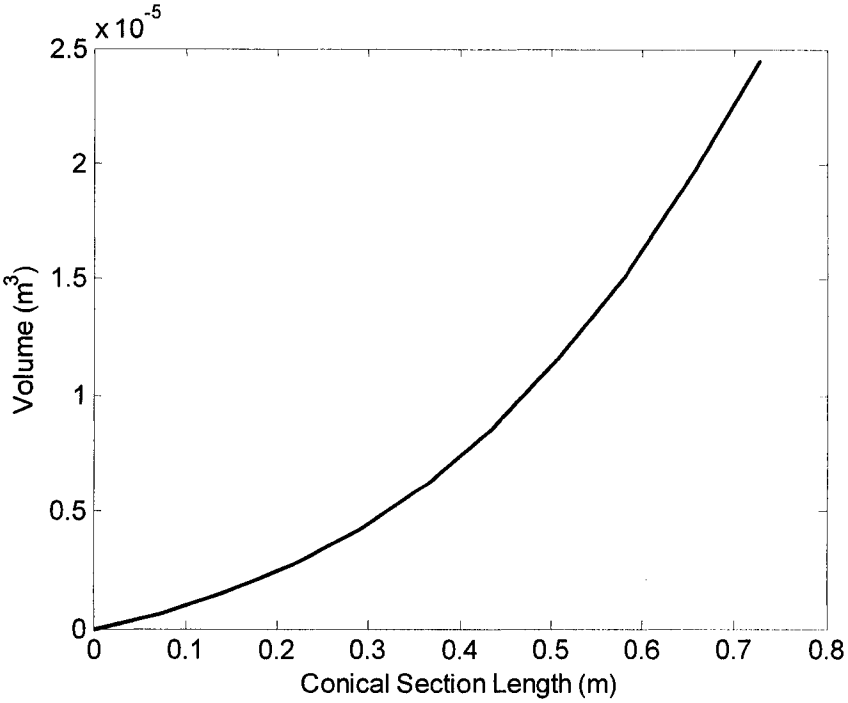

Figure 6-5: Increase in volume of the conical section

The equation describing the change in volume along the conical section is given below.

$$V_c = 3x10^{-5} z_c^3 + 2x10^{-5} z_c^2 + 8x10^{-6} z_c \quad \textbf{(6-8)}$$

Equation 6.7 was multiplied by the material density, ρ_s, and gravitational constant, g, to determine the force due to the mass of the tapered section. The bending moment created by the mass force is dependent on the location of the centre of gravity, lcg_s, for the conical section this is given at any point z_c as:

$$lcg_s = \left(z_c/4\right)\frac{\left(r_{1,o}^2 + 2r_{1,o}r_{2,o} + 3r_{2,o}^2\right) - \left(r_{1,i}^2 + 2r_{1,i}r_{2,i} + 3r_{2,i}^2\right)}{\left(r_{1,o}^2 + r_{1,o}r_{2,o} + r_{2,o}^2\right) - \left(r_{1,i}^2 + r_{1,i}r_{2,i} + r_{2,i}^2\right)} \quad \textbf{(6-9)}$$

where the notations 1 and 2 indicate the radius of the minor or major diameter of the section and the subscripts i and o represent the inner and outer radius. Therefore, $r_{1,o}$ denotes the outer portion at the minor (smaller) radius. The inner radius is simply the

outer radius minus the shaft wall thickness. Since the conical section has a linear taper, the radius at any point, n, along the section is given as:

$$r_n = r_1 + (r_2 - r_1)(z_c / L_c) \tag{6-10}$$

The minor radius is the radius of the cylindrical tip section and the major radius at L_c is the radius of the cylindrical butt section. The reactions on the conical section are as follows:

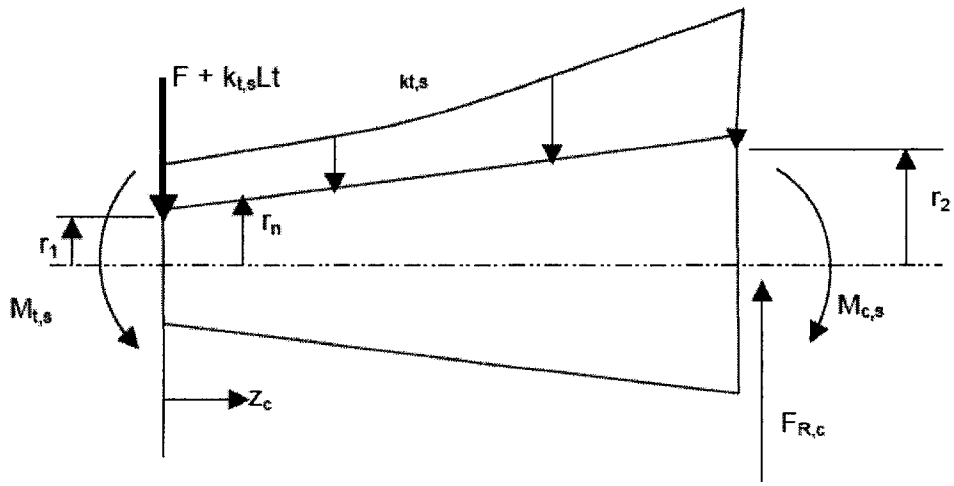

Figure 6-6: Free body diagram of the conical section

where:

$$M_{c,s} = M_{t,s} + (F + k_{t,s} L_t) z_c + k_{c,s} lcg \tag{6-11}$$

$$k_{c,s} = \rho_s g V(z_c)_{c,s} \tag{6-12}$$

$$\partial M_{c,s} / \partial F = z_c + L_t \tag{6-13}$$

$$F_{R,c} = F + k_{t,s} L_t + k_{c,s} L_c \tag{6-14}$$

where $V(z_c)_{c,s}$ is the volume of the conical sections as a function of the conical length, z_c, and $F_{R,c}$ is the reaction force on the conical section.

In the cylindrical butt section, $E_{b,s}$ and $I_{b,s}$ are constant (as for the tip section) and the force due to mass of the cylindrical section can be modeled as a uniformly distributed load, $k_{b,s}$. The reactions on the butt section are detailed in Figure 6-7.

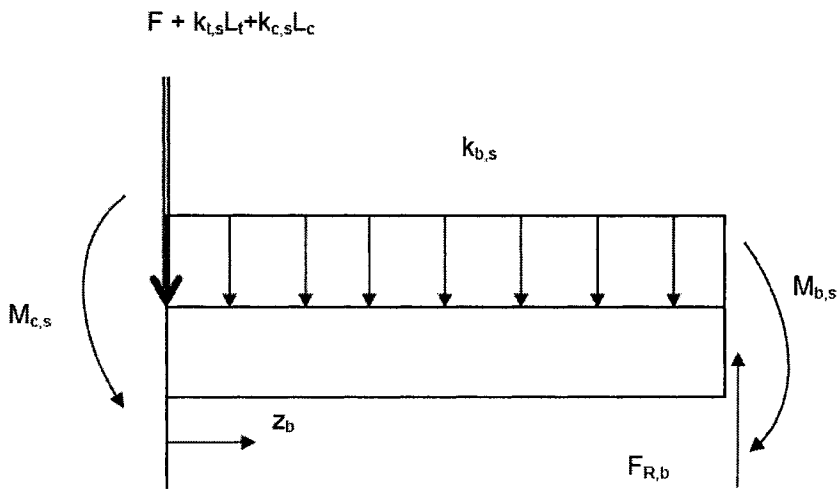

Figure 6-7: Free body diagram of the cylindrical butt section

Shown in Figure 6-7:

$$
\begin{aligned}
M_{b,s} &= M_{c,s} + \left(F + k_{t,s}L_t + k_{c,s}L_c\right)z_b + 1/2\,k_{b,s}z_b^2 \\
k_{b,s} &= \rho_s g A_{b,s} \\
A_{b,s} &= \pi\left(r_{o,b}^2 - r_{i,b}^2\right) \\
F_{R,b} &= F + k_{t,s}L_t + k_{c,s}L_c + k_{b,s}L_b
\end{aligned}
\qquad \textbf{(6-15)}
$$

where $A_{b,s}$ is the cross-sectional area of the cylindrical butt section and $r_{o,b}$ and $r_{i,b}$ are the outer and inner radius, respectively. Additionally, $F_{R,b}$ is the reaction force on the butt end section.

The final total shaft deflection-force is determined by equation 6-3.

Additionally, the mass of the shaft, $m_{total,s}$ can be calculated using the distributed loads from the mass for each section.

$$m_{total,s} = \frac{k_{t,s}L_t + k(L_c)_{c,s} + k_{b,s}L_b}{g} \tag{6-16}$$

The deflection of the shaft with the foam core was also determined. The deflection due to the mass of the core must be added to the hollow shaft deflection to find the total deflection.

The force due to the mass of a foam core, f, can be modeled as a uniformly distributed load, $k_{t,f}$. The free body diagram of the tip section is similar as that for the hollow shaft except that the total distributed load is the sum of $k_{t,s}$ and $k_{t,f}$.

$$M_{t,f} = Fz_t + \frac{(k_{t,s} + k_{t,f})z_t}{2} \tag{6-17}$$

where:

$$k_{t,f} = \rho_f g A_{t,f}$$
$$A_{t,f} = \pi(r_{i,t}^2)$$

The foam core cross-sectional area is denoted as $A_{t,f}$ and the foam material density by ρ_f. Similarly with the hollow conical shaft section, the volume of the foam core follows a cubic function and the resulting distributed load is found in the same manner. However, the center of mass for the core is not the same as for hollow shaft due to the difference in geometry.

$$V_{f,c} = (z_c\pi/3)(r_{1,i}^2 + r_{1,i}r_{2,i} + r_{2,i}^2) \tag{6-18}$$

$$lcg_f = (z_c/4)\left(\frac{r_{1,i}^2 + 2r_{1,i}r_{2,i} + 3r_{2,i}^2}{r_{1,i}^2 + r_{1,i}r_{2,i} + r_{2,i}^2}\right) \tag{6-19}$$

Using the volume, $V_{f,c}$, and centre of mass, lcg_f, of the core, the moment and the force due to the core mass, $k_{b,f}$, on the conical section, $M_{c,f}$ can be determined.

$$M_{c,f} = FL_t + 1/2\,k_{t,s}L_t + 1/2\,k_{t,f}L_t + \left(F + k_{t,s}L_t + k_{t,f}L_t\right)z_c + k_{c,s}lcg_s + k_{c,f}lcg_{c,f} \quad \textbf{(6-20)}$$

where

$$k_{c,f} = \rho_f g V_{f,c} \quad \textbf{(6-21)}$$

The butt section of the shaft with the foam core can again model the force due to the core mass as a uniformly distributed load.

$$M_{b,f} = \left(F + k_{t,s}L_t + k_{t,f}L_t + k_{c,s}L_c + k_{c,f}L_c\right)z_b + 1/2k_{b,s}z_b + 1/2\,k_{b,f}z_b + M_{c,f} \quad \textbf{(6-22)}$$

where:

$$\begin{aligned} k_{b,f} &= \rho_f g A_{b,f} \\ A_{b,f} &= \pi\left(r_{i,b}^2\right) \end{aligned} \quad \textbf{(6-23)}$$

Additionally, $M_{b,f}$ is evaluated with z_b equal to L_b.

6.2 Castigliano's Theorem for Angle of Twist

The evaluation of the twist of the shaft by Castigliano's Theorem is simpler to determine since the mass of the shaft does not need to be considered. The shaft is again modelled as a cantilevered shaft with a 1.35 N·m torque applied 50.4 mm from the tip end (as shown in Figure 3-2). This was done to produce comparable results to the previously compiled shaft data [12]. The calculation to determine the angle of twist was done using the sectional method as with the bending deflection calculation.

In this analysis there is one torque, i.e. the torque applied at the tip of the shaft. The angle of twist, θ, as a function of the applied torque, is given as:

$$\theta_i = \sum_{j=1}^{n} \int \frac{T_j}{G_j J_j} \frac{\partial T_j}{\partial T_i} dz \tag{6-24}$$

where T_j, G_j, J_j are the moment, in-plane shear modulus and polar moment of inertia of each section of the system. Since the cross-sectional area of the shaft changes between the tip, tapered and butt section the analysis was again divided into these three sections: the tip, tapered and butt sections. The total twist of the shaft is given below.

$$\theta = \int_0^{L_t} \frac{T_t}{G_t J_t} \frac{\partial T_t}{\partial T} dz_t + \int_0^{L_c} \frac{T_c}{G(z)_c J(z)_c} \frac{\partial T_c}{\partial T} dz_c + \int_0^{L_b} \frac{T_b}{G_b J_b} \frac{\partial T_b}{\partial T} dz_b \tag{6-25}$$

where t, c and b represent the tip, tapered (conical) and butt sections, respectively.

The twist of the tip section was determined using the FBD, shown in Figure 6-8..

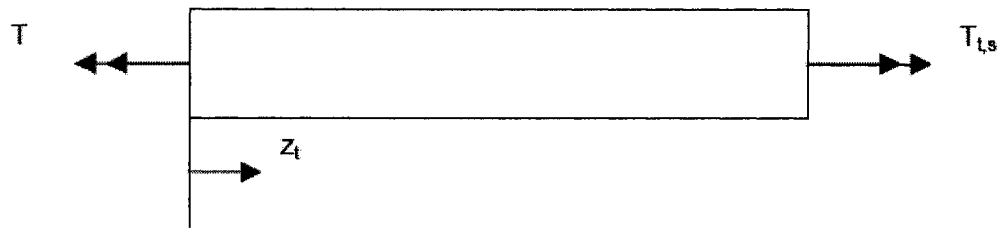

Figure 6-8: FBD of shaft tip section to determine the angle of twist

$$T_{t,s} = T \; and \; \partial T_{t,s} / \partial T = 1 \tag{6-26}$$

where $T_{t,s}$ is the torque on the tip section. In the tip section, $G_{t,s}$ and $J_{t,s}$ are constant since the tip section is cylindrical.

The twist of the conical section of the shaft is a function of the cross-sectional area and braid angle (of the minimum 95% cover factor lamina). As with the calculation to determine the deflection, a best-fit approach was used. The torque on the conical section does not change from that applied to the tip section. However, the in-plane shear

modulus, G, changes from the change in braid angle as previously discussed in Section 5.4. Additionally, the polar moment of inertia, J, changes due to the changing cross-section. Since the product of G and J remain in the denominator of the twist equation, a best-fit line of this product over the conical section was found. The change in torsional rigidity, GJ, was approximated using a cubic function. For a given shaft analysis, the values of GJ along the conical section were stored and fit with a cubic function. The cubic function was then evaluated at values along the data range for GJ to check for the accuracy of the best-fit line. The approximated values are denoted as GJ_A.

$$GJ_A = 0.6188x^3 + 4.3796x^2 + 9.0203x + 3.9949 \quad \textbf{(6-27)}$$

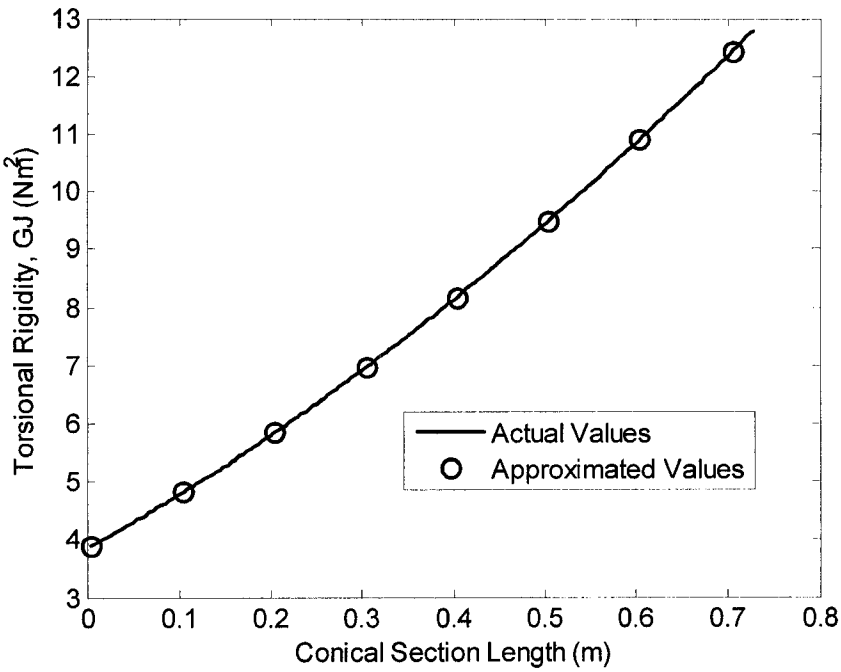

Figure 6-9: Best-fit line approximation of torsional rigidity for the conical shaft section

From Figure 6-9, the cubic approximation fits well to the actual values for GJ. The differences between the approximated values and actual values are detailed in Table 6-2.

Table 6-2: Approximated, actual and errors for the torsional rigidity of the conical section

Distance (m)	GJ (GPa)	GJ_A (GPa)	GJ error (%)
0.00425	4.036	4.033	0.067
0.10200	4.960	4.961	0.024
0.20400	6.022	6.023	0.009
0.30175	7.133	7.133	0.006
0.40375	8.392	8.392	0.006
0.50150	9.698	9.698	0.001
0.60350	11.169	11.170	0.007
0.70125	12.688	12.687	0.004

The values on this figure are for a shaft with only the minimum 95% cover factor layer made from AS4 carbon fibres. The error between the actual and approximated values is a maximum of 0.067%, which indicates that the approximated values are very close to the actual values.

The FBD for the conical section looks much like the tip section with the exception of the varying cross-section as seen in Figure 6-10.

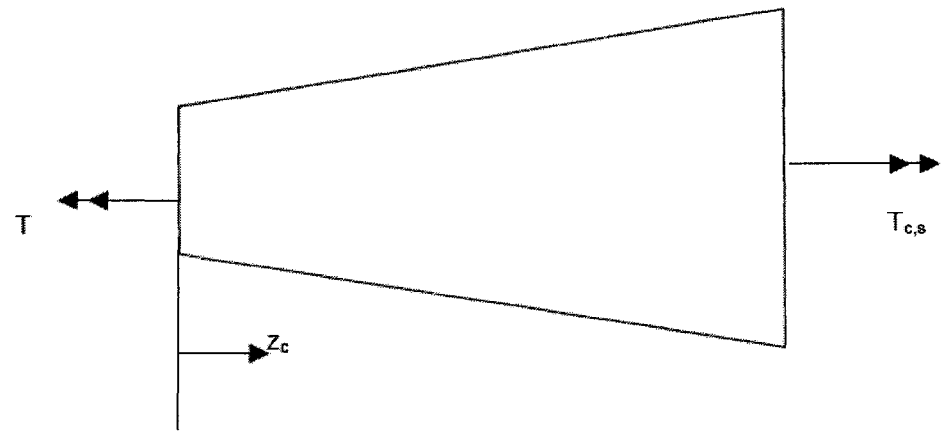

Figure 6-10: FBD of the conical shaft section to determine the angle of twist

$$T_{c,s} = T_{t,s} = T \; and \; {}^{\partial T_{c,s}}/_{T} = 1 \tag{6-28}$$

where $T_{c,s}$ is the torque on the conical section.

Finally, to determine the twist of the butt section, the analysis is the same as the tip section.

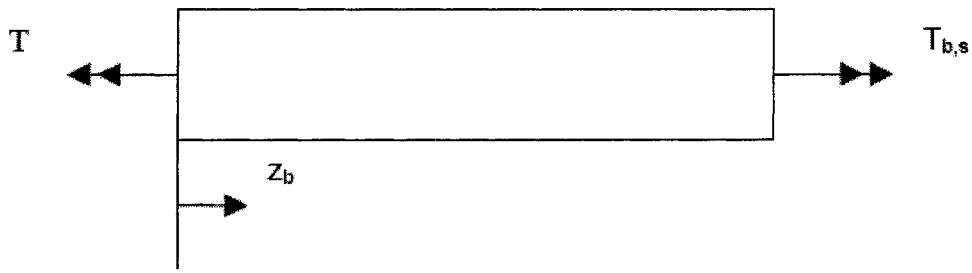

Figure 6-11: FBD of the butt section to determine the angle of twist

The torque on the butt section is still the initial torque applied to the tip section.

$$T_{b,s} = T \; and \; {}^{\partial T_{b,s}}/_{\partial T} = 1 \tag{6-29}$$

where $T_{b,s}$ is the torque on the butt section. As in the tip section, the values of G and J remain constant since the section is cylindrical and the braid angle and cross-section do not change.

To determine the angle of twist of the shaft with a foam core, the procedure is similar as for the hollow shaft. The torque applied to the tip section remains constant in each shaft section. The torsional rigidity of the shaft is the sum of the torsional rigidity of the hollow shaft, GJ_s, and the foam core, GJ_c.

$$\theta = \int_0^{L_t} \frac{T_t}{(GJ_{s,t} + GJ_{f,t})} \frac{\partial T_t}{\partial T} dz_t + \int_0^{L_c} \frac{T_c}{(GJ(z)_{s,c} + GJ(z)_{f,c})} \frac{\partial T_c}{\partial T} dz_c + \int_0^{L_b} \frac{T_b}{(GJ_{s,b} + GJ_{f,b})} \frac{\partial T_b}{\partial T} dz_b \quad \textbf{(6-30)}$$

where s and f represent the hollow shaft and foam core, respectively.

The free body diagrams for each section are identical as for the hollow section. The only difference is the sum of the hollow shaft and foam core rigidity in the denominator of the equation above and does not need to be repeated. The angle of twist for the conical section with the foam core is approximated using a cubic function based on the sum of hollow shaft and foam core GJ values.

In this chapter the methodology to determine the deflection-force and angle of twist was introduced. Castigliano's Theorem was used to determine both the deflection-force and twist by integrating over each of the three sections of the shaft. This procedure will be repeated for different lamina stacking sequences to determine an optimal shaft design.

7 SHAFT DESIGN

Design of the golf shaft was done using a progressive number of lamina. The lamina differed in number, fibre orientation and material. Mass, deflection-force, and twist were calculated for each stacking sequence and material using the methodology outlined in Chapter 6. Dimensions of the tip, conical and butt sections were modeled after a commercially available shaft but it is unknown how these lengths compare to other available shafts. However, the tip and butt end diameters are common dimensions for wood shafts produced by numerous manufacturers.

7.1 Shaft Laminate Stacking Selection

The candidate carbon fibre materials listed in Table 4-3 were evaluated to determine which material(s) would be used in the shaft design with the epoxy resin. The materials were first evaluated using three composite layers in the following sequence (from outermost to innermost): (1) braided layer with a cover factor greater than 95%, (2) braided layer with a constant 45° braid angle and (3) unidirectional layer. This stacking sequence gives a good overall picture of the rigidity that the material can produce.

The longitudinal modulus of typical fibres is much greater than the transverse modulus. Therefore, if a load is applied in the same direction as the fibres, the fibres can provide the greatest reinforcement. The longitudinal unidirectional (UD) layer is used to provide longitudinal reinforcement.

Conversely, fibres set at ±45° are used to provide shear reinforcement in golf shaft design [17]. Layers placed at ±45° provide optimal shear reinforcement due to the balance of the opposing fibre angles. As the fibre orientation rotates from 0° to 90°, the

longitudinal modulus decreases and the transverse modulus increases. Additionally, the shear modulus rises to at peak at 45° before declining. Braided laminates provide superior shear reinforcement compared to angle-ply laminates due to the interlocking of fibres between lamina. The interlocking fibres prevent shear failure from delamination.

Finally, the high cover factor (≥95%), CF, is used at the outermost layer due to superior out-of-plane properties it provides over UD lamina. It has been shown [80], that woven and braided fabrics have higher tensile, compressive and shear through-the-thickness modulus than unidirectional composites. A braided layer with a high cover factor (≥ 95%) would have higher elastic constants than a braided lamina with a low cover factor because for a given unit cell, the lower CF layer would have more matrix material. Matrix material generally has lower modulus values than strands. Therefore, a unit cell almost fully comprised of strands would have higher elastic constants. The difference in modulus values between matrix material and fibres is evident in Chapter 3. Additionally, it has been shown by Kim and Sham [81] that woven fabrics have a greater mode II failure, which may be due to tension in the through-thickness direction. The strand undulations create an uneven surface where resin pockets can provide greater plastic yield zones [81]. Strand undulations also create greater interlaminar shear strength to prevent de-bonding between fibres and matrix or fracture of the matrix between fibres [81]. Bending in the through-thickness direction, which would be experienced by a golf shaft during the swing, causes interlaminar shear stresses. Additionally, strand undulations decrease the damage from low velocity/low energy impacts compared to cross-ply lamina [81]. This is due to decreased coupling stresses due to the interlocking of the strands and the resin pockets, which may provide greater plastic yield zones.

Therefore, placing a high CF layer on the outside of the shaft may also decrease interlaminar shear in the interior UD layers in the shaft than if the UD layer was on the outside. The basic function of the CF layer is to provide additional strength against the bending forces experienced by the shaft during the swing and protection from low-velocity impacts that may be experienced by the shaft from a variety of causes (such as player neglect or miss hits).

7.2 Methodology

The mass, deflection-force and angle of twist were calculated for each material in multiple stacking sequences. The elastic constants of braided lamina were determined using the model introduced in Chapter 5. Similar elastic constants for UD lamina were found using CLPT, which was also used to determine the overall elastic constants of the laminate. The moment of inertia, I, and polar moment of inertia, J, were determined based on the thickness of the laminate. The methodology introduced in Chapter 6 was used to determine the mass, deflection-force and twist of the shaft.

The analysis was conducted to determine a lamina stacking sequence that would yield a golf shaft with a combination of mass, deflection and angle of twist (twist) comparable or better to commercially available shafts. Three basic types of lamina were considered in the analysis: (1) braided layer with strands at 45° (45), (2) unidirectional (UD) fibre lamina, with fibres oriented at 0° and (3) a braided layer with a minimum 95% cover factor (CF). Strands oriented at 45° result in braided layers with the greatest shear modulus [17]. Therefore for a given cross-sectional area, a higher shear modulus will produce a greater torsional rigidity. A 45° strand angle is commonly used for torsional reinforcement in golf shaft design [15,17].

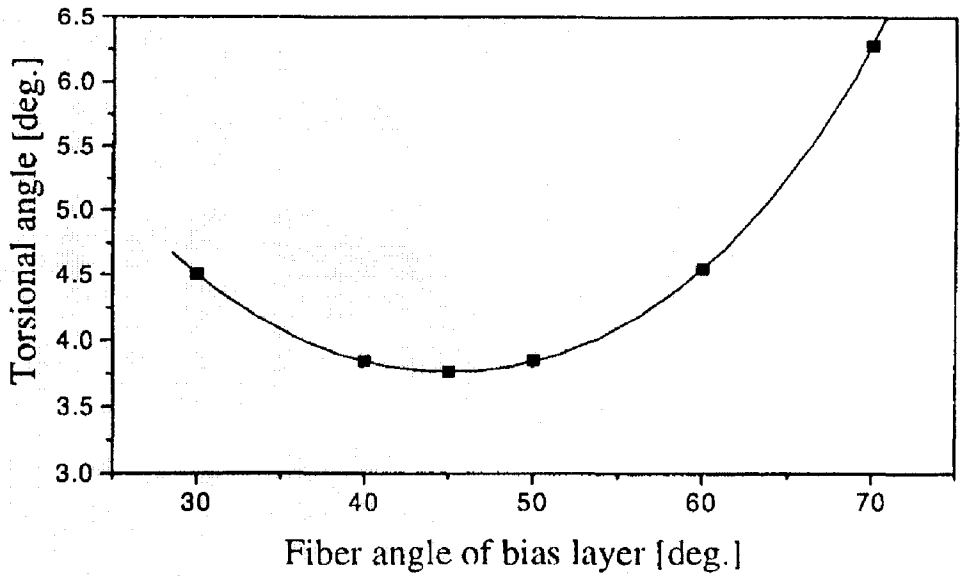

Figure 7-1: Relationship between angle of twist and fibre angle [15]

The minimum twist occurs when the strand angle is 45° as seen in Figure 7-1. Bias layers refer to intermediate layers that change in fibre angle but all other layers maintain constant fibre orientations [15]. A shaft with a low angle of twist can be interpreted as having high torsional rigidity since rigidity is defined as resistance to deformation. As previously mentioned, high shear modulus can be associated with high rigidity.

UD layers, with fibres oriented at 0°, are used for flexural reinforcement since they provide the greatest reinforcement when a force is applied in the direction of fibre orientation.

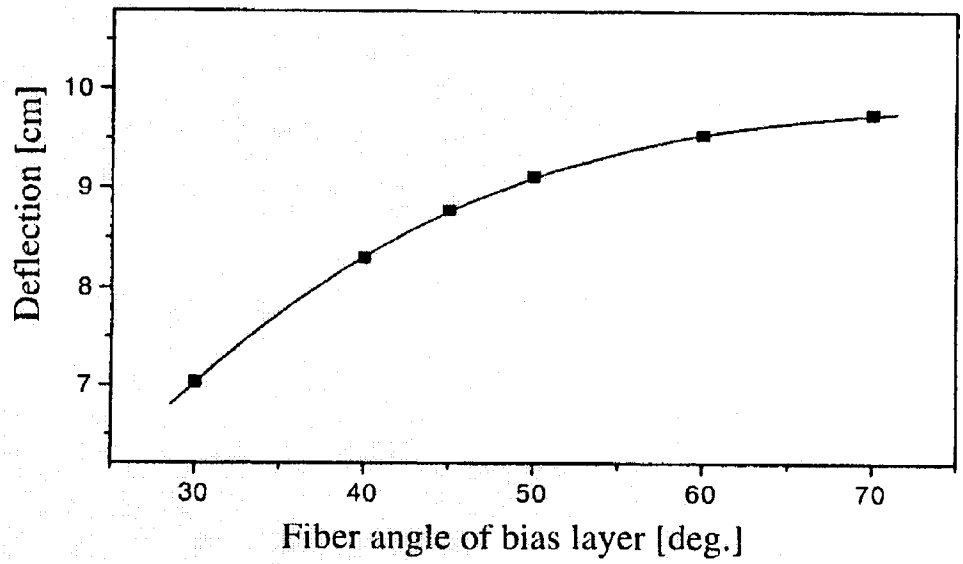

Figure 7-2: Relationship between fibre angle and deflection [15]

Figure 7-2, shows the deflection decreases with lower fibre angles. The slope of the curve can be interpolated that as the fibre angle decreases further, so shall the deflection.

The CF layer remains the outermost lamina for its high out-of-plane properties. The stacking sequence of the 45 and UD layers are evaluated to determine which order yields the lowest deflection and twist. To evaluate the optimal stacking sequence, laminates comprising of single CF, 45 and UD layers were compared. The two stacking sequences compared were [CF/UD/45] and [CF/45/UD]. [CF/UD/45] indicates that CF is the outer layer and 45 is the inner layer. The stacking sequence that yields the highest deflection-force and lowest twist will be followed. The general stacking sequence is used for the candidate design shaft materials with an initial fibre volume fraction of 60%. Also, fibre volume fractions of 50% and 70% were used to improve the shaft design. The resulting combination of shaft mass, deflection-force and twist, for each candidate

material, are compared to commercially available shafts. Based on the results, laminae are added to the shaft laminate. Data on shaft mass, deflection-force and twist for wood and irons club shafts has been accumulated [12]. Shafts are cut to pre-determined lengths according to individual manufacturers' specifications. Consistent shaft lengths are required to provide comparable test results. Both composite and steel shafts are included in the data. The shafts of interest in this study are composite and steel wood shafts. The shaft lengths for composite and steel wood shafts differ due to swingweighting. Woods shafts used in the study were built to a D-1 swingweight and used the same clubhead [12]. Since steel shafts are heavier than composite shafts, the steel shafts need to be shorter to maintain the same swingweight. The shaft mass is defined as the uncut shaft mass. For both the composite and steel shafts, the standard uncut length is 46" (1168 mm). The deflection and twist were determined using the cut shaft length. Composite shafts had a cut length of 44.2" (1122 mm) and steel shafts a cut length of 41.7" (1059 mm) [12]. The results from the analysis of each stacking sequence were compared to composite and steel woods shafts in Table 7-1.

Table 7-1: Commercial composite and steel woods shafts used for comparison with design shaft results [12]

Shaft Model	Flex	Shaft Type	Mass (g)	Deflection-Force (N)	Twist (degrees)
Aldila NVS 55	R	Composite	55.4	8.34	5.20
Aldila NVS 55	S	Composite	57.3	10.01	5.02
Aldila NVS 65	R	Composite	66.4	8.90	4.01
Aldila NVS 65	S	Composite	67.5	10.01	3.91
Aldila NV 75	R	Composite	79.4	9.17	3.26
Aldila NV 75	S	Composite	77.5	11.12	3.44
Grafalloy Blue	S	Composite	61.6	11.12	3.39
Grafalloy Blue	X	Composite	62.2	12.79	3.31
Grafalloy ProLite 35	S	Composite	64.8	11.40	4.14
Grafalloy ProLite 35	X	Composite	68.7	13.07	3.43
UST ProForce 65	R	Composite	70.5	9.17	3.73
UST ProForce 65	S	Composite	70.0	10.29	3.57
UST ProForce 75	R	Composite	79.9	11.68	3.72
UST ProForce 75	S	Composite	80.8	13.07	3.70
Royal Precision Rifle	R	Steel	122.5	12.23	2.60
Royal Precision Rifle	S	Steel	126.2	13.07	2.50
Royal Precision Rifle	X	Steel	130.5	13.90	2.50
True Temper Dynalite Gold	S	Steel	111.9	12.51	2.64
True Temper Dynalite Gold	X	Steel	117.3	13.07	2.41
True Temper Dynamic Gold	S	Steel	123.8	13.07	2.75
True Temper Dynamic Gold	X	Steel	120.5	13.62	2.67

7.3 Results for Golf Shafts Made of a Single Material

The initial analysis of the stacking sequence for the shaft design used a [CF/UD/45] and [CF/45/UD] layering. The thickness of UD and braided lamina for AS4, T800H, M40J and T700S is in Table 7-2.

Table 7-2: Material unidirectional and braid lamina thickness for 60% V_f [19*]

Material	UD Lamina Thickness* (mm)	Braided Lamina Thickness (mm)
AS4	0.160	0.320
T800H	0.112	0.224
M40J	0.083	0.166
T700S	0.119	0.224

The thickness of braided lamina for each material is twice that of UD lamina due to the strands undulating during the braiding process. Results for the mass, deflection-force and twist were calculated using equations from Chapter 6.

Table 7-3: Laminate thickness, mass, deflection-force and twist of [CF/45/UD] stacking sequence

Material	Laminate Thickness (mm)	Mass (g)	Deflection-Force (N)	Twist (degrees)
AS4	0.80	54.6	9.71	5.00
T800H	0.56	39.0	8.12	8.00
M40J	0.42	28.6	8.12	6.78
T700S	0.60	41.3	6.97	6.88

Table 7-4: Laminate thickness, mass, deflection-force and twist of [CF/UD/45] stacking sequence

Material	Laminate Thickness (mm)	Mass (g)	Deflection-Force (N)	Twist (degrees)
AS4	0.80	54.6	9.71	5.00
T800H	0.56	39.0	8.12	8.00
M40J	0.42	28.6	8.12	6.78
T700S	0.60	41.3	6.97	6.88

Results listed in Table 7-3 and Table 7-4, are identical for both [CF/UD/45] and [CF/45/UD] laminates. This indicates that for these laminates, the order to the 45 and UD laminae do not substantially affect the flexural or torsional rigidity. To compare the rigidity of the laminates, the results for the cylindrical tip section are presented in Table 7-5 and Table 7-6.

Table 7-5: Flexural and torsional rigidity for the [CF/45/UD] laminate

Material	$E_{x,tip}$ (GPa)	I_{tip} (mm^4)	$EI_{,tip}$ ($GPa \cdot m^4$)	$G_{xy,tip}$ (GPa)	J_{tip} (mm^4)	$GJ_{,tip}$ ($GPa \cdot m^4$)
AS4	43.49	145	6.3	23.98	290	7.0
T800H	49.78	111	5.5	19.27	222	4.3
M40J	63.04	86	5.4	30.34	172	5.2
T700S	39.48	116	4.6	22.14	232	5.1

Table 7-6: Flexural and torsional rigidity for the [CF/UD/45] laminate

Material	$E_{x,tip}$ (GPa)	I_{tip} (mm^4)	$EI_{,tip}$ ($GPa \cdot m^4$)	$G_{xy,tip}$ (GPa)	J_{tip} (mm^4)	$GJ_{,tip}$ ($GPa \cdot m^4$)
AS4	43.49	145	6.3	23.98	290	7.0
T800H	49.78	111	5.5	19.27	222	4.3
M40J	63.04	86	5.4	30.34	172	5.2
T700S	39.48	116	4.6	22.14	232	5.1

The tip section was chosen for comparison since the shear modulus is greatest along this segment. As detailed in Figure 5-18, the in-plane shear modulus for the CF lamina is a maximum in the tip section. Also, the shear modulus of the 45 lamina will remain constant along the shaft length since the cover factor is held constant. From the results in Table 7-5 and Table 7-6, it was expected that the moment of inertia, I_{tip}, and polar moment of inertia, J_{tip}, would not change since the laminate thickness remained constant. However, the longitudinal modulus, $E_{x,tip}$, and in-plane shear modulus, $G_{xy,tip}$, also did not change between the two laminates, for any material. It is evident that the change in distance of the of the UD or 45 lamina, with respect to the laminate midplane, is not sufficient to alter, $E_{x,tip}$ or $G_{xy,tip}$. The mass of each single material design shaft is less than each commercial shaft. The deflection-force, for the T800H, M40J and T700S shafts, are lower than the commercial shafts. However, the deflection-force, of 9.71 N,

for the AS4 shaft is greater than the Aldila NVS 55 R, Aldila NVS 65 R, Aldila NV 75 R and UST ProForce 65 R composite shafts. Additionally, only the twist for the AS4 shaft was lower than any of the commercial shafts. The AS4 shaft has a lower twist, at 5.00°, than the Aldila NVS 55 R and Aldila NVS S at 5.20° and 5.02°, respectively. The results in Table 7-3 and Table 7-4 do not indicate which lamina stacking sequence would provide the best combination of flexural and torsional rigidity. Since the deflection-force for the design shafts is comparable to a greater number of commercial shafts than the twist, a 45 layer was added to increase torsional rigidity. This increased the laminate thickness of the AS4, T800H, M40J and T700S to 1.12 mm, 0.74 mm, 0.58 mm and 0.83 mm, respectively.

Table 7-7: Laminate thickness, mass, deflection-force and twist of [CF/45$_2$/UD] stacking sequence

Material	Laminate Thickness (mm)	Mass (g)	Deflection-Force (N)	Twist (degrees)
AS4	1.12	74.4	10.86	3.55
T800H	0.78	53.6	9.30	5.04
M40J	0.58	39.5	9.20	4.30
T700S	0.83	56.7	7.87	4.77

Table 7-8: Laminate thickness, mass, deflection-force and twist of [CF/UD/45$_2$] stacking sequence

Material	Laminate Thickness (mm)	Mass (g)	Deflection-Force (N)	Twist (degrees)
AS4	1.12	74.4	10.86	3.55
T800H	0.78	53.6	9.30	5.04
M40J	0.58	39.5	9.20	4.30
T700S	0.83	56.7	7.87	4.77

There is no difference in the results for the stacking sequences in Table 7-7 and Table 7-8. This was also observed with the [CF/UD/45] and [CF/45/UD] laminates. The affect of lamina stacking on the longitudinal modulus, in-plane shear modulus, flexural rigidity and torsional rigidity, for both [CF/45_2/UD] and [CF/UD/45_2] laminates, is detailed in Table 7-9 and Table 7-10.

Table 7-9: Flexural and torsional rigidity for the [CF/45_2/UD] laminate

Material	$E_{x,tip}$ (GPa)	I_{tip} (mm^4)	$EI_{,tip}$ (GPa·m^4)	$G_{xy,tip}$ (GPa)	J_{tip} (mm^4)	$GJ_{,tip}$ (GPa·m^4)
AS4	36.78	181	6.7	25.52	362	9.2
T800H	44.66	143	6.4	22.75	286	6.5
M40J	51.80	114	5.9	34.48	227	7.8
T700S	33.07	150	4.9	23.53	299	7.0

Table 7-10: Flexural and torsional rigidity for the [CF/UD/45_2] laminate

Material	$E_{x,tip}$ (GPa)	I_{tip} (mm^4)	$EI_{,tip}$ (GPa·m^4)	$G_{xy,tip}$ (GPa)	J_{tip} (mm^4)	$GJ_{,tip}$ (GPa·m^4)
AS4	36.78	181	6.7	25.52	362	9.2
T800H	44.66	143	6.4	22.75	286	6.5
M40J	51.80	114	5.9	34.48	227	7.8
T700S	33.07	150	4.9	23.53	299	7.0

The trend is similar to that observed in Table 7-5 and Table 7-6. The results for all of the results in Table 7-9 and Table 7-10 are identical. Again, it appears that the midplane distance of the 45 and UD lamina does not affect $E_{x,tip}$ or $G_{xy,tip}$ of the design shafts. The laminate thickness of the AS4 exceeds the conditions of the thin-wall assumption for the tip section. The ratio of the outer tip diameter to wall thickness is 7.59, which is below the minimum of 10. Additionally, the T700S wall thickness is close to the minimum at 10.24. However, previous work [82] has shown that the thin-wall assumption may be

violated but still produce reliable results. Furthermore, the tip section of the shaft is only approximately 8.7% of the total shaft length, which represents a small segment of the overall length. The deflection-force of the AS4, T800H and M40J design shafts ranged from 9.20 N – 10.86 N, which was greater than the Aldila NVS 55 R/S, Aldila NVS 65 R/S, Aldila NV 75 R and UST Proforce 65 R composite shafts. The deflection-force for the Aldila NVS 55 R/S, Aldila NVS 65 R/S, Aldila NV 75 R and UST Proforce 65 R shaft ranged from 8.43 – 10.01 N. The twist of all the single material design shafts was lower than the Aldila NVS R/S. Additionally, the twist of the AS4 shaft is also lower than the Aldila NVS 65 R/S, Grafalloy ProLite 35 S, UST ProForce 65 R/S and UST ProForce 75 R/S, with a magnitude of 3.55°. The mass of the AS4 shaft was greater than most of the composite shafts but none of the steel shafts. The mass of the other materials was lower than any of the commercial shafts. Since the order of the 45 and UD laminae did not appear to change the longitudinal or in-plane shear moduli, a stacking order was arbitrarily set. The lamina order was set at [CF/45/UD], with additional 45 and UD layers added to increase flexural or torsional rigidity. A 45 layer was added to increase the torsional rigidity, since the design shafts were comparable to a lower proportion of shafts in terms of twist than deflection-force. This caused the AS4 laminate to increase in thickness to 1.44 mm, the T800H to 1.01 mm, the M40J 0.75 mm and the T700S to 1.07 mm.

Table 7-11: Laminate thickness, mass, deflection-force and twist of [CF/45$_3$/UD] stacking sequence

Material	Laminate Thickness (mm)	Mass (g)	Deflection-Force (N)	Twist (degrees)
AS4	1.44	93.0	11.59	2.89
T800H	1.01	67.6	10.10	3.81
M40J	0.75	50.1	9.93	3.24
T700S	1.07	71.5	8.50	3.79

The mass of the AS4 shaft, at 93.0 g, was greater than all of the composite shafts but lower than the steel shafts. The heaviest composite shaft is the UST ProForce 75 S at 79.9 g and the lightest steel shaft is the True Temper Dynalite Gold S at 111.9 g. The 71.5 g T700S and 67.6 g T800H shafts were heavier than the Aldila NVS 55 R/S, Aldila NVS R/S and Grafalloy Blue S/X. The T700S shaft was also heavier than the UST ProForce 65 R/S. The M40J was lighter, at 50.1 g, than all of the commercial shafts. The deflection-force for all the design shaft materials was comparable to the commercial composite shafts, which range from 8.90 N to 13.07 N, but lower than the steel shafts.. The twist of all the single material shafts is comparable to the composite shafts but not the steel shafts. The design shafts angle of twist ranged from 2.89° (AS4) to 3.81° (T800H). The lowest twist for the composite shafts is 3.26° (Aldila NVS 55 R) and 2.41° for the steel shafts (True Temper Dynamic Gold X). Since the twist was comparable to the commercial composite shafts, a UD layer was added to increase the flexural rigidity of the design shafts. The AS4, T800H, M40J and T700S laminate thickness increased to 1.60 mm, 1.12 mm, 0.83 mm and 1.19 mm, respectively.

Table 7-12: Laminate thickness, mass, deflection-force and twist of [CF/45$_3$/UD$_2$] stacking sequence

Material	Laminate Thickness (mm)	Mass (g)	Deflection-Force (N)	Twist (degrees)
AS4	1.60	101.8	16.14	2.93
T800H	1.12	74.4	14.06	3.83
M40J	0.83	55.2	14.62	3.28
T700S	1.19	78.6	12.01	3.84

As seen in Table 7-12, the mass of the 101.8 g AS4 shaft was greater than the composite shafts but lower than the steel shafts. The mass for the T800H, M40J and T700S shafts ranged from 55.2 g – 78.6 g, which was comparable to the composite shafts. The deflection-force of all the design material shafts was comparable to the commercial shafts, with the exception of the T700S shaft. The 12.01 N deflection-force of the T700S shaft was in the range for the composite shafts but lower than the steel shafts. One interesting observation between the [CF/45$_3$/UD] and [CF/45$_3$/UD$_2$] laminates was that the angle of twist increased. This was due to the change in polar moment of inertia and in-plane shear modulus.

Table 7-13: Comparison of in-plane shear modulus and polar moment of inertia between the [CF/45$_3$/UD] and [CF/45$_3$/UD$_2$] laminates

Material	[CF/45$_3$/UD] Laminate			[CF/45$_3$/UD$_2$] Laminate		
	$G_{xy,tip}$ (GPa)	J_{tip} (mm^4)	$GJ_{,tip}$ (GPa·m^4)	$G_{xy,tip}$ (GPa)	J_{tip} (mm^4)	$GJ_{,tip}$ (GPa·m^4)
AS4	26.37	415	10.9	24.28	435	10.6
T800H	24.67	339	8.4	22.65	362	8.2
M40J	36.78	276	10.2	33.50	297	9.9
T700S	24.31	352	8.6	22.32	375	8.4

As in Table 7-5 and Table 7-6, the tip section was used for comparison. As expected, the polar moment of inertia, J_{tip}, is greater for the [CF/45$_3$/UD$_2$] than the [CF/45$_3$/UD]

laminate due the increase in wall thickness. However, both the in-plane shear modulus, $G_{xy,tip}$, and torsional rigidity, $GJ_{,tip}$, decrease with the addition of a UD lamina. This is due to the influence of the UD layer on the overall shear modulus of the lamina. From CLPT, the in-plane shear modulus decreases as the braid angle goes to 0°. Consequently, the laminate shear modulus would decrease with the addition of a UD lamina. Additionally, the decrease in laminate in-plane shear modulus was proportionately greater than the increase in polar moment of inertia. The deflection-force of the AS4, T800H and M40J shafts, in Table 7-12, were greater than both the steel and composite shafts. In fact, the shafts may be too stiff. Recall, if a shaft is too stiff it will not properly "unload" during the downswing. However, this does show the potential of using braided lamina to produce stiff golf shafts. A 45 lamina was added and a UD layer removed to increase the torsional rigidity and decrease the flexural rigidity.

Table 7-14: Laminate thickness, mass, deflection-force and twist of [CF/45$_4$/UD] stacking sequence

Material	Laminate Thickness (mm)	Mass (g)	Deflection-Force (N)	Twist (degrees)
AS4	1.76	110.4	12.06	2.52
T800H	1.23	81.1	10.67	3.16
M40J	0.91	60.3	10.45	2.65
T700S	1.31	85.5	8.96	3.22

The results show a decrease in deflection-force and increase in both mass and twist for the [CF/45$_4$/UD] compared to the [CF/45$_3$/UD$_2$] laminate. The deflection-force for each design shaft was within the range of 8.34 N – 13.07 N for the composite shafts. However, the deflection-force was below the outside the minimum the range of 12.23 N – 13.90 N for the steel shafts. The twist for each design shaft was lower than all of the

composite shafts. Additionally, the 2.52° twist of the AS4 shaft and 2.65° twist of the M40J were comparable to the steel shafts. However, with the exception of the 60.3 g M40J shaft, the mass for the design shafts were greater than the composite shafts. Consequently, only the M40J shaft was within the range of composite shafts in terms of deflection-force, twist and mass. The angle of twist values for the [CF/45_4/UD] laminate details the potential of using braiding to produce torsionally rigid shafts.

Based on the results for the single material design shafts, it is apparent that a golf shaft can be designed, using braided lamina that is comparable to composite and steel shafts in terms of mass and flexural and torsional rigidity. However, the shaft design can be improved by utilizing the strengths of the individual shaft materials. Improvement of the shaft design may be possible by using laminates comprised of multiple shaft materials.

7.4 Results for Golf Shafts Made of Multiple Materials

The shaft design could be improved by creating a shaft of multiple materials. Based on the results in the previous section certain materials are better in either deflection or twist. The M40J is optimal weight reduction while maintaining flexural and torsional rigidity. The M40J has the lowest density, compared to the other materials, and was therefore expected to produce a lighter shaft. The T800H was utilized to increase torsional rigidity and preserving mass. These materials were chosen to create a shaft comparable to the composite shafts. The AS4 provides good flexural and torsional rigidity but also adds mass. This material, in tandem with the M40J, may be used to create a shaft comparable to the steel shafts. Two shafts were designed using a [CF/45_4/UD] laminate. This stacking sequence was chosen because the single material

shaft results due to the torsional rigidity produces. One design shaft was produced to compare to the composite commercial shafts and another to the steel commercial shafts. A shaft laminate, 0.95 mm thick, comprised of M40J UD and CF layers and T800H 45 layers were analyzed to compare with the composite shafts. A shaft, with a wall thickness of 1.14 mm, consisting of M40J CF and UD layers and AS4 45 layers was modeled to evaluate against the steel shafts.

Table 7-15: Laminate thickness, mass, deflection-force and twist for multiple shaft materials for [CF/45_4/UD] stacking sequence

Material	Laminate Thickness (mm)	Mass (g)	Deflection-Force (N)	Twist (degrees)
M40J/T800H	0.95	75.2	10.66	2.97
M40J/AS4	1.14	96.8	11.77	2.58

The M40J/T800H was comparable to the composite shafts in terms of deflection-force and twist. The 10.66 N deflection-force, of the design shaft, was in the upper range of listed composite shafts. The 2.97° twist was lower than any composite shaft but has a greater mass, at 75.2 g, than all of composite shafts except the Aldila NV 75 R/S and UST ProForce 75 R/S shafts. The M40J/AS4 shaft has a lower mass, at 83.4 g, than any of the steel shafts. Additionally, the 2.58° twist was in the range of 2.41° - 2.75° for steel shafts. However, the deflection-force, of 11.77 N, was lower than any steel shaft.

To further attempt to optimize the shaft design, the fibre volume fraction, V_f, was changed to 50% and 70%. This was done to determine the effect of V_f on the mass, deflection-force and twist of the design shaft. The variation in fibre volume fraction was actually a change in the matrix volume. The fibre volume remained constant while the corresponding matrix volume either increased or decreased. This was applied to the

M40J/T800H and M40J/AS4 shaft to improve the results from Table 7-15. The thickness of the 50% V_f and 70% V_f AS4 and T800H laminates change with fibre volume fraction. The thickness of the M40J, T800H and AS4 laminae, for 50% V_f, is 0.0996 mm, 0.134 mm and 0.192 mm, respectively. This corresponds to a laminate thickness of 0.1.10 mm, 1.47 mm and 2.11 mm, respectively. With a 70% V_f, the lamina thickness decreases to 0.071 mm, 0.096 mm and 0.137 mm for the M40J, T800H, and AS4 materials. The resulting laminate thicknesses are 0.78 mm, 1.06 mm and 1.51 mm for the M40J, T800H and AS4, respectively. The increase in lamina mass with a 50% V_f, compared to 60% V_f, is due to the increase in matrix material relative to the fixed fibre volume fraction. This also contributes to the increase in 50% V_f lamina thickness. Likewise for the 70% V_f lamina, the mass and thickness decrease due to the reduced matrix volume.

Table 7-16: Laminate thickness, mass, deflection-force and twist for [CF/45$_4$/UD] laminate and 50% V_f

Material	Laminate Thickness (mm)	Mass (g)	Deflection-Force (N)	Twist (degrees)
AS4	2.11	123.4	10.74	2.80
M40J	1.10	68.7	9.89	2.80
T800H	1.47	91.6	9.88	3.34

Table 7-17: Laminate thickness, mass, deflection-force and twist for [CF/45$_4$/UD] laminate and 70% V_f

Material	Laminate Thickness (mm)	Mass (g)	Deflection-Force (N)	Twist (degrees)
AS4	1.51	100.4	13.54	2.31
M40J	0.78	54.1	11.06	2.54
T800H	1.06	73.2	11.56	2.97

Comparing the results in Table 7-12, Table 7-16 and Table 7-17, the mass for M40J, T800H and AS4 decreased 14.6 g, 18.4 g and 23.0 g, respectively from a 50% V_f to 70%. The deflection-force increased 1.17 N for the M40J, 2.80 N for the AS4 and 1.68 N for the T800H with an increase from 50% V_f to 70% V_f. Additionally, the twist decreased for the AS4, T800H and M40J, 0.49°, 0.37° and 0.26°, respectively from 50% V_f to 70%. The 18.4 g change in mass for the T800H is a 20.1 % decrease, while the 0.37° decrease in twist corresponds to 11.1%. The deflection-force increased 26.1%, 11.8% and 17.0% for the AS4, T800H and M40J, respectively over the V_f range. Similarly, the M40J decreased 21.3% in mass and 9.29% in twist from a 50% to 70% fibre volume fraction. Consequently, the laminas with a 70% V_f appeared to provide lower mass and superior flexural and torsional rigidity with respect to the 50% and 60% V_f. An increase in fibre volume fraction increases flexural and torsional rigidity and increases mass. Therefore, a design shaft with 70% V_f should yield better results than with 60% V_f.

Table 7-18: Laminate thickness, mass, deflection-force and twist for modified [CF/45$_4$/UD] laminates

Material	Laminate Thickness (mm)	Mass (g)	Deflection-Force (N)	Twist (degrees)
M40J/T800H	0.86	67.8	11.47	2.81
M40J/AS4	0.97	87.7	13.09	2.39

The mass of the M40J/T800H shaft decreased 9.84% with a 70% V_f compared to a 60% V_f. Additionally, the deflection-force increased 7.60% while the angle of twist decreased 5.39%. These are all improvements over the results in Table 7-15. This design shaft has lower twist, than all of the composite shafts, of 2.81°. The deflection-force, of 11.47 N, is only lower than the Grafalloy Blue X, Grafalloy ProLite 35 X and UST

ProForce 75 S. However, the mass is greater than half of the composite shafts including the Aldila NVS 55 R/S, Aldila NVS R/S, Grafalloy Blue S/X, Grafalloy ProLite 35 S.

The M40J/AS4 shaft decreased in mass and twist by 9.40% and 7.36%, respectively from a 60% - 70% V_f. Additionally, the deflection-force increased 11.21%. In comparison to the steel shafts, the M40J/AS4 design shaft has lower twist, of 2.39°, than any steel shaft listed. Additionally, the 87.7 g mass of the design shaft is 21.6% lower than the lightest steel shaft (True Temper Dynalite Gold S). However, the deflection-force, of 13.09 N, is lower than the Royal Precision Rifle X and True Temper Dynamic Gold X shafts.

Both of the final design shafts, listed in Table 7-18, are comparable to composite and steel shafts. In case of the M40J/T800H, the relatively high flexural and torsional rigidity is offset by the mass. The mass is in the median of values for the commercial composite shafts. This shaft may be beneficial to a player with a relatively fast swing, where the mass will not hamper generation of clubhead speed. The M40J/AS4 shaft is much lighter than the listed steel shafts. Additionally, the twist is lower compared to the commercial shafts. The deflection-force is among the highest of the steel shafts. This shaft would also be useful to a player with a fast swing and a problem getting the clubface square to the ball at impact.

8 ANALYSIS OF THE INFLUENCE OF A FOAM CORE ON SHAFT DESIGN

An analysis on the influence of using the foam core materials was conducted using the materials listed in Table 4-5 and M40J/T800H design shaft from Table 7-18. Either design shaft from Table 7-18 could have been used, but the M40J/T800H was chosen for its lower mass and higher deflection-force and twist. By using the design shaft as a baseline, the influence of the core materials may be better analyzed. The results for the mass, deflection-force and twist for each of the foam materials is in Table 8-1.

Table 8-1: Mass, deflection-force and twist of design shaft with a foam core

Material	Total Shaft Mass (g)	Mass Diff. (g) / (%)	Deflection Force (N)	Defl. Force Diff. (N) / (%)	Twist (deg.)	Twist Diff. (deg.) / (%)
M40J/T800H	67.8	-	11.47	-	2.81	-
Sawbones Rigid Polyurethane	155.3	87.5 / 129.1	13.18	1.71 / 14.9	2.62	-0.19 / -6.76
Cymat Aluminum Foam	100.6	32.8 / 48.4	12.96	1.49 / 13.0	2.58	-0.23 / -8.19
Degussa Rohacell 110 IG PMI	79.9	12.1 / 17.8	12.73	1.26 / 11.0	2.64	-0.17 / -6.05
DIAB Klegecell R 260 PVC	90.2	22.4 / 33.0	12.75	1.28 / 11.2	2.63	-0.18 / -6.41
DIAB Divinylcell HT 110 IPN	80.0	12.2 / 18.0	12.73	1.26 / 11.0	2.64	-0.17 / -6.05
DIAB Divinylcell H 250 Semi-rigid PVC	95.8	28.0 / 41.3	12.74	1.27 / 11.1	2.63	-0.18 / -6.41

The differences in mass, deflection-force and twist are with respect to the M40J/T800H design shaft. When discussing a shaft with a particular foam core material, it is referred to by the core material name. It is assumed that composite portion of the shaft is the M40J/T800H from Table 7-18. The mass of the shafts with foam cores were all lighter than the steel shafts of Table 7-1, with the exception of the Sawbone at 155.3 g.

Additionally, the cored shafts were heavier than all of the commercial composite shafts, with masses ranging from 79.9 g–155.3 g (17.8%-129.1%). Each of the cored shafts yielded a higher deflection-force and lower twist than the design shaft. The increase in deflection-force ranged from 1.26 N–1.71 N (11.0%-14.9%) and the decrease in twist ranged from 0.17°–0.23° (6.05%-8.19%). Only the 13.18 N deflection-force of the Sawbone was greater than of the commercial composite shafts. The deflection-force of the cored shafts was comparable to the steel shafts. Additionally, the twist of the cored shafts was comparable to the steel shafts and greater than composite shafts.

Using foam cores to reinforce composite golf shafts may be a possible design consideration. However, the increase in mass was a *minimum* of 17.8% while the change in deflection-force and twist was a *maximum* of 14.9% and -8.19%, respectively. Therefore, it may be necessary to only use the core in a portion of the shaft to minimize the increase in mass and maximize the increase in flexural and torsional reinforcement. For example, using a core in the tip section of the shaft may provide optimal torsional reinforcement since this is the location of maximum twist. A foam core in the tip section may also provide flexural reinforcement without adding significant mass.

Golf shafts were designed using carbon fibre and epoxy resin materials and compared to commercially available composite and steel golf shafts. Multiple laminate stacking sequences were evaluated based on the resulting mass, deflection-force, and angle of twist compared to commercial shafts. Laminates were used with single or multiple materials. A fibre volume fraction of 50%, 60% and 70% was used for the multiple material laminates. It was found that using a laminate comprised of multiple materials could produce design shafts with comparable mass, deflection-force and twist

to commercially available shafts. This showed that braiding could be used as an alternative technology to hand lay-up and filament winding. A preliminary investigation into the benefit of using foam materials as a solid core for a golf shaft was conducted. Multiple foam core materials were used and evaluated based on the increase in shaft mass and deflection-force and the decrease in twist. The *minimum* increase in shaft mass was 17.8% while the *maximum* increase in deflection-force and decrease in twist was 14.9% and -8.19%, respectively.

9 CONCLUSIONS AND FUTURE WORK

9.1 Conclusions

Braiding is not currently a widely used manufacturing technique in the production of golf shafts. The objective of this thesis was to design a composite golf shaft, using braiding that would be comparable to commercially available composite and steel golf shafts. The comparison between shafts was based on shaft mass, deflection-force and angle of twist. To achieve this, a predictive model was developed to calculate the cover factor and elastic constants of a single-layered, conical braided composite. The model was validated through comparisons with previous works and applied to model a golf shaft. The model was expanded to also calculate the cover factor and elastic constants of the cylindrical tip and butt sections. The design of the golf shaft utilized both braided and unidirectional lamina in multiple stacking sequences. The results of the analysis showed that a composite golf shaft could be produced that was comparable to commercially available shafts. Additionally, a preliminary investigation into the use of foam materials as shaft core yielded mixed results.

The goal of the work is to show that 2D braiding is a viable technology in the production of golf shafts. The thesis contains a review of previously published literature on golf shafts, braided composite materials and foam core materials. Information presented on golf shafts included previous work detailing the deformation of the golf shaft during the golf swing, typical golf shaft design parameters and the use of composites in golf shaft design. Literature presented on braided composites included work on modelling the braiding process and determining the cover factor. Additionally,

previous models to determine the elastic constants of braided composites were detailed. A review of the use of foam core materials in tubular structures was given.

Second, a predictive model to determine the cover factor and elastic constants of a conical braided composite was developed from previous works. A constraint of the model was to sustain a minimum cover factor of 95%. The cover factor was determined using a trapezoidal unit cell while the elastic constants were predicted using a rectangular unit cell and was based on the CLPT. A condition of the model was to maintain a maximum unit cell area difference of 5%. The resulting difference in unit cell area was below 1%. Comparing the results to previous works validated the model. The conical model was expanded to also calculate the cover factor and elastic constants of the cylindrical tip and butt sections of a golf shaft. Comparing the results to those produced by the conical model validated the model for a golf shaft.

The golf shaft model was used, along with Castigliano's Theorem, to determine the mass, deflection-force and angle of twist. The methodology to determine the deflection-force consisted of dividing the golf shaft into its three sectional components, i.e. the tip, tapered and butt sections and applying a point load the to tip of the cantilevered shaft. The mass of the shaft was included in the analysis to provide accurate results. The twist of the shaft also consisted of using a cantilevered shaft and had a torque applied 50.4 mm (2 inches) from the tip. Both the deflection-force and twist were also calculated with a foam material used as a solid golf shaft core.

The design of the golf shaft consisted of using multiple materials and stacking sequences to produce a golf shaft with comparable mass, deflection-force and twist with commercially available composite and steel shafts. The data on commercial shafts was

taken from previous work [12] that tested numerous shafts for properties such as mass deflection-force and twist. Additionally, the affect of changing the fibre volume fraction on the properties of the design golf shaft was detailed to optimize the design. Fibre volume fractions of 50%, 60% and 70% were used in the design process. It was found that by using a combination of braided and unidirectional lamina and multiple materials a design shaft could be produced that was comparable in mass, deflection-force and twist. Golf shafts that utilize braided lamina offer the golf industry an alternate form of production from hand lay-up and/or filament winding. Manufacturing costs may be decreased since hand lay-up requires manual labour to produce shafts, while braiding is a fully automated process. Lower productions costs could yield lower commercial prices for golfers. This may allow players to purchase shafts, at a lower price, that provide the desired characteristics of current shafts. The variability of braiding, in terms of braid angle and fibre volume fraction, would allow for a multitude of different shaft designs to better match player requirements.

Finally, a preliminary evaluation into using foam materials as a solid golf shaft core was conducted. Multiple foam core materials were evaluated based on the affect on shaft mass, deflection-force and twist. The results were mixed. While the deflection-force increased and the twist decreased with the foam cores, the increase in mass was proportionately greater.

9.2 Future Work

The work presented in this thesis offers areas of continuing research in the field of both braided composites and golf shaft design. Some possible areas of future work are given below:

1) Development of a model to predict elastic constants using trapezoidal unit cell. Eliminating the need to check the difference in unit cell area between the trapezoidal and rectangular unit cells would allow for greater application of the model to conical composites with a greater cone angle.

2) Further investigation using foam core materials. Perhaps only using the core in a section of the shaft rather than the entire length to minimize the increase in mass. Another possibility for core materials in golf shaft design may be for their dampening capabilities.

3) Dynamic analysis of the design shafts to evaluate the deformation of the design shaft during the swing. This may be done using FE models.

4) Further optimization of the design shafts. Using different materials, braid angles, braid types (regular and Hercules), fibre volume fractions and laminate stacking sequences may be possible areas of investigation.

All of the above are possible areas of future research based on the work detailed in this thesis.

REFERENCES

1 Summit, J. (2000), The Modern Guide to Shaft Fitting, 2nd edition, Dynacraft Golf Products Inc., Newark, Ohio

2 Naik, N.K., Nemani, B. (2001), Initiation of Damage in Composite Plates Under Transverse Central Static Loading, Journal of Composite Structures, v. 52, Pg. 167-172

3 Ko, F., Pastore, C., Head, A. (1989), Atkins and Pearce Handbook of Industrial Braiding, Atkins and Pearce, Covington, Kentucky, 1989

4 Horwood, G.P (1994), Golf Shafts – A Technical Perspective, Science and Golf II: Proceedings of the World Scientific Congress of Golf, 1st edition, E & FN Epon, London, England

5 The Tutelman Site, Dave T's Golf Technology Articles, from website: http://www.tutelman.com/golfclubs, accessed June 2006

6 Milne, R.D., Davis, J.P. (1992), The Role of the Shaft in the Golf Swing, Journal of Biomechanics, 25(9): 975-983

7 Butler, J.H., Winfield, D.C. (1994), The Dynamic Performance of the Golf Shaft During the Downswing, Science and Golf II: Proceedings of the World Scientific Congress of Golf, 1st edition, E & FN Epon, London, England

8 Penner, A.R. (2002), The Physics of Golf, Reports on Progress in Physics, 66: 131-171

9 Club Head Speed Golf, from website: http://www.clubheadspeed.net, accessed November 2006

10 Pelz, D. (1990), A Simple, Scientific, Shaft Test: Steel Versus Graphite, Science and Golf: Proceedings of the First World Scientific Congress of Golf, 1st edition, E & FN Epon, London, England

11 Hireko Golf, from website: http://www.hirekogolf.com, accessed September 2006

12 Summit, J. (2006), 2006 Shaft Fitting Addendum, 1st edition, Dynacraft Golf Products Inc., Newark, Ohio

13 Matsumoto, T., Kojima, A., Horii, H., Mohri, M. (1996), Golf Club Shaft Application of High Modulus Pitch-Based Carbon Fibre, 41st International SAMPE Symposium, March 24-28, 1996: 405-414

14 Fujikura Composites America Inc., Fujikura: The Only Value is Performance, from website: http://www.fujikuragolf.com, accessed December 2006

15 Cheong, S.K., Kang, K.W., Jeong, S.K. (2004), Evaluation of the Mechanical Performance of Golf Club Shafts, Engineering Failure Analysis, 13: 464-473

16 United Sports Technologies Inc., United Sports Technologies: High Performance Golf Shafts, from website: http://www.ustgolfshaft.com, accessed June 2006

17 Howell, D. D. (1992), The Design of Filament Wound Graphite/Epoxy Golf Shafts, 37th International SAMPE Symposium, March 9-12, 1992: 1392-1405

18 Rules of Golf 2004-2007: As approved by the R&A Rules Ltd and the United States Golf Association, The Royal and Ancient Golf Club of St. Andrews and the United States Golf Association

19 Takemura, S., Ohno, H., Kobayashi, A. (2001), Improved Flexural Properties of Circular Cylinder for Sporting Goods, 46th International SAMPE Symposium, May 6-10, 2001: 636-646

20 Zhang, Q., Beale, D., Broughton, R.M. (1999), Analysis of Circular Braiding Process, Part 1: Theoretical Investigation of Kinematics of the Circular Braiding Process, Journal of Manufacturing Science and Engineering, vol. 121, Pg. 345-350

21 Chou, T-W., Ko, F. (1989), Composite Materials Series 3 – Textile Structural Composites, 1st edition, Elsevier Science Publishing Company Inc., New York, N.Y.

22 Du, G.W., Popper, P. (1994), Analysis of a Circular Braiding Process for Complex Shapes, Journal of the Textile Institute, 85(3): 316-337

23 Brunnschweiler, D. (1953), Braids and Braiding, Jounral of Textile Institute, 45: 668-686

24 Michaeli, M., Rosenbaum, U. (1989), Structural Braiding of Complex Shaped FRP Parts – A New Approach for Higher Productivity, 34th International SAMPE Symposium, May 8-11, 1989: 1834-1884

25 Brunnschweiler, D. (1954), The Structure and Tensile Properties of Braids, Journal of the Textile Institute, 45: T55-T87

26 Soebroto, H.B., Hager, T., Pastore, C., Ko, F. (1990), Engineering Design of Braided Structural Fibreglass Composites, 35th International SAMPE Symposium April 2-5, 1990: 687-696

27 Pastore, C., Ko, F. (1990), CIM of Braided Preforms for Composites, Computer Aided Design in Composite Materials Technology, Springer Verlag: 133-155

28 Du, G.W., Popper, P. (1990), Process Model of Circular Braiding, Processing of Polymers and Polymetric Composites, ASME Materials Division, 19: 119-133

29 Mazzawi, A. (2002), The Steady State and Transient Behaviour of 2D Braiding, PhD Thesis, University of Ottawa

30 Rawal, A., Potluri, P. (2005), Geometrical of the Yarn Paths in Three-Dimensional Braided Structures, Journal of Industrial Textiles, 35(2): 115-135

31 Carey, J. (2003), Axial, Flexural and Torsional Rigidities of 2D Braided Fibre Composite Medical Catheters, Ph.D. Thesis, Department of Mechanical Engineering, University of Ottawa, Ottawa, Canada

32 Falzon, P.J., Herzberg, I., Baker, A.A. (1993), Stiffness Analysis of Textile Composites, 5th Australian Aeronautical Conference, Melbourne, Australia, IE Australia, 1(93): 219-224

33 Ishikawa, T., Chou, T.-W. (1982), Stiffness and Strength Behaviour of Woven Fabric Composites, Journal of Materials Science, 17: 3211-3220

34 Huang, Z. (2000), The Mechanical Properties of Composites Reinforced with Woven and Braided Fabrics, Composites Science and Technology, 60: 479-498

35 Naik, N.K., Ganesh, V.K. (1995), An Analytical Method for Plain Weave Fabric Composites, Composites, 26(4): 281-289

36 Raju, I.S., Wang, J.T. (1994), Classic Laminate Theory Models for Woven Fabric Composites, Journal of Composites Technology and Research, 16(4): 289-303

37 Carey, J., Munro, M., Fahim, A. (2003), Longitudinal Modulus Prediction of a 2-D Braided Fiber Composite, Journal of Reinforced Plastics and Composites, 22(9): 813-831

38 Simpson, K. (2003), Balancing Properties for Core Success, Reinforced Plastics, April 2003

39 Klempner, D., Sendijarevic, V. (2004), Polymeric Foams and Foam Technology, 2nd edition, Hanser Gardner Publications, Inc., Cincinnati, OH, 2004

40 Kanny, K., Mahfuz, H., Carlsson, L.A., Thomas, T., Jeelani, S. (2002), Dynamic Mechanical Analyses and Flexure Fatigue of PVC Foams, Composite Structures, 58: 175-183

41 Cecchini, L.S., Weaver, P.M. (2003), The Optimisation of Foam-Filled Cylindrical Shells Subject to Flexural Loading, Structures, Structural Dynamics and Materials Conference, April 2003, 1: 180-187

42 Harte, A-M., Fleck, N.A., Ashby, M.F. (2000), Energy Absorption of Foam-Filled Circular Tubes with Braided Composite Walls, European Journal of Mechanics A: Solids, 19: 31-50

43 Mantena, P.R., Mann, R. (2003), Impact and Dynamic Response of High-Density Structural Foams Used as Filler Inside Circular Steel Tube, Journal of Composite Structures, 61: 291-302

44 Brachos, V., Douglas, C.D. (1995), Energy Absorption Characteristics of Hybrid Composite Structures, 27th International SAMPE Technical Conference, 27: 421-435

45 Ekstrom, E.A. (1996), Vibrations on the Golf Course, The Engineering of Sport, 1st edition, A.A. Balkema, Netherlands, 1996

46 True Temper Sports Inc., True Temper: The #1 Shaft in Golf, from website: http://www.truetemper.com/golf, accessed October 2006

47 Ashida, H., Ishii, T., Hironaka, S. (2006), Fiber Reinforced Plastic Golf Shaft, Mizuno Corporation, US 7,037,212

48 Hisamatsu, G., Ashida, H., Matsui, Y. (2003), FRP Golf Club Shaft, Mizuno Corporation, US 6,652,389

49 Ashida, H. (2003), FRP Golf Club Shaft, Mizuno Corporation, US 6,572,490

50 Ashida, H. (2001), FRP Golf Club Shaft, Mizuno Corporation, CA 2,363,756

51 Ashida, H. (2001), FRP Golf Club Shaft, Mizuno Corporation, US 6,666,778

52 Ashida, H. (2001), FRP Golf Club Shaft, Mizuno Corporation, CA 2,363,812

53 Earle III, G.A., Kruesi, A. H., Stockton, J. E., Kruesi, D. C. (1995), Asymmetric Braiding of Improved Fiber Reinforced Products, U.S. Composites Corp., US 5,419,231

54 Earle III, G.A., Kruesi, A. H., Stockton, J. E., Kruesi, D. C. (1992), Asymmetric Braiding of Improved Fiber Reinforced Products, U.S. Composites Corp., CA 2,104,669

55 Ngishi, I., Minowa, T. (1995), Golf Club Shaft and Method of Producing the Same, Fujikura Rubber Ltd., US 5,653,646

56 Walton, T., Fanton, F. (1992), Golf Club Shaft Having Selective Reinforcement, Spalding & Evenflo Companies Inc., US 5,083,780

57 Sutherland, T. (2006), Composite Over-wrapped Lightweight Core, CE Baseball Inc, US 7,008,339

58 Cundiff, T.R., Bennett, H.H., Lund, B.G., Renz, R.S., Wright, D.E. (2005), Resin Transfer Molding Process, The Boeing Company, US 6,872,340

59 Crow, T.L., Newmiller, B.A., Davidson III, W.F., Weaver, D.L., Hwang, T.H., Wever III, G.D., Stolz, P. (2000), Golf Club Shaft, Cobra Golf Incorporated, US 6,117,021

60 Bocoviz, C.D., Gautier, A., Barquet, H.F. (1999), Method of Making a Composite Flow-Straightener Vane, Eurocopter France, US 5,855,709

61 Grove, D.W. (1997), Center Beam Golf Club Shaft, CA 2,154,370

62 Goodwin, S.L., Spencer, R.W. (1996), Molded Products Made from Preforms of Tubular Braids, US 5,580,627

63 Tutleman, D. (1998), What Does Swingweight Really Mean?, from website: http://www.clubmaker-online.com, accessed October 2006

64 Kaw., A. (1997), Mechanics of Composite Materials, 1st edition, CRC Press LLC, Boca Raton, Florida, 1997

65 Kutz, M. (2002), Handbook of Materials Selection, John Wiley & Sons, New York

66 Mazumder, S.K. (2001), Composites Manufacturing: Materials, Product and Process Engineering, CRC Press LLC, Boca Raton, Florida

67 Buck, M. (2003), The Use of Thermoplastic Matrix Composite Materials in Making Tubular Composite Structures, Such as Golf Clubs, 48th International SAMPE Symposium, May 11-15, 2003: 1310-1319

68 Gill, R.M. (1972), Carbon Fibres in Composite Materials, 1st edition, Iliffe Books, London, England

69 Matweb, The Online Materials Information Resource, from website: www.matweb.com, accessed May 2006

70 Granta, Material Intelligence, from website: www.grantadesign.com, accessed October 2006

71 Landrock, A.H. (1995), Handbook of Plastic Foams: Types, Properties, Manufacture and Applications, 1st edition, Noyes Publications, New Jersey, 1995

72 Agarwal, B.D., Broutman, L.J. (1990), Analysis and Performance of Fiber Composites, 2nd edition, John Wiley & Sons, Inc., New York

73 Barbero, J. (1999), Introduction to Composite Materials Design, Taylor and Francis, Philadelphia, Pennsylvania, 1999

74 Naik, N.K., Shembekar, P.S. (1992), Elastic Behaviour of Woven Fabric Composites: III – Laminate Design, Journal of Composite Materials, 26(17): 2522-2541

75 Raju, I.S., Wang, J.T. (1994), Classic Laminate Theory Models for Woven Fabric Composites, Journal of Composite Technology and Research, 16(4): 289-303

76 Horneck, R.W. (1975), Numerical Methods, Quantum Publishers, Inc., New York, New York, 1975

77 Burden, R.L., Faires, J.D., Reynolds, A.C. (1981), Numerical Analysis, 2nd edition, Prindle, Weber & Schmidt, Boston, Massachusetts, 1981

78 Carey, J., Munro, M., Fahim, A. (2005), Regression-Based Model of Elastic Constants of 2D Braided/Woven Open Mesh Angle-Ply Composites, Journal of Polymer Composites, 26(2): 152-164

79 Huang, Z. (2000), The Mechanical Properties of Composites Reinforced with Woven and Braided Fabrics, Journal of Composites Science and Technology, 60: 479-498

80 Abot, J.L. (2004), Through-thickness Mechanical Characterization of Woven Fabric Composites, Journal of Composite Materials, 38(7): 543-553

81 Kim, J., Sham, M. (2000), Impact and Delamination Failure of Woven-Fabric Composites, Journal of Composites Science and Technology, 60: 745-761

82 Carey, J., Fahim, A., Munro, M. (2004), Design of Braided Composite Cardiovascular Catheters Based on Required Axial, Flexural and Torsional Rigidities, Journal of Biomedical Materials Research, 70(1): 73-81